Please cite the Published Version

Development of a Cell Based Assay for Candidate Drug Screening using Transcription Factor Activated Reporter (TFAR) Construct

A thesis submitted in fulfilment of the requirements of the Manchester Metropolitan University for the degree of Master of Science (by Research)

Alysha Burrows

School of Healthcare Science

Faculty of Science and Engineering

2018

Abstract

There is a need for new high throughput drug screening models that are able to reliably and efficiently predict drug safety and efficacy during preclinical studies. Transcription factor activated reporter gene (TFAR) cassettes can be utilised *in vitro* and *in vivo* to quantify and define modulation of transcription factor activity in response to pharmacological stimulation. Insertion of such genetic constructs into target cells or tissues necessitates the use of genetic manipulation technologies and lentiviral vectors enable permanent integration of these TFAR constructs into a range of cell types. The aim of this project was to create a cell based model for drug screening using a range of previously constructed lentiviral TFARs responsive to NFκB, NRF2, TFEB, AP-1, TCF/LEF (Wnt Signalling), STAT3 and HIF transcription factors. Human embryonic kidney (HEK)293T cells were transduced with a lentiviral TFAR construct. Clonal selection and expansion was performed in response to known agonists for each TFAR. The clonal TFAR-HEK293T cell line panel was provisionally evaluated for responses to a pro-inflammatory cytokine (TNF-α), a cytokine-mediated phorbol ester (PMA) and a GSK-3β inhibitor ($LiCl_2$). Fully quantitative luciferase luminometry data showed that all three factors activated the predicted canonical cell signalling pathways (NFκB, AP-1 and TCF/LEF respectively) but also activated non-canonical pathways. Results were broadly consistent with current literature, demonstrating that the clonal TFAR transduced cell based model could be a valuable first stage platform for evaluating newly synthesised drugs or screening drug libraries.

<u>Contents</u>

List of Figures

List of Tables

1.0 Introduction

1.1 Drug Screening Models

The development of preclinical assays with improved target specificity readouts would improve intelligent drug design and drug library screening efficiency. There is a critical need for new models that are able to reliably predict drug specificity in human cells (Esch *et al.,* 2015). *In vivo* evaluations remain a critical component of preclinical drug safety and efficacy and currently remain more applicable to human use than 2D cell based models (Szabo *et al.,* 2017). Models may range from simple organisms such as yeast (*Saccharomyces cerevisiae),* to lower vertebrates such as zebrafish (*Danio rerio*) and mammals such as mice (*Mus musculus*); each having varying degrees of similarity to humans and thus provide different benefits. Models that are of higher complexity tend to be lower throughput. Zebrafish are a particularly useful model for investigation of metabolic regulation and for study of conserved genes associated with human metabolic dysfunction, as they conserve function of the liver, pancreas and adipose tissue (Kamel and Ninov, 2017). Limitations of drug screening using animal models are that they can be costly and tend to be lower throughput than cell based models. It is broadly agreed that human cell models are the first line for drug development but traditional models lack scalability to high throughput and fidelity in data outputs.

Human Pluripotent Stem cell (hPSC) derived 3D Organoids are an emerging cell-based model for drug screening. For example induced pluripotent stem cells (iPSCs) derived from patients with neurodevelopmental disorders have been shown to produce 3D organoids which display disease phenotype *in vitro*, demonstrating that hPSC derived brain organoids may be useful for neurodevelopmental disease modelling (Lee *et al.,* 2017). Liver organoids also have significant potential to be used for the investigation of the systemic toxicity and liver toxicity which may occur during drug metabolism (Ranga *et al.,* 2014). Due to their potential applications in toxicology studies and in investigation of drug metabolism within organs such as the liver, 3D organoids have the capacity to bridge the translational gap between drug testing in animal models and in human clinical

trials. However, organoids are time consuming and costly to produce on the scale necessary for drug screening and results may be challenging to reproduce due to variation in organoid formation, for example, 3D brain organoids have been noted to vary in the size and number of ventricular zone (VZ)-like regions which they develop (Lee *et al.,* 2017). This is indeed an exciting area of research and development but the widespread application of organoid culture in the drug development field is some way off. A further iteration of this technology for drug screening is the 'organ-on-a-chip', described as a biomimetic system which aims to simulate the complex physiological functionality, structure and microenvironment of key human organs (Esch *et al.,* 2015). Organ-on-a-chip technology uses microfluidics technologies to control the microenvironment of cultured cells. This results in an *in vitro* cell culture model that is able to simulate physiological responses to pharmacological stimulation. This technology is also amenable to high throughput drug screening, however is costly to produce and currently not scalable.

There are currently remarkably few industry standard cell assays employed for pre-clinical drug screening; cytochrome p450 assays in the HepG2 liver cell line is one example. However, many drugs still present with off-target effects during the clinical trials phase, which leads to significant increases in costs and a reduction in progress during drug development. Hence, there remains an unmet need for inexpensive, high-throughput preclinical drug screening models, which are able to better define the expansive range of biological modulations that occur on pharmacological stimulation. Improved understanding of these biological effects earlier in the process of drug development will facilitate selection of drugs more appropriate for further screening, and will potentially aid the development of pharmaceuticals with reduced off target effects.

1.2 Cell Signalling and Transcription Factors

Transcription factors (TFs) have a fundamental role in control and regulation of cellular processes. They almost always contain a DNA binding domain (DBD) specific to a particular region of DNA. Binding to this region causes recruitment of RNA polymerase

and initiation of nuclear transcription. TF activation can lead to the expression or repression of a multitude of genes with diverse functions. The modulation of transcription factors that occurs on pharmacological stimulation is an important indicator of the on-target and off-target effects that may present during human clinical trials. Cell signalling pathways have been well defined for biological processes implicated in disease such as; inflammation, autophagy, cell proliferation, apoptosis, the antioxidant response, hypoxia and development. Examples of TFs characteristic of these pathways are; NFκB, TFEB, AP-1, STAT3, NRF2, HIF and TCF/LEF (Wnt signalling). Measuring TF modulation on pharmacological stimulation enables evaluation of these specific biological responses to drug administration. For example, NFκB gene expression can be used to determine if a drug is activating the inflammatory response or, alternatively, acting as an anti-inflammatory.

1.2.1 Canonical NFκB signalling

Nuclear factor kappa light chain enhancer of activated B cells (NFκB) refers to a family of transcription factors involved in regulation of inflammation, immunity, cellular growth, differentiation, apoptosis and tumorigenesis (Ghosh and Dass, 2016), (Nennig and Schank 2017). NFκB regulates gene expression in response to pro-inflammatory cytokines including TNF-α and Interleukins (IL) -1, 2, 6, 8 and 12. NFκB also acts as an activator of transcription for a range of proteins with anti-apoptotic function (IAPs, FLIP, Bcl-xL, Bfl-1, survivin) and adhesion molecules (E-selectin, VCAM-1 and ICAM-1) (D'Ignazio et al., 2017). NFκB signalling has also been demonstrated to mediate complex behaviours including learning and memory, stress responses, anhedonia and drug reward (Nennig and Schank, 2017). NFκB family proteins RelA (p65), RelB, c-Rel, NFκB1 (p105) and NFκB2 (p100) are the principle signalling molecules (Park and Hong, 2016) but canonical pro-inflammatory responses are mediated through the p65/p50 heterodimer. NFκB1 and NFκB2 are synthesised as polypeptides which are later cleaved to produce subunits p50 and p52 which are able to bind DNA and initiate transcription (Hoesel and Schmid, 2013), other family proteins function to expose activation sites during activation and transcription (Ghosh and Dass, 2016). All NFκB subunits contain an N-terminal with a Rel Homology domain (RHD), which mediates DNA binding to sites in promoters of target genes (Caamaño and Hunter, 2002). NFκB has been identified in

almost all cell types and is generally found in the form of a homo/heterodimer complex, which is formed from dimerization of Rel-like proteins. NFκB transcriptional response is determined by NFκB dimerization, and association of dimers with co-activators, repressors and other transcription factors such as STAT3, p53 and HIFs.

NFκB based regulation of gene expression may occur via canonical, non-canonical or atypical pathways. Dysregulation of NFκB canonical and non-canonical pathways has been linked with increased risk of malignancies (D'Ignazio *et al.,* 2017), (Hoesel and Schmid, 2013). In canonical NFκB signalling, binding of ligands such as Tumour Necrosis Factor α (TNF-α), Interleukin-1 (IL-1) or Lipopolysaccharides (LPS) to cell surface receptors induces intracellular recruitment of the 'activation platform'. This consists of adaptors and protein kinases and is able to phosphorylate and therefore activate the Inhibition of κB Kinase (IKK) complex. On activation, the IKK complex phosphorylates IκB inhibitor molecules which hold NFκB inactive in the cytoplasm (D'Ignazio et al., 2017). Phosphorylated IκB inhibitor molecules subsequently undergo polyubiquitination and proteasomal degradation, thus enabling NFκB nuclear translocation and gene transcription (Park and Hong, 2016).
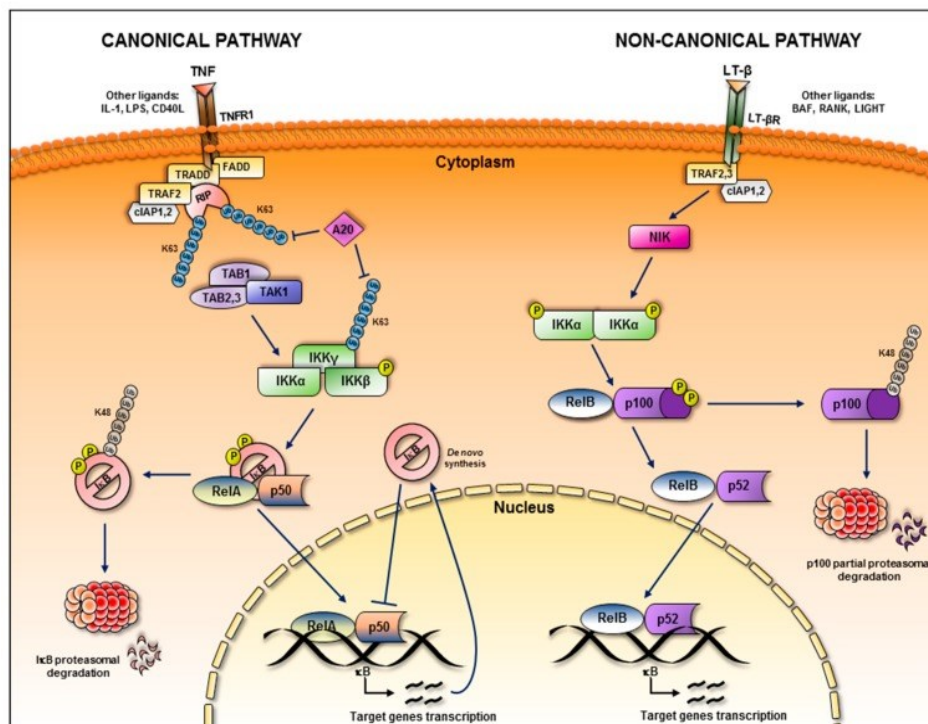
Figure 1. Mechanisms for canonical and non-canonical NFκB signalling. Image taken from D'Ignazio *et al.,* (2017).

Inflammation is a biological stress response and is associated with activation of canonical NFκB signalling (Hoesel and Schmid, 2013). Dysregulated NFκB signalling is associated with chronic inflammation and can be seen in disorders such as asthma, arthritis and inflammatory bowel disease. Chronic inflammation can also lead to cancer development via inhibition of apoptosis and promotion of angiogenesis and cell proliferation. NFκB has been shown to both promote and suppress tumour progression, depending on the cellular situation (Xia *et al.,* 2014)

1.2.2 NRF2 signalling

Nuclear factor erythroid 2-related factor 2 (NRF2) is a master regulator of the response to oxidative stress (Smith *et al.,* 2016). NRF2 plays an important role in maintaining redox homeostasis balance between levels of reactive oxygen species (ROS) inducers and ROS scavengers (Gorrini *et al.,* 2013). Controlled production of oxidants is important for regulating signalling pathways such as inflammation, immune function, cell division and autophagy. However, uncontrolled levels of oxidants result in oxidative stress and impaired cellular functions, and may lead to development of chronic disease, toxicity and cancer (Ma, 2013). The antioxidant response comes in the form of ROS scavengers, which prevent ROS induced damage to cellular organelles. ROS scavengers include glutathione (GSH), NADPH, tumour suppressors and dietary antioxidants. NRF2 upregulates antioxidant-response genes leading to expression of GSH and thioredoxin (TXN), both of which are able to reduce ROS and regenerate using NADPH (also expressed as a result of NRF2 DNA binding).

Under non-stressful conditions, cytoplasmic NRF2 is bound to kelch-like enoyl-CoA hydratase-associated protein 1 (KEAP1), a protein in the cytosol, which is anchored to actin in the cytoskeleton. When NRF2 is held in the KEAP1-NRF2 complex, the protein ubiquitin is able to bind and cause poly-ubiquitination of NRF2 via cullen3 (Cul3) binding. Poly-ubiquitination of NRF2 leads to proteasomal degradation and thus prevents DNA transcription (Zhou *et al.,* 2016). Nuclear KEAP1 proteins can also target NRF2 for

proteasomal degradation. In the nucleus, NRF2 is constitutively expressed to maintain basal expression of antioxidant genes (Smith *et al.,* 2016). Within the KEAP1 protein, there are cysteine residues containing thiol groups (R-S-H). Under conditions of oxidative stress, ROS and electrophiles reduce the thiol group of KEAP1 to disassociate the KEAP1-NRF2 complex. Disassociated NRF2 becomes phosphorylated at Ser40 and is translocated to the nucleus to bind with antioxidant response elements (ARE) of promoter regions of target genes. ARE binding regulates expression of genes associated with cellular response to oxidative stress. After DNA transcription has occurred, phosphorylation at Tyr568 causes exportation of NRF2 from the nucleus. Cellular oxidants may also cause dissociation of the KEAP1-NRF2 complex by activation of the PI3K enzyme and subsequent depolymerisation of the actin cytoskeleton, which holds the KEAP1 protein in place (Smith *et al.,* 2016).
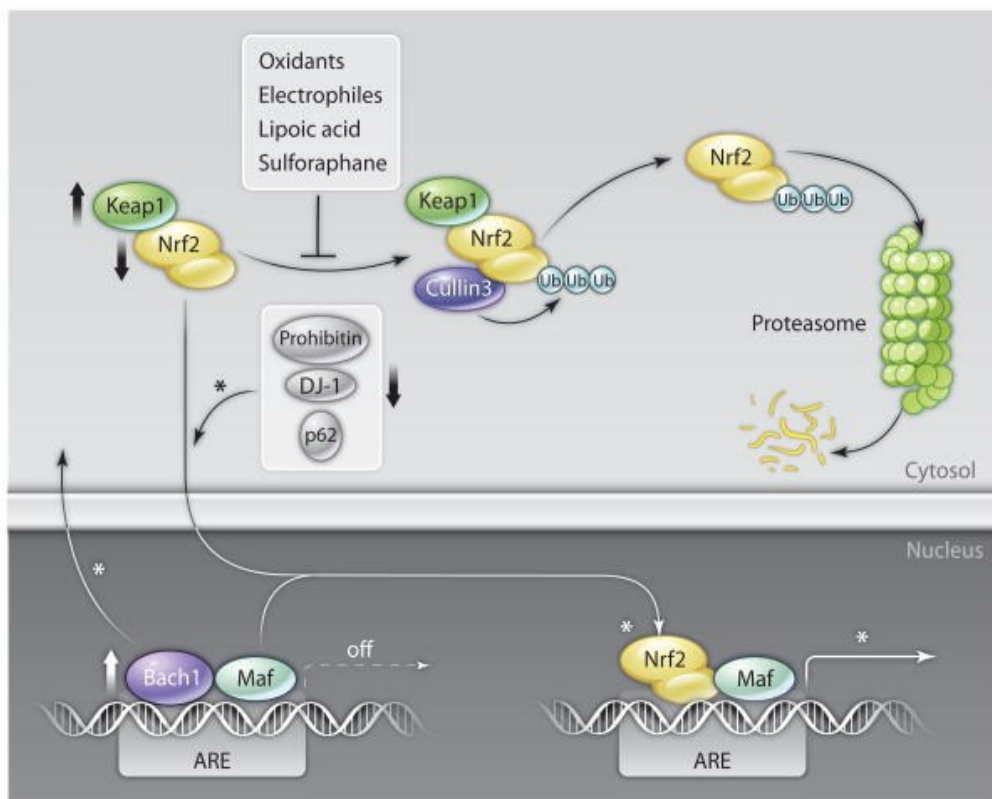
Figure 2. Mechanisms for NRF2 degradation and nuclear translocation. Image taken from Sykiotis and Bohmann (2010).

NRF2-ARE signalling is involved in modulating gene expression of over 500 genes, coding for detoxification enzymes, transport proteins, growth factors, receptors and other TF's. (Kim *et al.,* 2017), (Bryan *et al.,* 2013), (Velichkova and Hasson, 2005), (Smith *et al.,* 2016). Dysregulation of NRF2 expression is associated with increased cellular toxicity and over-activation of NRF2 can lead to multi-drug resistant cancer and cardiovascular disease.

1.2.3 HIF signalling

Hypoxia is a pathophysiological condition in which there is diminished oxygen availability to cells (Kim and Lee, 2017). In response to low oxygen availability, cells upregulate expression of hypoxia Inducible Factors (HIFs), which promote adaptive mechanisms to hypoxia. HIFs are a family of basic-helix-loop-helix TFs and each HIF is a heterodimeric complex formed by binding of a HIFα subunit to a HIF-1β subunit. Three isoforms of HIF-α have thus far been identified, HIF-1α, HIF-2α, and HIF-3α. HIF-1α is ubiquitously expressed, HIF-2α expression has been detected in the kidney, endothelial cells, heart, lungs and placenta and expression of HIF-3α is thought to occur primarily in the kidneys and in lung epithelial cells (D'Ignazio *et al.,* 2017). HIFs mediate DNA transcription for cellular adaptions to hypoxia (Jun *et al.,* 2017). In areas of localised ischaemia, HIF promotes vascularisation in hypoxic areas via upregulation of processes such as angiogenesis. HIF-1β is expressed constitutively and is nuclear (Xiong and Liu, 2017), (Garziera *et al.,* 2017). HIF-1α is cytoplasmic and its concentration is regulated by oxygen. Under normoxic conditions, HIF-1α is hydroxylated on proline residues by a prolyl-4-hydroxylase (PHD) enzyme (Garziera *et al.,* 2017). This enables binding with the von Hippel-Lindau protein (pVHL), a tumour suppressor protein, which targets HIF-1α for polyubiquitination and subsequent degradation by the proteasome. PHDs are oxygen dependent, and thus have limited function in hypoxia where lack of hydroxylation permits HIF-1α to translocate to the nucleus and form a heterodimeric complex with HIF-1β. This complex 'HIF-1' binds to hypoxia response elements (HREs) and upregulates expression of immune pathways and hypoxia response genes (Garziera *et al.,* 2017).
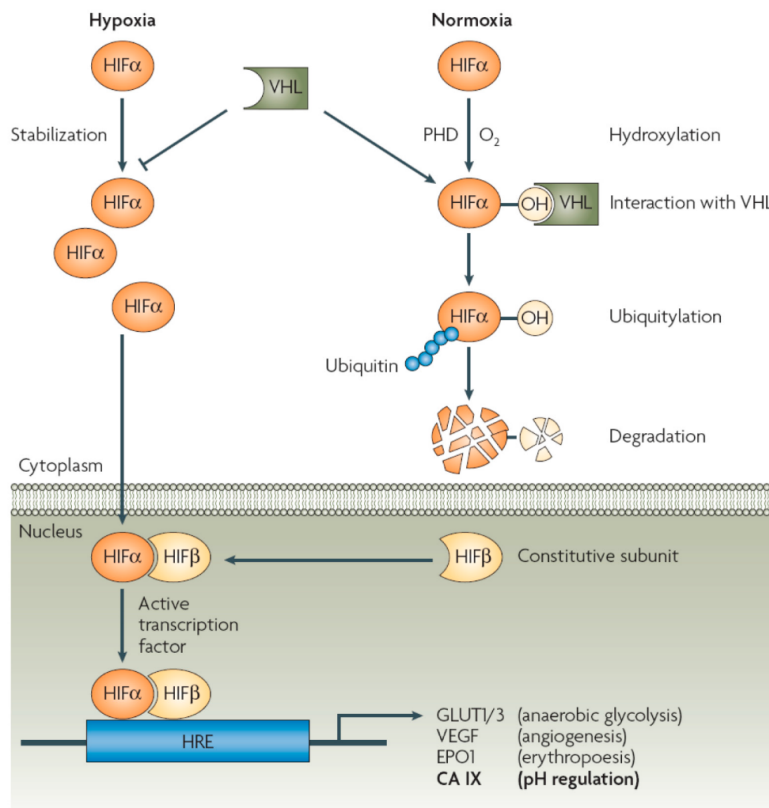
Figure 3. Mechanisms for HIF dimerization and gene transcription. Image taken from Supuran (2017).

HIF-1 binding to its consensus sequence in the promoter of target genes upregulates expression of proteins such as; vascular endothelial growth factor (VEGF), glucose transporters (GLUT1-3), enzymes CA IX and XII, and erythropoietin 1, which respectively mediate cellular mechanisms such as angiogenesis, aerobic glycolysis, pH regulation and erythropoiesis (Supuran, 2017).

HIF-1 is increased in many cancers through upregulation of genes implicated in angiogenesis, and re-modelling of the extracellular matrix (ECM), HIF-1 also improves cancer cell survival in oxygen depletion conditions via metabolic reprogramming. Furthermore HIF signalling can increase secretion of cytokines that are able to suppress both adaptive and innate immune responses (Garziera *et al.,* 2017). High levels of HIF-1 at the tumour site indicate reduced response to chemotherapy and radiotherapy and are associated with poor patient prognosis (Supuran, 2017). HIF inhibitors are in various

stages of clinical and pre-clinical drug development for treatment of a range of cancer types: topoisomerase 1 inhibitors, for example function in part by inhibition of HIF-1α expression (Yu *et al.,* 2017), (Kumar and Choi, 2015). Inhibitors of HIF PHD have been shown to improve outcome in ischemic and haemorrhagic models of stroke (Karuppagounder and Ratan, 2012) and results from Guo *et al.,* (2016) supported involvement of HIF-1-VEGF-vascular endothelial growth factor receptor (VEGFR) signalling in development of new vessels during recovery after cerebral ischemia. Depletion of HIF-1 is also associated with impaired wound healing by preventing normal cell signalling responses to hypoxia, whereas HIF hyperactivity can cause excessive production and deposition of matrix, leading to fibrosis (Hong *et al.,* 2014). Huang *et al.,* (2017) treated skin flaps on mice with hypertonic glucose (sapylin) and found improved wound healing correlating with increased VEGF-A and HIF-1α in comparison with the control, saline. HIF and its TF targets therefore represent druggable targets in the treatment of cancer, ischaemia and wound healing (Jun *et al.,* 2017).

1.2.4 AP-1 signalling

Activator protein–1 (AP-1) is the name given to dimeric transcription factors comprised of Jun, Fos, musculoaponeurotic fibrosarcoma (Maf) or activating transcription factor (ATF) family subunits, which bind to a common DNA site (AP-1 binding site) (Tewari *et al.,* 2017). AP-1 TFs contain a basic a leucine-zipper (bZIP) consisting of a leucine zipper domain and a basic DNA-binding domain. The bZIP domain is required for formation of dimers with other bZIP proteins and the DNA binding domain determines the genes regulated by that specific protein (Kappelmann *et al.,* 2013).

Dimerization between AP-1 subunits- (members of JUN, FOS, ATF, MAF families) enables formation of DNA binding complexes and stimulation of gene transcription for genes which contain AP-1 DNA recognition element 5'-TGA(C/G)TCA-3' (Kappelmann *et al.,* 2013). When activated, AP-1 can bind with the cMAP response elements (CRE) or the 12-O-tetradecanoylphorbol-13-acetate (TPA) response element (TRE) to induce gene transcription (Gào and Schöttker, 2017). AP-1 gene transcription is associated with regulation of cellular proliferation, metabolism, differentiation, oncogenic

transformation, apoptosis and cell migration (Tewari *et al.,* 2017) and AP-1 can be activated by chemokines, cytokines, growth factors, hormones and environmental stress. AP-1 proteins may be activated by Jun-N-terminal kinases (JNKs), which occurs via involvement of mitogen activated protein kinase (MAPK) pathways and can be mediated by stress. The three subfamilies of MAPKs are; Jun N-terminal kinases (JNK)/stress-activated protein kinases (SAPK), extracellular signal-regulated kinases (ERK1/2) and p38 MAPK. MAPK pathways lead to activation and phosphorylation of proteins Fos and Jun and AP-1 led tumour progression may occur through phosphorylation and activation of MAPKs pathways. Dysregulation of AP-1 is associated with progression of inflammatory disorders such as asthma, rheumatoid arthritis, psoriasis, transplant rejection and cancer (Tewari *et al.,* 2017). AP-1 and its TF targets may therefore be a potential target for prevention or treatment of cancer and inflammatory disorders.
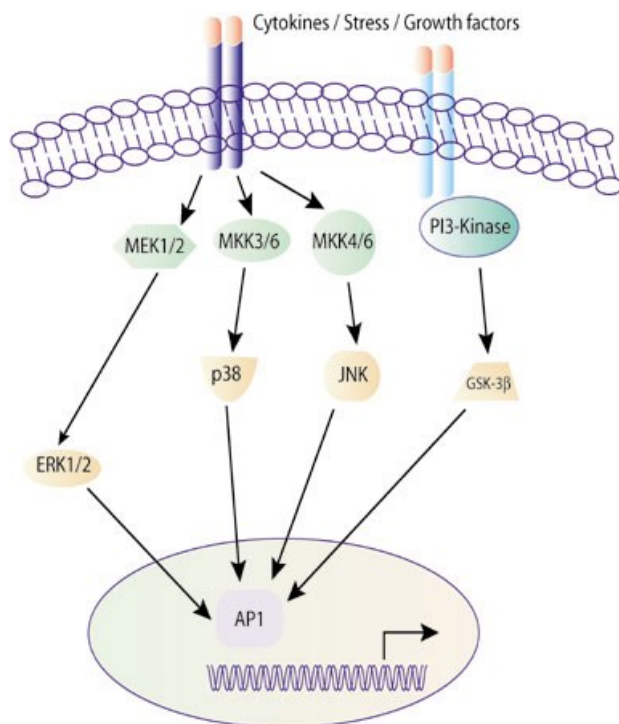
Figure 4. Mechanisms for AP-1 nuclear translocation and gene transcription. Image taken from http://www.isogen-lifescience.com/ap1-293

1.2.5 TCF/LEF (Wnt) Signalling

During mammalian development Wnt signaling is essential for regulation of cell proliferation, cell-fate specification, and asymmetric cell division. In adults, Wnt regulates tissue homeostasis and stem cell maintenance (Rapp *et al.,* 2017). There are 19 Wnt ligands and 10 main Frizzled (FZD) receptors identified in mammals. Two sub-categories of Wnt signalling are the β-catenin dependent canonical pathway, and the β-catenin independent non-canonical pathways. The non-canonical pathways are termed the planar cell polarity (PCP) and Wnt/Ca^{2+} pathways. In canonical Wnt signaling, absence of Wnt initiates formation of a complex between glycogen synthase kinase 3-beta (GSK-3β), adenomatous polyposis coli (APC) and axis inhibition protein (AXIN), termed the β-catenin destruction complex, which phosphorylates β-catenin at serine and threonine sites to tag it for degradation by the proteasome. When Wnt is present in the canonical signaling pathway, Wnt ligand binding to a FZD receptor initiates formation of a receptor complex composed of FZD, Wnt, Disheveled (DVL), lipoprotein receptor–related protein (LRP) and AXIN. Phosphorylation of DVL within the complex enables inhibition of GSK-3β, preventing it from phosphorylating beta-catenin and thus preventing its degradation. β-catenin therefore accumulates and translocates to the nucleus to form a complex with T-cell factor (TCF)/ Lymphoid enhancer-binding factor (LEF) transcription factors (Rapp *et al.,* 2017). TCF/LEF gene targets include cyclin and c-myc (Rapp *et al.,* 2017).
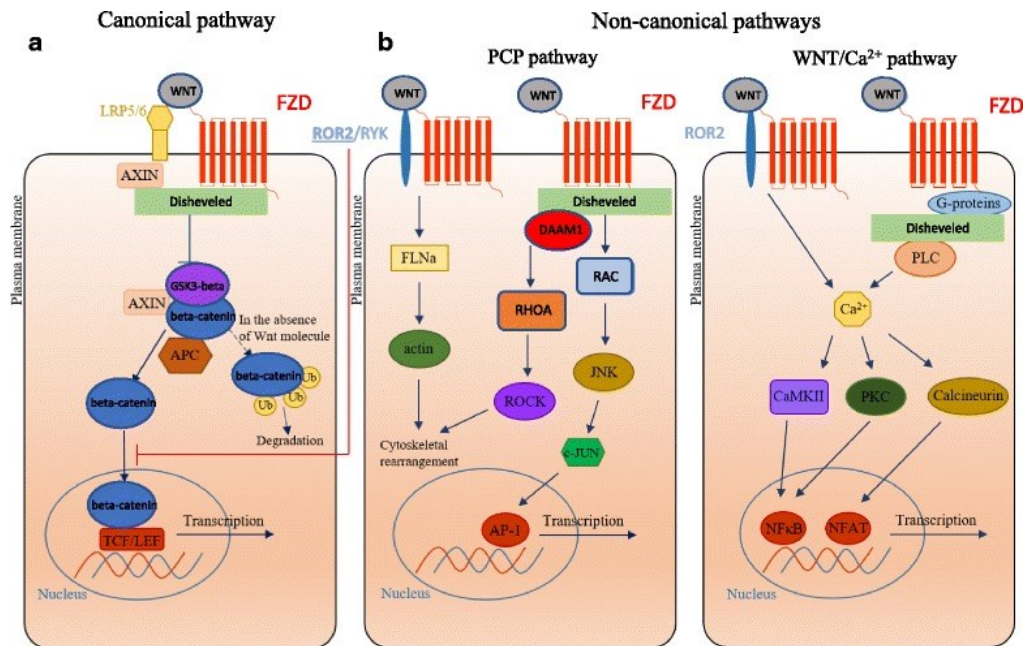
Figure 1. Schematic diagram of canonical and non-canonical Wnt (TCF/LEF) signaling pathways taken from Rapp *et al.,* (2017

1.2.6 TFEB signalling

Transcription Factor EB (binds E-box sequences) is a master regulator of lysosomal biogenesis and autophagy (Medina *et al.,* 2015), which is also involved in regulation of energy metabolism. TFEB is part of a family of TFs that positively regulates gene expression of a network of genes termed the coordinated lysosomal expression and regulation (CLEAR) network. Under normal growth conditions, TFEB in the cytoplasm is phosphorylated at ser211 and is associated with 14-3-3 family proteins; this retains TFEB in the cytoplasm/cytosol and prevents translocation to the nucleus. MTORC1 is a protein kinase complex present on the surface of the lysosome, which positively regulates this phosphorylation, and promotes upregulation of cell growth and downregulation of autophagy. Conditions such as lysosomal stress and nutrient deprivation lead to inhibition of mTORC1 and release of Ca^{2+} from the calcium channel mucolipin 1 (MCOLN1) on the lysosomal membrane. Increased cytoplasmic Ca^{2+} leads to activation of calcineurin (Cn), which binds to TFEB and causes de-phosphorylation. De-phosphorylated TFEB is able to dissociate from the TFEB/14-3-3 complex and translocate to the nucleus to form homo/ heterooligomers with other members of the

microphthalmia transcription factor (MiTF) family, leading to transcription of autophagic and lysosomal genes (Medina *et al.,* 2015).
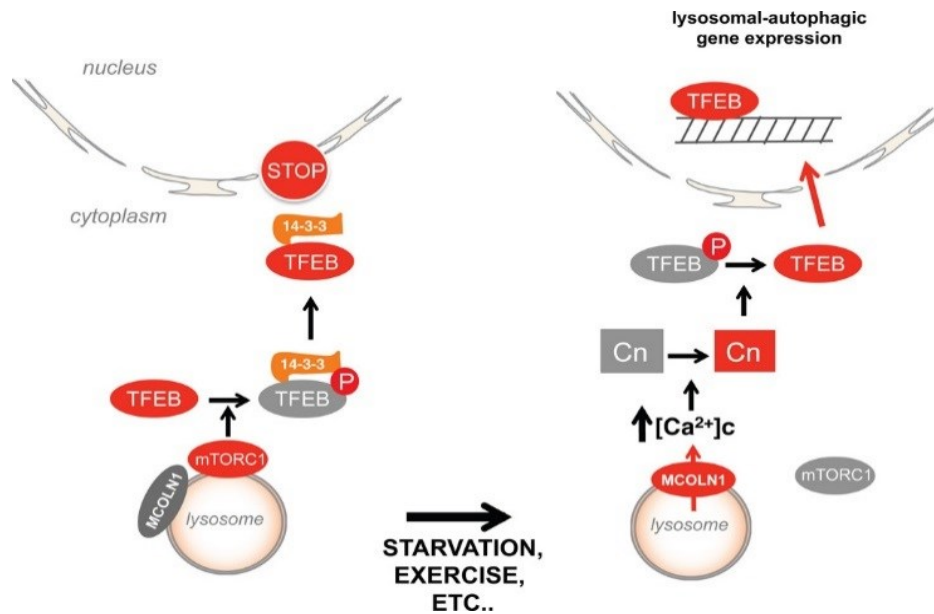
Figure 6. Mechanisms of TFEB de-phosphorylation and translocation to the nucleus. Image taken from Medina *et al.,* (2015).

1.2.7 STAT3 signalling

Signal transducer and activator of transcription (STAT) proteins are transcription factors and signal transducers that regulate cellular proliferation, cell survival, proliferation, and the inflammatory response. STAT proteins include STAT3, STAT1-4, and STAT5A and can be modulated by ROS and RNS (Gào and Schöttker, 2017). Activation of STAT3 may occur as a result of cytokine-Janus kinase (JAK) signalling. Oxidative stress can cause oxidation of STAT and JAK, which inhibits cytokine-JAK-STAT signalling. Conversely, increased levels of H_2O_2 can result in inhibition of tyrosine phosphatases and activation of tyrosine kinases and thus activation of cytokine-JAK-STAT signalling pathways (Gào and Schöttker, 2017). STAT proteins modulate inflammation and tumorigenesis and may promote angiogenesis, proliferation and metastasis of cancer cells. Upregulation of STAT3 and STAT5 has been detected in various cancer types. STAT3 activation promotes gene expression of interleukin-6 (IL-6) and COX-2 which may be involved in mediation of cancer-promoting immunity (Gào and Schöttker, 2017).
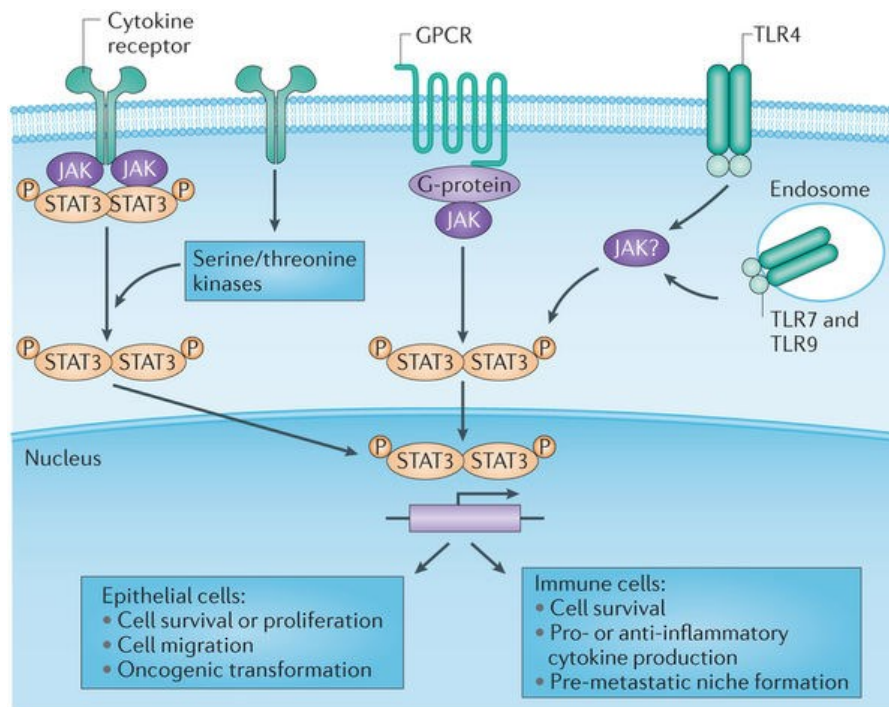
Figure 7. Activation of JAK-STAT3 signaling in Cancer. Image taken from Yu et al., (2014).

1.3 Measuring cell signalling: Reporter gene constructs

Mechanisms of gene expression may be elucidated through measuring modulations in transcription factor (TF) concentration, and may be determined via measurement of protein concentration through methods such as western blotting. These measurements require cell lysis meaning that measures can only be taken at a single time point (Dai *et al.,* 2014). However mechanistic fluctuations during drug metabolism mean that repeated or continuous measures are more relevant to drug function in vivo. Reporter gene constructs which produce secreted luciferase enable continuous and quantifiable measurements of protein modulation in response to pharmacological stimulation and have provided accurate results both *in vitro* and *in vivo*. A reporter gene is a gene attached to a regulatory sequence that produces a measurable signal upon modulation of gene expression (Ghim *et al.,* 2010). A reporter construct consists of a reporter gene whose activation is regulated by a promoter. In mammalian cells, promotor regions regulate DNA transcription. They contain functional DNA sequences which interact with

regulatory proteins such as TFs and gene specific binding proteins. On binding to a gene promoter, TFs can form 'transcriptional switches' which control gene expression. Promoters may be constitutively active, inducible in response to stimuli or active in a specific stage of development or a particular cell type (Xu *et al.,* 2013), they also may be endogenous or exogenous. Endogenous promoters commonly utilized in reporter gene constructs include cAMP response element (CRE), oestrogen response element and c-fos. These endogenous promoters however, may be affected by interference from intracellular signalling, thus exogenous promoters such as the Gal4 response element system in yeast may be used in order to reduce non-specific promoter activation (Liu *et al.,* 2009).

Cells engineered with reporter constructs express gene products on activation with given stimuli. These products may have measurable enzymatic activity or may fluoresce when viewed under a specific wave length. Gene products are either intracellular or secreted extracellularly. Intracellular products can be quantified in situ or after cell lysis and include firefly luciferase (Luc), aequorin, green fluorescent protein (GFP) and β-galactosidase (LacZ). Extracellular products secreted into the extracellular medium are collected for analysis and include β-lactamase, secreted placental alkaline phosphatase (SPAP), and variations of luciferase such as nano-luciferase (NLuc) (Liu *et al.,* 2009). Secreted products enable repeated sampling and measurements without altering the cellular environment or damaging cells.

Reporter gene constructs are versatile and sensitive and are commonly employed as 'biodetectors' for monitoring cellular signalling pathways and identifying regulatory regions involved in transcriptional control of gene expression (Liu *et al.,* 2009). They have also been used in promoter deletion analysis as well as high-throughput drug screening programmes (Xu *et al.,* 2013). Reporter gene assays may be applied for investigation of targets such as TFs, nuclear receptors, G-protein coupled receptors (GPCRs), receptor tyrosine kinases and enzymes (Xu *et al.,* 2013). We used a dual reporter gene construct developed by Buckley *et al.,* (2015) for investigation of TF modulation and for development of a clonal transcription factor activated reporter (TFAR) drug screening assay. The reporter construct contained a TF binding motif

upstream of a minimal promoter, which upon TF binding, drove gene expression of NLuc and GFP.

| TFBE | MP | — | FLAG | NanoLuc | 2A | eGFP |

A.   B.   C.   D.   E.   F.
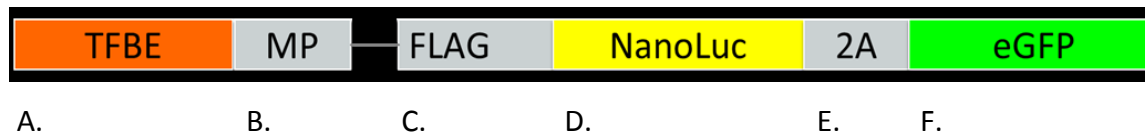
Figure 8. Representation of TFAR Gene Construct. A.) Transcription Factor Binding Motif, B.) Minimal Promoter, C.) Gene for production of Flag antibody, D.) Gene for production of nano-luciferase (NLuc), E.) Bisotronic Linker Peptide. F.) Gene for expression of Green Fluorescent Protein.

The TF binding site contained serial repeats of known transcription factor consensus sequences derived from current literature, some examples of which are displayed in Table 1. The amount of GFP and Luciferase produced was proportional to TF binding (Buckley *et al.,* 2015).

Transcription Factor	Disease Model	Response Element sequence (TF binding Motif)	*In vitro* agonist
NFκB	Inflammation/Cancer	(GGGACTTTCC) x8	TNF-α
HIF	Ischemia/Cancer	(TACGTGCT) x8	$CoCl_2$/ Low O_2
TCF/LEF (Wnt signalling)	Development	(AGATCAAAGGGGGTA) x8	$LiCl_2$
AP-1	Cancer	(TGAGTCAG) x8	PMA
STAT3	Cancer/Development	(GTCGACATTTCCCGTAAATCGTCGA) x4	IL-6
NRF2	Toxicity	(TCACAGTGACTCAGCAAAATT) x8	H_2O_2
TFEB	Autophagy	(TCACGTGA) x8	Serum starvation/Torin1

Table 1. TFs chosen for investigation, disease models which may be investigated by these, specific response elements for TF binding and in vitro agonists used for activation.

NLuc is a 19.1 kDa ATP-independent secreted nano-luciferase derived from *Oplophorus gracilirostris.* It is a highly stable bioluminescent protein able to react with a

coelenterazine analog (furimazine) to produce high intensity luminescence (Boute *et al.,* 2016). Coelenterazine acts as a substrate for NLuc catalysis in a reaction which results in the production of photons of bioluminescent light that can be quantified in a luminometer and used as a quantitative measure of gene expression. Vargulin acts as a substrate for catalysis of the the Cypridina Luciferin in a separate reaction which also produces bioluminescence. GFP is a stable fluorescent protein which can be visualised using fluorescent microscopy and used as a qualitative measure of gene expression. GFP and NLuc genes were used within this construct due to their biocompatibility and high sensitivity. GFP and NLuc are non-overlapping and may be regulated by the same promoter, thus were used to produce dual measurements of TF modulation and gene expression. Dual reporter systems which use GFP and luciferase give a more complete and accurate idea of molecular signalling (Zhang *et al.,* 2017).
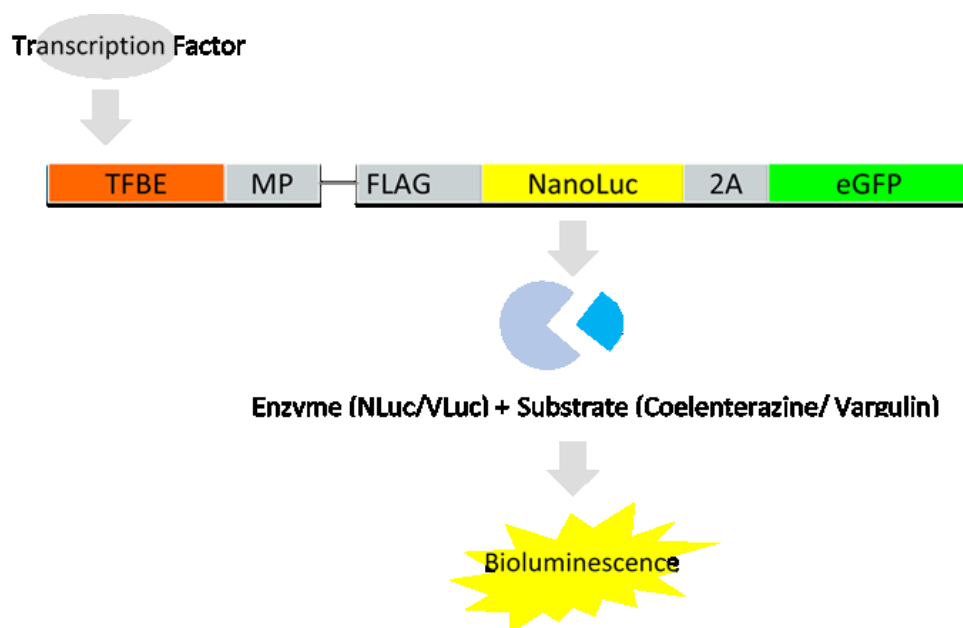
Figure 9. Representation of TF binding to the reporter construct that results in quantifiable production of luminescence.

A lentiviral vector was employed for transduction of the TFAR gene construct into HEK293T cells. In comparison with plasmid based transduction, viral vectors broaden viral tropism and increase length of expression of the reporter cassette (Zhang *et al.,* 2017).

1.3.1 Lentiviral vectors

Viral and non-viral vectors may be used to deliver and integrate reporter gene constructs within a range of cell types. Buckley *et al.,* (2015) used lentiviral vectors to successfully integrate cells with a range of TFAR constructs.
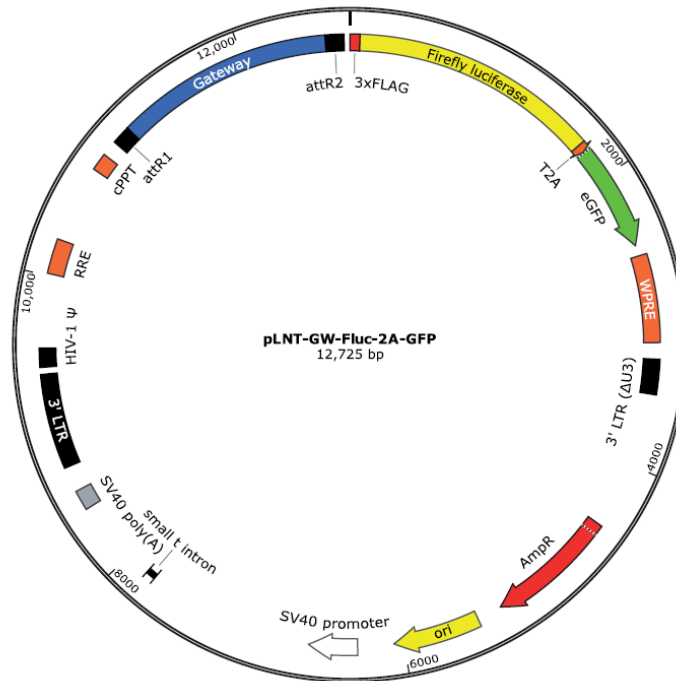
Figure 10. Schematic diagram of the lentiviral vector construct used by Buckley et al., (2015) to integrate TFAR cassettes into a range of cell types. The vector contains a firefly luciferase-2A-eGFP reporter construct.

The McKay lab have produced a range of plasmid vector constructs for lentiviral integration of TFAR cassettes. These plasmids may be delivered to cells via a second-generation lentiviral packaging system. As part of this system three plasmid vectors are delivered to a host cell; the vector construct, the plasmid for production of VSV-G envelope proteins and the packaging plasmid containing essential gag/pol viral genes. On successful delivery of all three plasmid vectors to a host producer cell, plasmid DNA is used to produce lentivirus. The lentiviral vector produced can be collected and used to deliver the TFAR cassette to another cell for genomic integration.
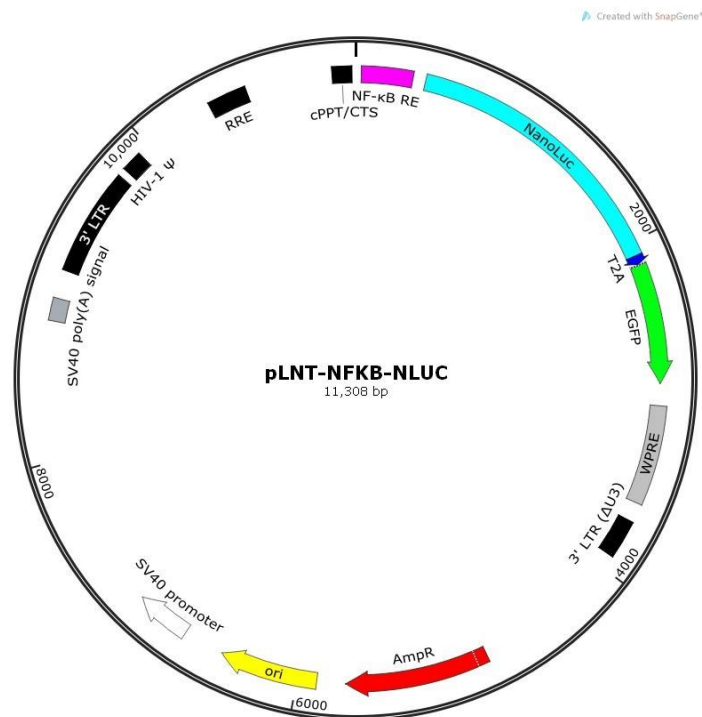
Figure 11. Plasmid map of vector construct used for lentiviral integration of the NFκB TFAR. Image courtesy of Lorna Fitzpatrick.

Lentiviral vectors are able to transduce both dividing and non-dividing cells, have a broad tropism and are SIN vectors. Lentiviruses are of the genera retrovirus. All retroviruses contain similar genomic make up consisting of gag, pol and env coding regions. Gag and pol code for structural proteins and enzymes involved in viral replication. Env codes for viral envelope proteins which enable host specific binding. Lentiviruses also contain essential gene expression activators (rev1, tat 1, RRE, rev 2, tat 2) and genes for factors involved in pathogenesis (vpr, vif, vpu, nef) (Elsner and Bohne, 2017). Lentiviral vectors may be useful in cellular reprogramming, RNA interference, CRISPR-Cas9 based genome editing and gene delivery and integration.

Many recombinant lentiviral systems are based on the HIV-1 virus. For creation of replication defective lentiviral vectors, viral genes required for delivery of transgene are identified and unnecessary sequences deleted. Antigens present on the viral surface determine viral tropism. HIV-1 envelope proteins may be substituted with different envelope glycoproteins during viral production to broaden tropism in a process called

pseudotyping. Vesicular stomatitis virus glycoprotein (VSV-G) proteins enable gene delivery and genomic integration into a wide range of cell types (Farley *et al.,* 2007).

Plasmids used for lentiviral generation are replication defective and may contain a deletion in the 3'LTR, to produce self-inactivating (SIN) virus that inactivates after integration. Lentiviral vectors are efficient for gene delivery as they are genome integrating and are able to transduce both dividing and non-dividing cells. Lentiviral vector systems may be used may be used in gene delivery of siRNA, CRISPR Cas9 and miRNA, for molecular investigation and treatment of diseases such as HIV infection, cancer and Parkinson's.

First, second and third generation lentiviral packaging systems have been developed for intracellular generation of lentiviral vectors. First generation systems are no longer in use due to the replication potential of viral products. Second-generation systems deliver genes to produce virus via three separate plasmids: a transfer plasmid containing the transgene, a packaging plasmid carrying gag and pol genes, and an envelope plasmid that delivers genes encoding for viral envelope proteins. Third generation lentiviral packaging systems divide genes for virus production between four plasmids to reduce viral pathogenicity. Second generation lentiviral systems are safe enough for non-clinical use and are able to produce a higher viral titre than third generation lentiviral production, thus are often the preferred method for lentiviral production.

Limitations of lentivectors are that they are randomly integrating and thus raise concerns of insertional mutagenesis, abhorrent protein expression and cancer (Elsner and Bohne, 2017). Viral coding and non-coding sequences may also lead to production of background noise which may interfere with reporter gene expression (Zhang *et al.,* 2017). Furthermore, lentiviral vectors may be immunogenic and cytotoxic (Ramamoorth and Narveka, 2015). Alternative gene delivery vectors may offer a safer, less immunogenic option for therapeutic purposes and include non-viral vectors which may be lipid, polymer, bacterial or inorganic. Non-viral gene delivery vectors have been employed for gene delivery of pDNA, SiRNA, shRNA, miRNA (Jayant *et al.,* 2016). Despite the limitations that may present with lentiviral vectorology, lentiviruses have been used successfully *in vitro* and *in vivo* to stably integrate genetic material including complex gene constructs into host cell genomes.

2.0 Aims

The overall objective of this project is to utilise lentiviral vectorology techniques to generate HEK293T cell lines transduced with selected TFAR constructs (developed by Buckley *et al.,* (2015)). In order to achieve this objective, I will first develop clonal HEK293T cell lines with single lentiviral integration of the expression cassette for candidate TFARs. I will then measure modulation of selected TFs on pharmacological stimulation using known agonists/antagonists and drugs. Finally, I will use these measurements to hypothesise cellular response to administration of specific drugs.

3.0 Materials and Methods

3.1 Materials

Material	Origin	Catalogue Number
Dulbecco's Modified Eagles Medium (DMEM)	Gibco	BE12-614F
Foetal bovine serum (FBS)	Fisher Scientific UK	11550356
Dimethyl Sulfoxide DMSO	Fisher Scientific UK	BP231-100
Penicillin/Streptomycin (P/S) antibiotics	Lonza	DE17-603E
Plasmocin	Invitrogen	ant-mpp
L-Glutamine	Lonza	17-605E
Human Embryonic Kidney cell line (HEK293T)	ATCC	CRL-3216
Trypsin/EDTA	Lonza	CC-5012
Plasmid pCMVR8.74	Addgene	22036
Plasmid pMD2.G	Addgene	12259
OptiMEM®	Gibco™	31985070
Polyethylenimine (PEI)	Sigma-Aldrich	03880
Cypridina Luciferin (Vargulin)	NanoLight	305

Coelenterazine	NanoLight	303
ELISA 2.0 kit	ZeptoMetrix	0801002
Plasmid Mini Kit	QIAGEN	27104

Table 2. Materials used, origin and catalogue number.

3.2 Methods

3.2.1 Cell Culture

The human embryonic kidney cell line HEK293T was cultured in DMEM, supplemented with 10% FBS, 100x Penicillin/Streptomycin antibiotics and 4mM L-Glutamine, herein after referred to as complete DMEM (cDMEM). Cells were incubated at 37°C and 5% CO_2.

3.2.2 Large scale production of VLuc expressing lentivirus vector

$2x10^7$ HEK293T cells were seeded in a T175cm^2 flask and incubated overnight at 37˚C, 5% CO_2 to reach >90% confluence. Cells were then transfected with a cocktail of 3 plasmids to produce replication defective lentiviral particles; 17.5µg pMD.G2, a VSV-G envelope expressing plasmid; 32.5µg pCMVΔR8.74, a second-generation lentiviral packaging plasmid and 50µg of vector construct containing the TFAR cassette. pCMVR8.74 was a gift from Didier Trono, as was pMD2.G. Plasmid DNA was complexed with 10mM PEI in OptiMEM® medium for 20 minutes. After this time, HEK293T cell culture media was removed and replaced by the OptiMEM® containing DNA/PEI complexes. Cells were incubated at 37°C and 5% CO_2 for 3 hours, after which transfection media was replaced with complete DMEM.

After 48 hours, cell supernatant containing budding lentivirus was collected and subjected to centrifugation at 5000 rpm/ for 10 minutes (Eppendorf 5804 R). Supernatant was removed and filtered using a 0.45µm PVDF filter to remove cellular debris. Lentivirus was concentrated by centrifugation in a benchtop centrifuge at 5000 rpm for 16-20 hours at 4˚C in 50mL Falcon tubes. Supernatant was then completely removed by aspiration and 50µL OptiMEM® added to the pellet (50µl OptiMEM® added per T175 flask). This was incubated on ice for 1 hour to resuspend the pellet. Primary

supernatant was then stored in the fridge overnight and the whole process repeated to yield a second harvest of supernatant. After 72 hours the second supernatant was then collected and centrifuged as described. Viral pellets were completely resuspended and lentivirus suspensions pooled, aliquoted, and stored for future use at -80 ˚C.

3.2.3 Viral Titration

Titration of VLuc expressing lentivirus (LNT-VLuc) produced from large scale viral prep was carried out as per the HIV-1 p24 antigen ELISA 2.0 kit. To prepare reagents, plate wash buffer was diluted 1:10 in distilled water (dH_2O) and used to wash the microplate wells. A series of 6 standards were prepared from the HIV-1 p24 antigen standard using the dilution scheme in table. Standards were not treated with Lysing buffer. 450µl of sample was treated with 50µl of Lysing buffer.

Standard Number	Concentration of HIV-1 p24 (pg/ml)	HIV-1 p24 antigen standard (µl)	Assay diluent (µl)
1	125.0	50	950
2	62.5	500 of #1	500
3	31.3	500 of #2	500
4	15.6	500 of #3	500
5	7.8	500 of #4	500
6	3.9	500 of #5	500
7	0	0	500

Table 3. Preparation of HIV-1 p24 antigen standard.

Each well of the microplate was washed (x3) with 350µl of 1X plate wash buffer. The microplate was blotted to remove all droplets from the wells. Two strips of the microplate were made up with prepared standards. 1 well of the microplate was left empty for use as a substrate blank. 200µl of standards 1-6 was pipetted into duplicate wells and for standard number 7 (0pg/ml) into triplicate wells.

	1 (pg/ml)	2 (pg/ml)
A	125	125

B	62.5	62.5
C	31.3	31.3
D	15.6	15.6
E	7.8	7.8
F	3.9	3.9
G	0	0
H	Substrate Blank	0

Table 4. Representation of two strips of microplate configured with prepared standards.

200 μl of each test sample, (prepared as described in the preparation of reagents section), was pipetted into duplicate wells. The microplate was covered with a plate sealer and incubated for 1.5 hours at 37°C ± 1°C. Wells were aspirated and washed (x6) taking care not to allow the plate to dry out. 100μl of HIV-1 p24 Detector Antibody was pipetted into each well, except the substrate blank. The microplate was then covered with a plate sealer and incubated for 1 hour at 37°C ± 1°C. The wells were then aspirated and washed (x6). 100 μl of Substrate was then pipetted into all wells and incubated uncovered for 30 minutes at room temperature (18°- 25°C). A blue colour developed in wells containing the p24 viral antigen. The reaction was stopped by pipetting 100 μl of Stop Solution into each well, which resulted in a colour change from blue to yellow. The optical density of each well was read at 450nm using the HT Synergy Plate Reader within 15 minutes of the initial colour change.

 The optical density of the standards were within given ranges indicating test validity. The mean absorbance readings of the test samples were within the linear range of the assay and within the standard curve so could be used for accurate quantification of viral titre.

HIV-1 Antigen Concentration (pg/ml)	Average Optical Density at 450nm
125	1.974
62.5	1.049
31.3	0.596
15.6	0.345
7.8	0.217
3.9	0.155
0	0.082

Table 5. Known densities of standard HIV-1 antigen concentrations.

A cut-off value was determined and a HIV-1 p24 ELISA Standard Curve was plotted to quantitate levels of HIV-1 p24. Mean absorbance was calculated for each p24 standard and test sample. Using computer graphing software, the concentration of HIV-1 p24 Antigen Standard (pg/ml) was plotted on the X-axis versus the mean optical densities for each standard on the Y-axis. Then the concentration of HIV-1 p24 antigen was determined in specimens by interpolation or linear regression analysis from the standard curve. Dilutions were corrected for, including the 1.1 dilution made during the addition of Lysing Buffer.

3.2.4 Isolation of Plasmid DNA

DNA extraction was carried using QIAGEN Plasmid Mini Kit. GM work was carried out according to appropriated SOPs, COSHH and risk assessments. *Stbl3* chemically competent *E.Coli* bacteria were defrosted from glycerol stocks and used for inoculation of a starter culture of 5 ml LB broth containing ampicillin (0.1mg/ml) for antibiotic selection. The culture was incubated at 37°C for 12–16 hours with vigorous shaking using SciQuip Incu-Shake MAXI shaking incubator (approx. 300 rpm). Bacterial cells were harvested by centrifugation at >8000 rpm (6800 xg) in a table-top microcentrifuge for 3 minutes at room temperature (15-25°C). After centrifugation, the bacterial pellet was resuspended in 250μl Buffer P1 (with added RNAse A) and transferred to a 1.5 ml microcentrifuge tube. DNA lysis occurred on addition of 250 μl of Buffer P2 (mixed by

inversion 4–6 times). The lysis reaction was neutralised by addition of 350 μl of Buffer N3 (mixed immediately and thoroughly by inversion of the tube). A homogeneous colourless suspension indicated effective precipitation of SDS. After lysis and neutralisation, bacterial DNA was centrifuged for 10 min at 13,000 rpm (~17,900 x g) in a table-top microcentrifuge to form a compact white pellet. Supernatants from the previous step were applied to the QIAprep spin column by pipetting to enable DNA binding to the spin column. This was then centrifuged for 30–60 s, and flow-through discarded. QIAprep spin column was washed with 0.5 ml buffer PB and centrifuged for 30–60 s; flow-through was discarded (in order to remove trace nuclease activity). The QIAprep spin column was then washed with 0.75 ml buffer PE and centrifuged for 30–60 seconds at maximum speed. Flow-through was discarded and tube centrifuged at full speed for an additional 1 min to remove residual wash buffer (Residual ethanol from Buffer PE may inhibit subsequent enzymatic reactions). QIAprep column was placed in a clean 1.5 ml microcentrifuge tube. For elution of plasmid DNA, 40 μl of water was added to the centre of each QIAprep spin column, let stand for 1 min, and centrifuged for 1 min. All microfuge centrifugation steps were conducted at maximum speed (13,000 rpm or ~17,900 x g).

3.2.5 Production of TFAR lentivirus

HEK293T cells were seeded at a cell density of 0.3×10^6 cells in a 6-well plate, grown to >90% confluence and transfected using a series of plasmids; 0.96μg pMD.G2, a VSV-G envelope expressing plasmid; 1.79μg pCMVΔR8.74, a 2nd generation lentiviral packaging plasmid and 2.75μg of vector construct. pCMVR8.74. Plasmid DNA was complexed with Polyethylenimine (PEI) at 0.1mM (Sigma-Aldrich) in OptiMEM® (Gibco™) for 20 minutes. After this time HEK293T cell growth medium was removed and replaced by the OptiMEM® containing DNA/PEI complexes. Cells were incubated at 37°C and 5% CO_2 for 3 hours, after which transfection medium was replaced with complete DMEM. Transfected cells were incubated for 48h to produce budding lentivirus, then supernatant containing lentivirus was harvested. Second viral supernatant was collected at 72 hours.

3.2.6 Lentiviral transduction of HEK293T cells

Lentiviral supernatant was filtered using a 0.45 μm filter and added directly to HEK293T cells. Transduction of HEK293Ts was achieved by adding 0.5ml of virus containing supernatant directly onto HEK293T cells seeded at 0.3×10^6 per well in 6-well cell culture plates.

3.2.7. Activation of heterogeneous population using known agonist.

Heterogeneous populations of cells transduced with the reporter construct were activated with known transcription factor agonists. Fluorescence microscopy was used to confirm that cells had been transduced and therefore were integrated with the reporter construct.

Transcription Factor	*In Vitro* Agonist Used for Validation	Concentration	Incubation Time (Hours)
NFκB	Tumour Necrosis Factor-alpha (TNF-α)	10ng/ml	16
HIF	Cobalt (II) Chloride ($CoCl_2$)	100μM	16
TCF/LEF (Wnt signalling)	Lithium Chloride ($LiCl_2$)	50mM	48
AP-1	Phorbol 12-myristate 13-acetate (PMA)	10ng/ml	21
STAT3	Interleukin-6 (IL-6)	10ng/ml	6-16
NRF2	Pyocyanin	5μg/ml	16
TFEB	Torin1	15μg/ml Torin1	48
	Serum Starvation	N/A	3-6

Table 6. Table displaying TFs, Agonists used for activation, the concentration and duration of use. (Concentrations and durations of agonist addition were determined based on current literature and titrations done in the McKay Lab).

3.2.8 Clonal Expansion of transduced cells

HEK293T cells were transduced with LNT-TFAR at a multiplicity of infection (MOI)<1. Subsequently cells were trypsinised, diluted and plated at approximately one cell per

well in a 96-well plate. Fluorescence microscopy was used to select clones based on pre-defined inclusion and exclusion criteria. Selected clones were amplified, and re-plated for clonal expansion.

3.2.9 Inclusion/Exclusion Criteria:

Clones must express basal levels of GFP and luciferase as measured by fluorescent microscopy and luciferase luminometry, respectively. Mixed populations were excluded.

3.2.10 Agonist induction of clonal HEK293T-TFAR cell lines

HEK293T-TFAR clonal cell lines expressing basal GFP were expanded and activated with a known agonist (See Table 1.) Modulations in gene expression in response to a known agonist were measured using both fluorescent microscopy and luciferase luminometry.

Selected HEK293T clones were each split 1:6 and plated at equal cell density into 6 wells of a 24-well plate. Cells were amplified to ~70% confluence prior to activation. For each HEK293T-TFAR clone 3 wells were treated with a vehicle control and 3 wells were treated with known agonist in a 24-well plate (as detailed in Table 1.) After 24-72 h cell medium containing agonist was replaced with Complete DMEM. Cells were maintained in Complete DMEM for 4 hours, and then cell medium was collected to assay using luciferase luminometry.

3.2.11 Cell Based Assay for Candidate Drug Screening using HEK-293T-TFAR

For all future experiments, the chosen seven HEK293T-TFAR cell lines were plated in triplicate in a 24-well plate. One 24-well plate acted as a control for vehicle administration, agonist was added to the other identical plate. The activity of each transcription factor with and without a drug or agonist was quantified by luciferase assay and used to determine which transcription factors were modulated by drug addition.

3.2.12 Imaging

All GFP Images were taken using the Leica Live Cell Imager. All below GFP images are displayed with a corresponding Phase Contrast image, taken simultaneously to show GFP expression relative to cell number.

3.2.13 Statistical analysis

Statistical analysis on data from *in vitro* vector analysis was performed using Independent Samples t-tests. *All* data is expressed as mean values ± SEM of at least three independent experiments performed in triplicate. A value of $p < 0.05$ was considered statistically significant. All statistical analyses were performed by SPSS (Version 22.0, 2013, IBM Corp., Armonk, NY, USA; SPSS Inc., Chicago, IL, USA).

4. Results

Transcription factor activated gene reporter (TFAR) constructs can be used *in vitro* and *in vivo* to quantify and define modulation of gene expression in response to pharmacological stimulation, and may be used to predict drug safety and efficacy during preclinical studies. I sought to generate a panel of TFAR cell lines for application in drug evaluation by transducing HEK293T cells with lentiviral vectors containing seven different TFAR cassettes.

4.1 Lentiviral-TFAR production

Transcription factor activated reporter gene (TFAR) constructs were originally generated and provided for this project by the McKay Lab (Buckley *et al.,* 2015). TFAR constructs were developed with a transcription factor binding motif (TFBM) upstream of a minimal promoter, which drives expression of green fluorescent protein (GFP) and luciferase (Luc) reporter genes *(Figure 9.)* TFBM were selected and originally isolated from those described and independently validated in the current literature. Serial repeats of these known transcription factor consensus sequences were commercially *de novo* synthesised (Aldevron, ND, USA) and cloned into the parental lentiviral vector by Buckley *et al.,* (2015) using rapid *Gateway®* cloning. The TFBM consisted of serial transcription factor binding sequences, which varied in length and repeat number depending on the transcription factor under investigation. Binding of transcription factor (TF) to the TFBM resulted in activation of the promoter region and thus upregulated gene expression of Luc and GFP reporter genes in a dose responsive manner (Table 1. and Table 2.). I have employed gene expression cassettes containing a secreted variant of luciferase called NanoLuc. NanoLuc is a strong flash luciferase variant and contains a protein secretory signal so is actively exported from the cell and can be quantitated in conditioned media by luciferase luminometry. Expression of GFP enables qualitative measurement of activity by fluorescent microscopy. Gene expression of NanoLuc and GFP are controlled by the same synthetic promoter enabling multi-modal TF activity evaluations. The construct also contains a FLAG antibody that can be used for easy detection of transgenic protein.

HEK293T cells were co-transduced with a TFAR lentiviral vector and a second lentiviral cassette expressing a constitutively active control promoter driving expression of secreted vargula vuciferase (VLuc) (Appendix: Figure 37.) VLuc luciferase is the luciferase produced by *Cypridina hilgendorfii*, it catalyses the conversion of vargulin substrate in an enzymatic reaction to produce light. This reaction can also be quantified using luciferase luminometry and can be measured in the same conditioned media as NLuc as neither NLuc nor VLuc show activity catalysing the opposite's substrate. HEK293T cells are a human embryonic kidney cell line widely used in cell biology because they are comparatively easy to grown, maintain and transfect with DNA vectors. In this project I have used these cells for two purposes: a) to generate lentiviral preps and b) to act as TFAR expressing cell lines delivered by lentivirus. In this section HEK293T cells were used as lentivirus generating factories.

4.2 Production and Titration of VLuc virus

Titration of VLuc expressing lentivirus (LNT-VLuc) produced from large scale viral prep was carried out as per the HIV-1 p24 antigen ELISA 2.0 kit. During this assay, microplate wells were coated with a monoclonal antibody specific for the HIV-1 capsid protein p24. During incubation of the sample, p24 antigen is bound to the immobilized antibody. Bound antigen is able to react with a human anti-HIV-1 antibody conjugated to horseradish peroxidase (HRP). When a substrate is added, reaction of the HRP enzyme produces colour. The optical density is proportional to the concentration of HIV-1 p24 antigen within the sample. The absorbance values of a set of standard dilutions are plotted and p24 sample concentration can be determined by interpolation from a point-to-point plot or from a linear regression analysis of the standard curve.
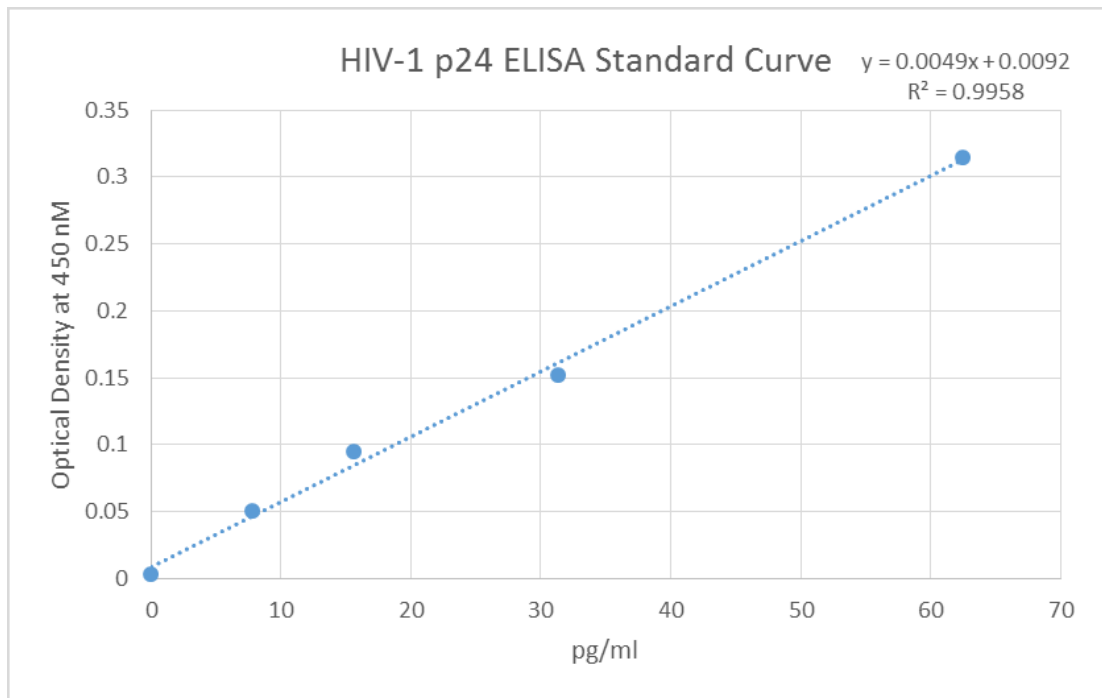
Figure 12. HIV-1 p24 ELISA Standard Curve. Results for the standard curve were based on configured standards.

Viral titre was determined by first calculating the value of X using the equation of the line derived from the HIV-1 p24 ELISA standard curve (X= 19.551pg/ml). This value was multiplied by 100 to account for the number of p24 antigens per viral particle, and then multiplied by the dilution factor used (10^6). Viral titre of LNT-VLuc produced was 1.9 x 10^9 viral particles per ml. As VLuc expression is controlled by the constitutively active spleen focus forming virus (SFFV) promoter, the concentration of vargulin luciferase in cell media could be taken as a measure of cell number. This measure was therefore used to normalise results for cell number and all cells were transduced with VLuc virus before the experiments described below were carried out.

4.3 Transfection

HEK293T cells were transfected with a cocktail of three plasmids: pMD.G2, a VSV-G envelope expressing plasmid, pCMVΔR8.74, a second generation lentiviral packaging plasmid and the vector construct, a plasmid containing the lentiviral construct expressing the TFAR (Figure 8). For this project, I focused on seven TFARs: AP-1, HIF, STAT3, TCF/LEF, NFκB, TFEB and NRF2. HEK293T cells were transfected and then

transfection efficiency assessed after 72 h by fluorescence microscopy detection of GFP. Figure 13. shows phase and GFP images demonstrating broad transfection efficiency for each TFAR. Broadly, the McKay lab have previously noted that the TFARs tend to express irrespective of agonist activation after transient plasmid transfection in HEK293T cells and only gain agonist-specific activity once the expression cassette is integrated into the host cell genome. Consequently, we are able to assess successful transfection of HEK293T cells at ~70-90% efficiency. Previous experience has indicated that these levels of transfection yield lentiviral titers in the region of $1 \times 10^{5-6}$ transduction units (ti)/ml supernatant. Interestingly, the intensity of expression of each construct varies (AP-1 is very strong, TCF/LEF is less intense) after transient transfection.
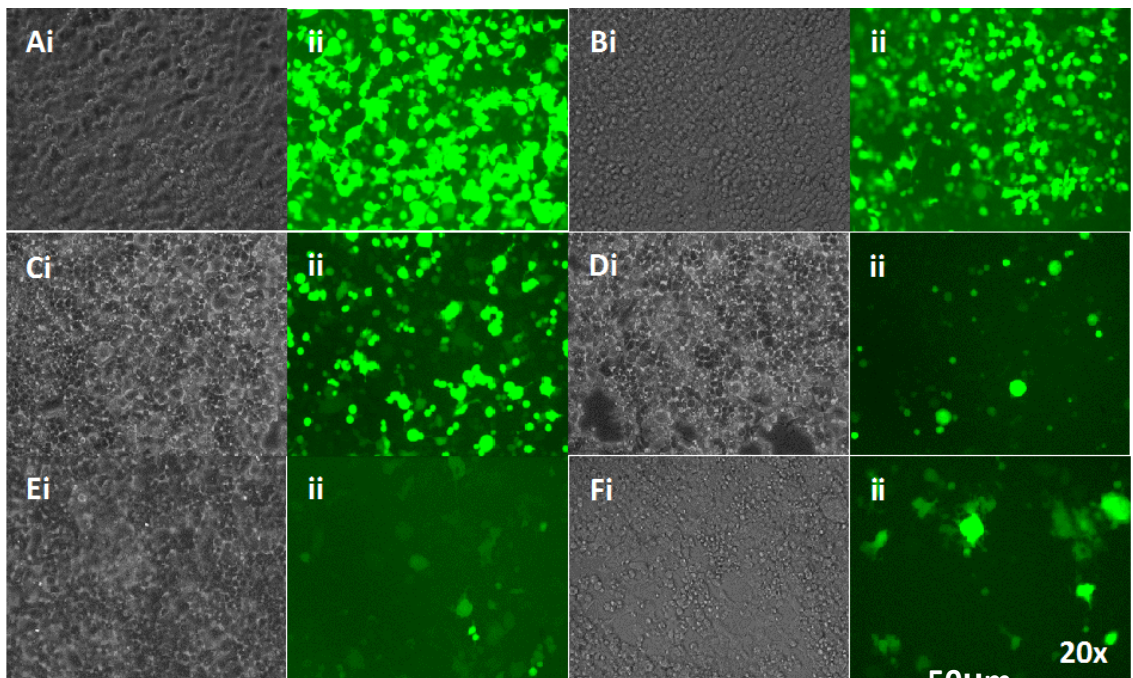

Figure 13. HEK293Ts Transfected with plasmids for integration of a range of TFARs. Ai). Phase-contrast images of HEK293Ts transfected with plasmid vectors for integration of the AP-1 TFAR construct. Aii).Corresponding GFP images. Bi). Phase-contrast images of HEK293Ts transfected with plasmid vectors for integration of the HIF TFAR construct. Bii).Corresponding GFP images. C). Phase-contrast images of HEK293Ts transfected with plasmid vectors for integration of the STAT3 TFAR construct. Cii). Corresponding GFP images. D). Phase-contrast images of HEK293Ts transfected with plasmid vectors for integration of the TCF/LEF TFAR construct. Dii.) Corresponding GFP images. E). Phase-contrast images of HEK293Ts transfected with plasmid vectors for integration of the NFκB TFAR construct. Eii). Corresponding GFP images. Fi). Phase-contrast images of HEK293Ts transfected with plasmid vectors for integration of the NRF2 TFAR construct. Fii). Corresponding GFP images. All images were taken at 20X magnification using Leica Live Cell Imaging System. Scale bar 50μm.

4.4 Titration of Lentivirus and Transduction

Lentivirus produced was titred to determine the amount of viral media that was required for minimal transduction of reporter construct. Due to the relatively high basal expression of NFκB seen in HEK293T cells, NFκB virus was selected for this titration. Lentiviral integration of the reporter construct within host cell genome occurred at an average transduction efficiency of 30%. Low transduction efficiency was desired to prevent the occurrence of multiple viral integrations per cell. Based on the transduction efficiency achieved, 0.5ml of viral media was diluted with 0.5ml media not containing virus for transduction of all future TFARs. HEK293T cells were transduced with LNT-TFAR at a multiplicity of infection (MOI) < 1. On average, it was estimated that each transduced cell contained a single viral genome integration.
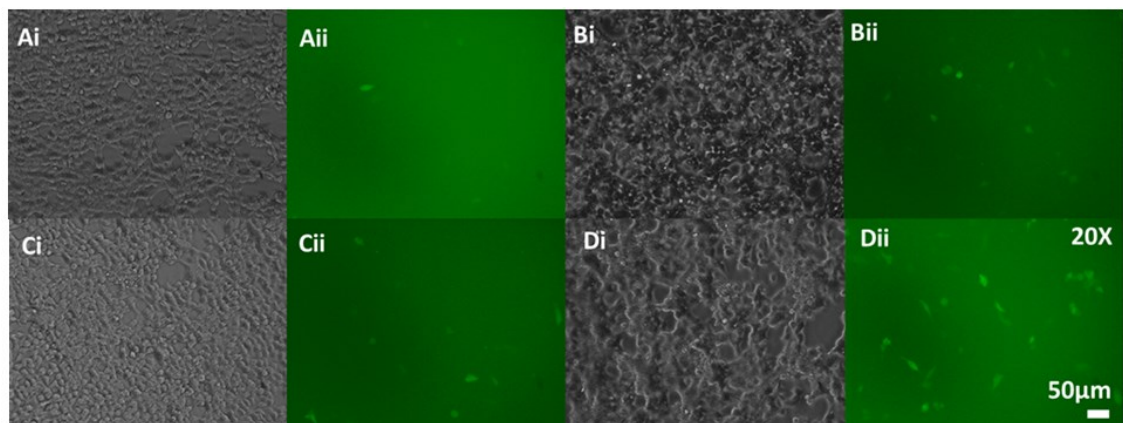

Figure 14. Transduction of HEK293Ts with NFκB virus. Each well of cells were transfected with virus diluted in varying ratios of media. Ai.) Phase-contrast images of HEK293Ts transduced with 0.0625ml viral media to 0.9375ml media. Aii.) Corresponding GFP images display low levels of lentiviral integration. Bi.) Phase-contrast images of HEK293Ts transduced with 0.125 ml virus to 0.875ml media. Bii.) Corresponding GFP images display an intermediate level of lentiviral integration. Ci.) Phase-contrast images of HEK293Ts transduced with 0.25ml virus to 0.75ml media. Cii.) Corresponding GFP images display a greater level of lentiviral integration. Di.) Phase-contrast images of HEK293Ts transduced with 0.5ml virus to 0.5ml media. Dii.) Corresponding GFP images display greatest levels of lentiviral integration. All images were taken at 20X magnification using Leica Live Cell Imaging System. Scale bar 50μm.

4.5 Activation of Heterogeneous Population of TFARs with Known Agonists

After lentiviral transduction of HEK293Ts, the resultant population of heterogeneously transduced cells was treated with a known agonist (refer to Table 1.) and imaged using fluorescence microscopy (Leica Live Cell Imager). GFP expression indicated lentiviral integration of the reporter construct. Transduced cells expressed NLuc and GFP on TF binding to the TFAR construct and the resultant activation of the synthetic promoter sequence. Expression of reporter genes was assumed to be proportional to the level of the nuclear translocation of the transcription factor under investigation. Low transduction efficiency was desired to reduce the probability of multiple lentiviral integrations. Due to the low rate of viral transduction achieved, variations in GFP expression are thought to result from diversity in cell signalling within the population rather than from multiple viral integrations.

In order to validate our TFAR lentivirus transduced HEK293T cell lines we chose to use agonists that have been previously extensively validated in the literature. In brief these were: TNF-α for NFκB (Wu and Zhou, 2010), pyocyanin for NRF2 (Liu *et al.,* 2017). PMA for AP-1 (Colin *et al.,* 2011), IL-6 for STAT3 (Attia *et al.,* 2017), $CoCl_2$ for HIF (Zhou *et al.,* 2017) and serum starvation for TFEB TFAR transduced cell lines (Medina *et al.,* 2015). Figures 15-22 show representative images of GFP upregulation in HEK293T-TFAR cells treated with the appropriate agonists.
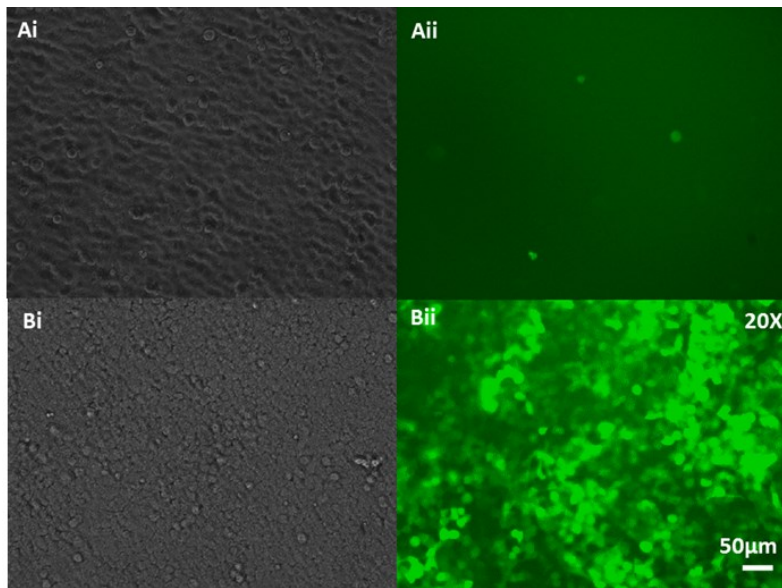
Figure 15. Heterogeneous Population of HEK293Ts Transduced with NFκB TFAR Activated by TNF-α.
Ai.) Phase-contrast images of HEK293Ts transduced with the TFAR for NFκB treated with the vehicle control. Aii.) Correlating GFP images for vehicle Control. Bi.) Phase-contrast images of Heterogeneous NFκB treated with TNF-α (10ng/ml) for 16 hours. Bii.) Corresponding GFP images for treatment with TNF-α. GFP images display activation of the NFκB reporter construct on addition of the known NFκB agonist TNF-α, indicating successful genomic integration of the NFκB TFAR. All images were taken at 20X magnification using Leica Live Cell Imaging System. Scale bar 50μm.
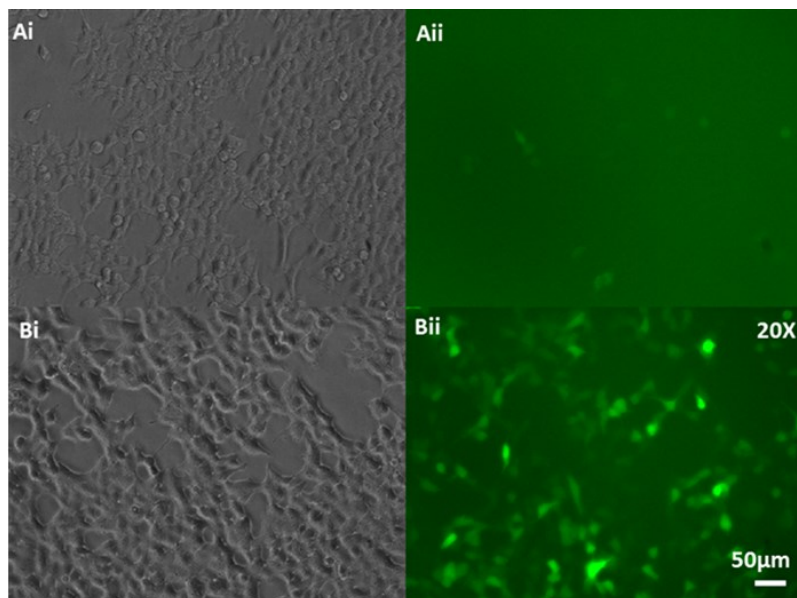
Figure 16. Heterogeneous Population of HEK293Ts Transduced with NRF2 TFAR Activated by Pyocyanin.
Ai.) Phase-contrast images of HEK293Ts transduced with the TFAR for NRF2 treated with the vehicle control. Aii.) Correlating GFP images for vehicle Control. Bi.) Phase-contrast images of Heterogeneous NRF2 treated with pyocyanin (5µg/ml) for 16 hours. Bii.) Corresponding GFP images for treatment with pyocyanin. GFP images display activation of the NRF2 reporter construct on addition of the known NRF2 agonist pyocyanin, indicating successful genomic integration of the NRF2 TFAR. All images were taken at 20X magnification using Leica Live Cell Imaging System. Scale bar 50µm.
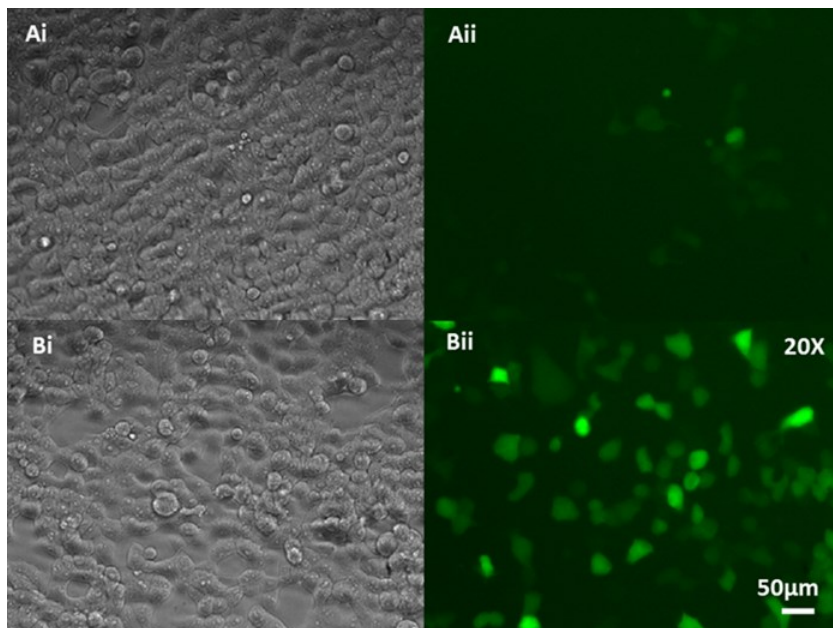

Figure 17. Heterogeneous Population of HEK293Ts Transduced with AP-1 TFAR Activated by PMA.
Ai.) Phase-contrast images of HEK293Ts transduced with the TFAR for AP-1 treated with the vehicle control. Aii.) Correlating GFP images for vehicle Control. Bi.) Phase-contrast images of Heterogeneous AP-1 treated with PMA (10ng/ml) for 21 hours. Bii.) Corresponding GFP images for treatment with PMA. GFP images display activation of the AP-1 reporter construct on addition of the known AP-1 agonist PMA, indicating successful genomic integration of the AP-1 TFAR. All images were taken at 20X magnification using Leica Live Cell Imaging System. Scale bar 50µm.
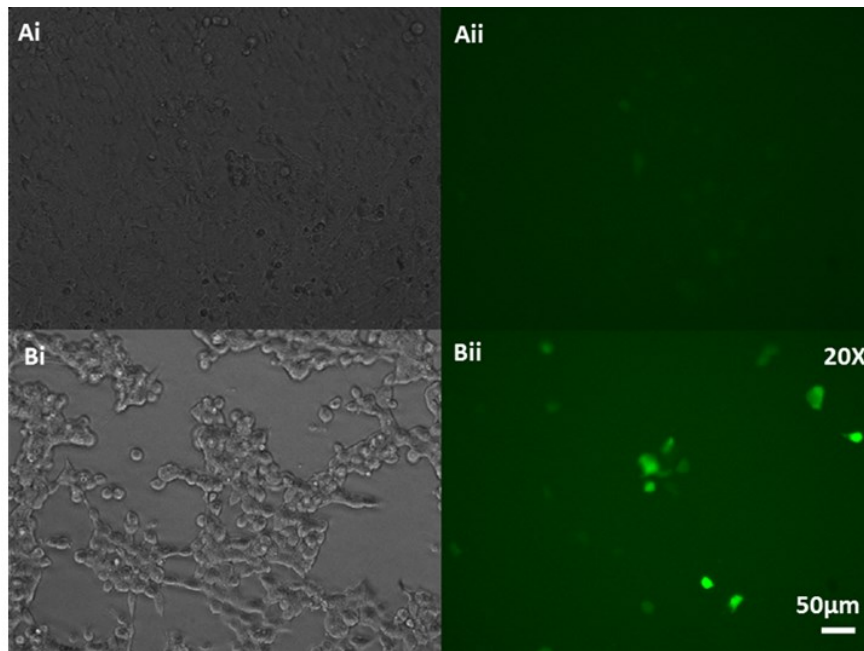
Figure 18. Heterogeneous Population of HEK293Ts Transduced with TCF/LEF (Wnt signalling) TFAR Activated by LiCl. Ai.) Phase-contrast images of HEK293Ts transduced with the TFAR for TCF/LEF treated with the vehicle control. Aii.) Correlating GFP images for vehicle Control. Bi.) Phase-contrast images of Heterogeneous TCF/LEF treated with LiCl (50nM) for 48 hours. Bii.) Corresponding GFP images for treatment with LiCl. GFP images display activation of the TCF/LEF reporter construct on addition of the known TCF/LEF agonist LiCl, indicating successful genomic integration of the TCF/LEF TFAR. All images were taken at 20X magnification using Leica Live Cell Imaging System. Scale bar 50μm.
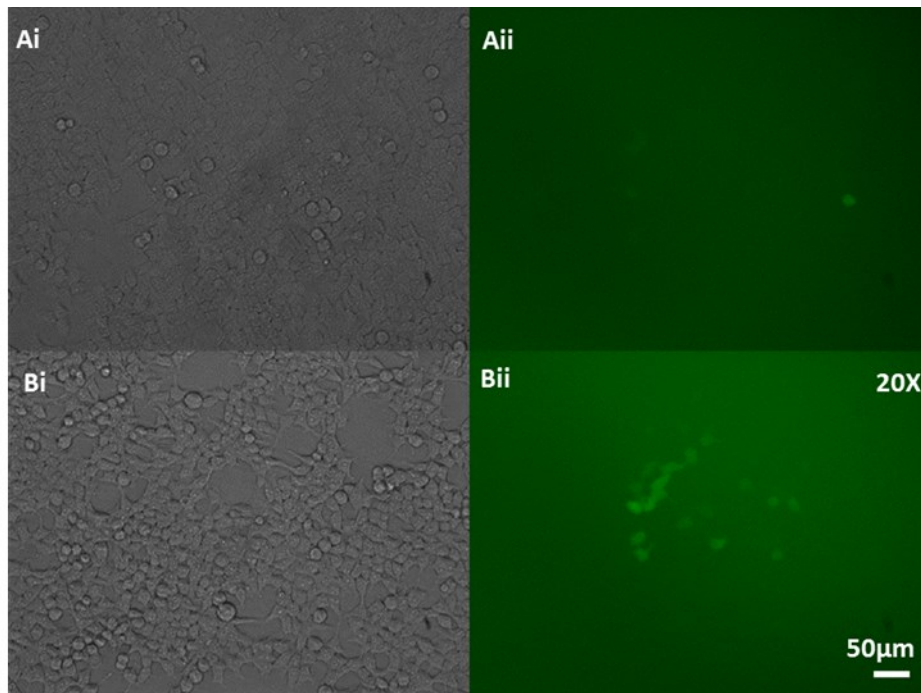
Figure 19. Heterogeneous Population of HEK293Ts Transduced with STAT3 TFAR Activated by IL-6.
Ai.) Phase-contrast images of HEK293Ts transduced with the TFAR for STAT3 treated with the vehicle control. Aii.) Correlating GFP images for vehicle Control. Bi.) Phase-contrast images of Heterogeneous STAT3 treated with IL-6 (10ng/ml) for 16 hours. Bii.) Corresponding GFP images for treatment with STAT3. GFP images display activation of the STAT3 reporter construct on addition of the known STAT3 agonist IL-6, indicating successful genomic integration of the STAT3 TFAR. All images were taken at 20X magnification using Leica Live Cell Imaging System. Scale bar 50µm.
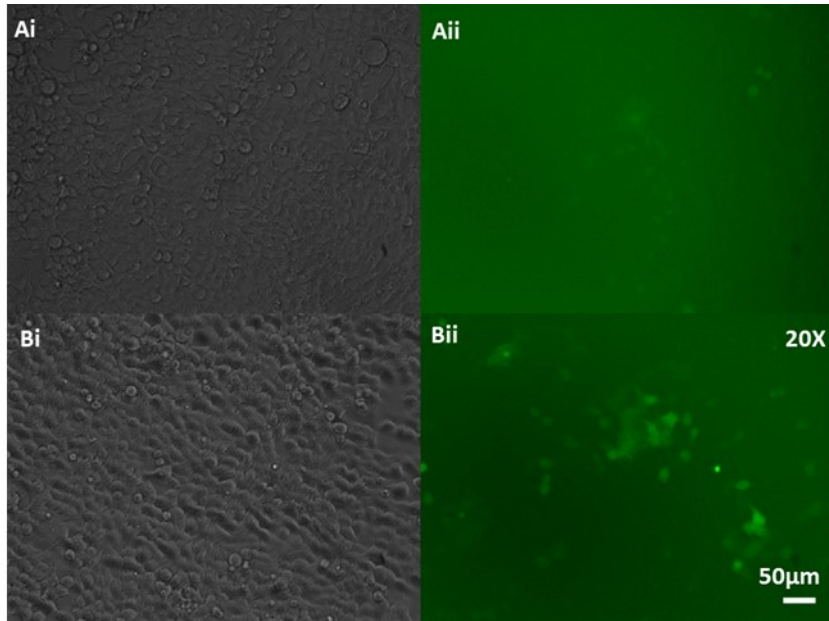
Figure 20. Heterogeneous Population of HEK293Ts Transduced with HIF TFAR Activated by CoCl₂. Ai.) Phase-contrast images of HEK293Ts transduced with the TFAR for HIF treated with the vehicle control. Aii.) Correlating GFP images for vehicle control. Bi.) Phase-contrast images of HEK293Ts transduced with the HIF TFAR treated with CoCl₂ (100μM) for 16 hours. Bii.) Corresponding GFP images for treatment with CoCl₂. GFP images display activation of the HIF reporter construct on addition of the known HIF agonist CoCl₂, indicating successful genomic integration of the HIF TFAR. All images were taken at 20X magnification using Leica Live Cell Imaging System. Scale bar 50μm.
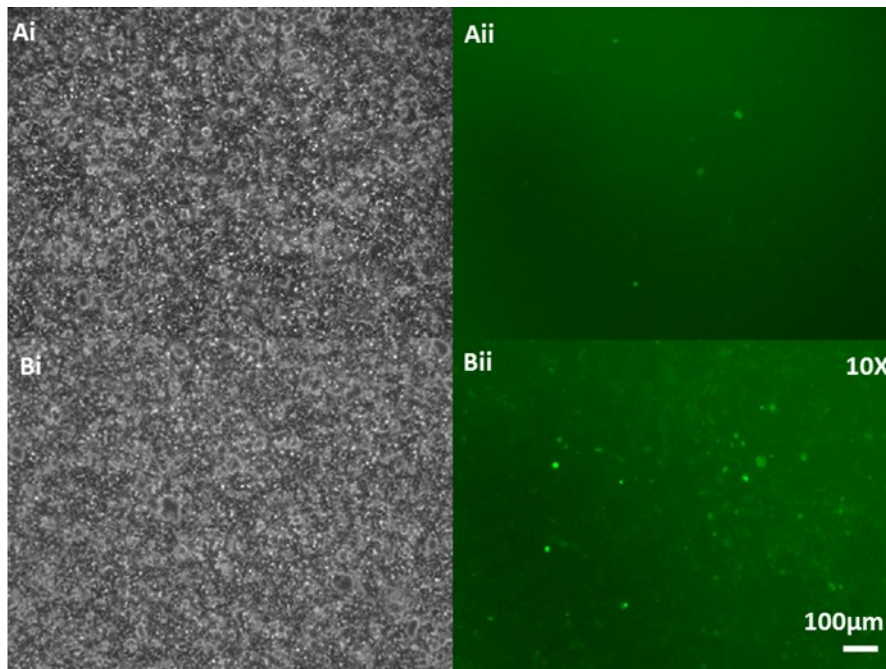
Figure 21. Heterogeneous Population of HEK293Ts Transduced with TFEB TFAR Activated by Serum Starvation. Ai.) Phase-contrast images of HEK293Ts transduced with the TFAR for TFEB treated with the vehicle control. Aii.) Correlating GFP images for vehicle control. Bi.) Phase-contrast images of HEK293Ts transduced with the TFEB TFAR treated with serum starvation for 4 hours. Bii.) Corresponding GFP images for treatment with serum starvation. GFP images display activation of the TFEB reporter construct on addition of the known TFEB agonist serum starvation, indicating successful genomic integration of the TFEB TFAR. All images were taken at 10X magnification using Leica Live Cell Imaging System. Scale bar 100µm.
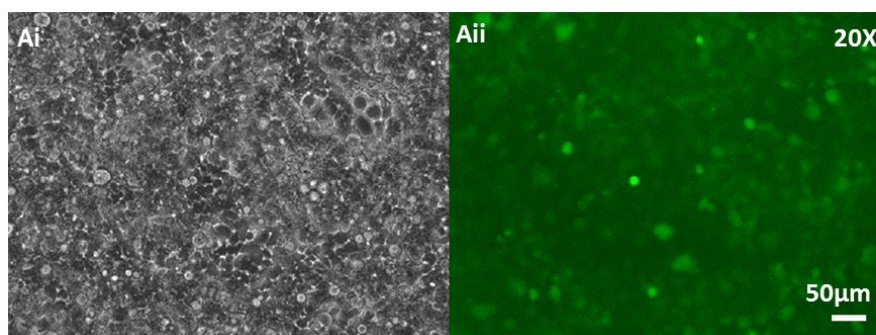

Figure 22. Heterogeneous TFEB 4 hours with Serum Starvation. All images were taken at 20X magnification using Leica Live Cell Imaging System. Scale bar 50µm.

4.6 Clonal Expansion of transduced cells

After validation of lentiviral integration within the heterogeneous populations of HEK293T cells they were trypsinised, counted using a hemocytometer, diluted in suspension and plated at one cell per well in a 96-well plate. Clonal populations that exhibited basal GFP expression (as shown in Figure 23.) were selected and expanded for further testing. On average ~30% of the colonies picked expressed GFP, thus it was assumed that average transduction efficiency was in the region of 30%. Due to the lentiviral transduction efficiency achieved based on previous experiments, it was assumed that transduced clones contained a single integration of the reporter construct.
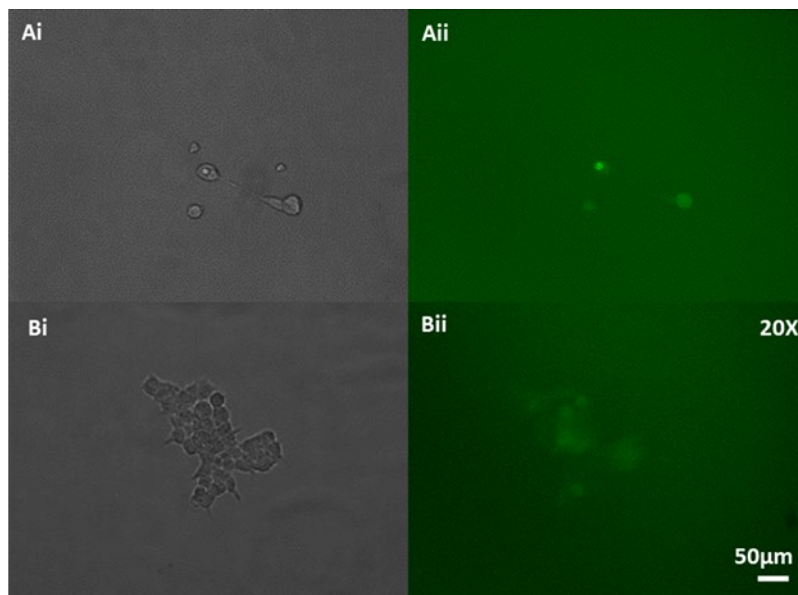

Figure 23. Expansion of a single cell plated in well of a 96 well plate during the process of Clonal Expansion. Ai). Phase-contrast images of clonal cells transduced with the TFAR for NFκB. Aii.) Corresponding GFP images. Bi.) Phase-contrast images of clonal cells transduced with the TFAR for TFEB. Bii). Corresponding GFP images. All images were taken at 20X magnification using Leica Live Cell Imaging System. Scale bar 50μm. Lentiviral integration is indicated by basal GFP expression.

4.7 Clonal Selection: Activation of Clonal Population of TFARs with Known Agonists

Clonal HEK293T cell lines transduced with a selected Lenti-TFAR (HIF, AP-1, TCF/LEF, STAT3, NRF2, NFκB and TFEB) that expressed basal levels of GFP were expanded initially in the 96-well format. They were then trypsin passaged at a dilution of 1:6 and plated at

equal densities into a 24 well plate. Selected clones were then activated using known *in vitro* agonists as previously described in table 1. GFP images were taken for qualitative measures of gene expression using fluorescent microscopy and then conditioned cell media was harvested for analysis by luciferase luminometry. For each HEK293T-TFAR clone, there were three biological repeats for each TFAR; three wells treated with vehicle control, and three wells treated with a known agonist. For each well three technical repeat luminometry readings were taken. The HEK293T-TFAR clones that displayed the greatest increase in activation compared to baseline were selected and amplified for further experiments.
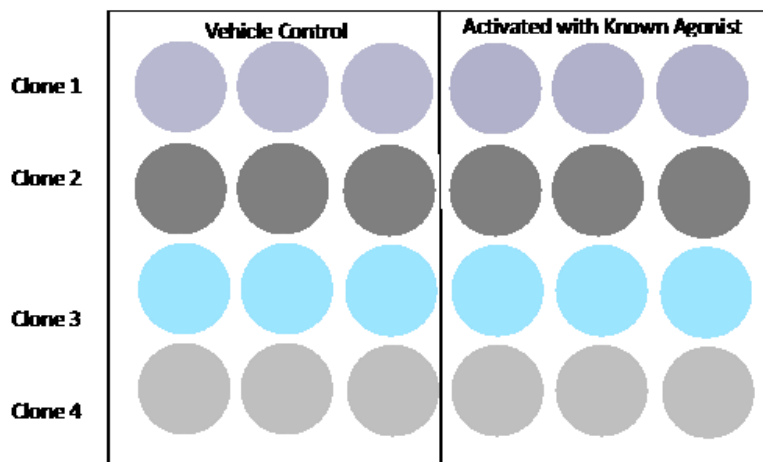

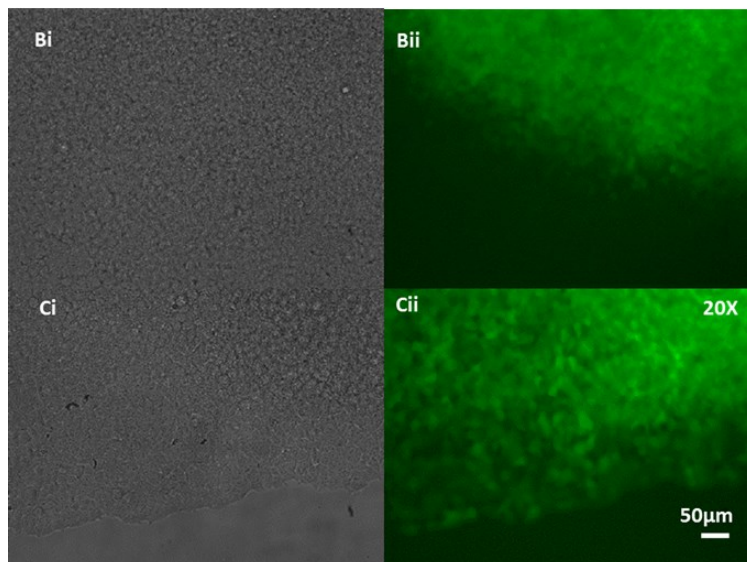**Figure 24. Representation of plate format during clonal selection.**

Figure 25. Clonal Population of HEK293Ts Transduced with HIF TFAR Activated by CoCl₂. A). Graph displaying activation of clonal populations integrated with the TFAR for HIF with the known agonist CoCl$_2$. On activation, clone B5 displayed a significant increase (p=0.007) in NanoLuc expression compared with the control. Clone B7 also displayed a significant increase in luciferase expression in response to the agonist (p=0.011). Clone B5 was most responsive to agonist thus was selected for further testing. Fold change results were attained using Luciferase Luminometry data. For all p-values: p*<0.05, p**<0.01 and p***<0.001. Bi.) Phase-contrast images displaying selected HIF transduced clone B5 treated with the vehicle control. Bii). Corresponding GFP images. Ci.) Phase-contrast images displaying selected HIF transduced clone B5 treated with (100μM) the known agonist CoCl$_2$ for 16 hours. Cii.) Corresponding GFP images. All images were taken at 20X magnification using Leica Live Cell Imaging System. Scale bar 50μm.
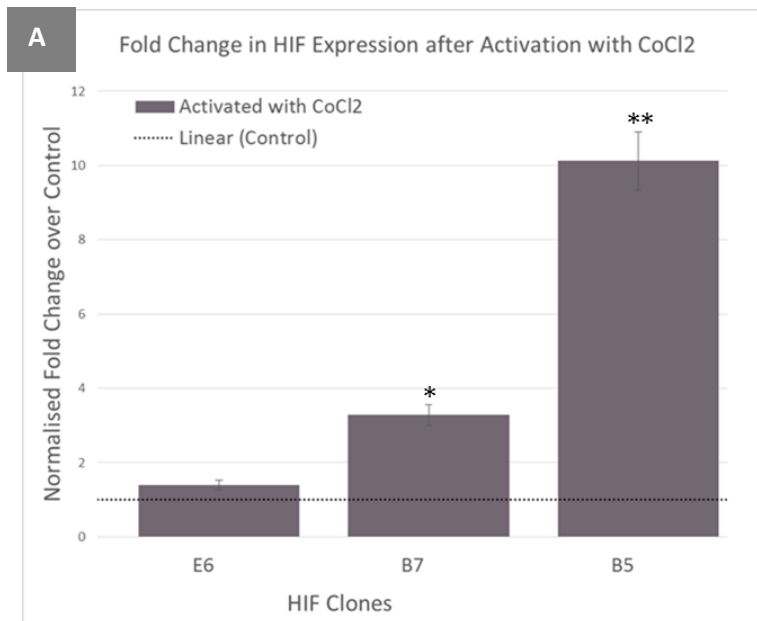
Figure 26. Clonal Population of HEK293Ts Transduced with AP-1 TFAR Activated by PMA. A). Graph displaying activation of clonal populations integrated with the TFAR for AP-1 with the known agonist PMA. On activation, clone F4 displayed the most significant increase (p=0.0129) in luciferase expression relative to its control. Clone G4 (p=0.0434). Clone F4 was selected for further testing. Fold change results were attained using Luciferase Luminometry data. For all p-values: p*<0.05, p**<0.01 and p***<0.001. Bi.) Phase-contrast images displaying selected AP-1 transduced clone F4 treated with the vehicle control. Bii). Corresponding GFP images. Ci.) Phase-contrast images displaying selected AP-1 transduced clone F4 treated with (10ng/ml) PMA for 24 hours. Cii.) Corresponding GFP images. All images were taken at 20X magnification using Leica Live Cell Imaging System. Scale bar 50µm.
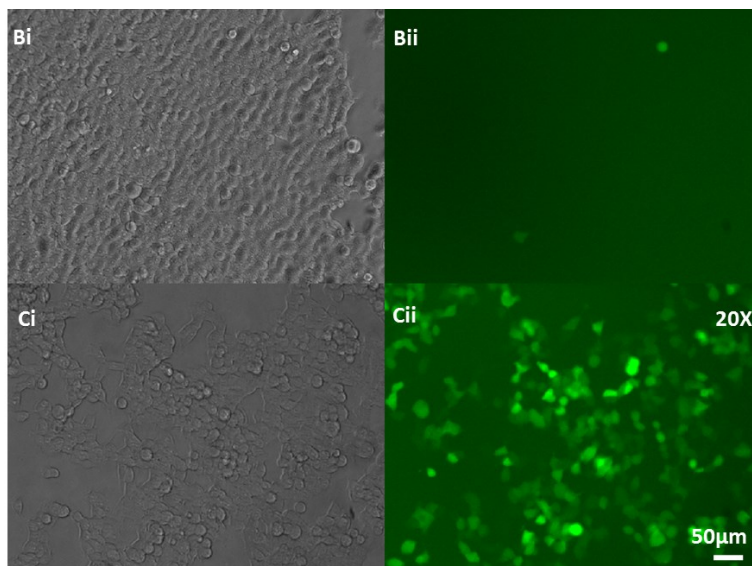
Figure 27. Clonal Population of HEK293Ts Transduced with TCF/LEF (Wnt signalling) TFAR Activated by LiCl$_2$. A.) Graph displaying activation of clonal populations integrated with the TFAR for TCF/LEF with the known agonist LiCl$_2$. On activation, clone C5 was significantly upregulated by LiCl$_2$ addition (p=0.018), but clone D12 displayed the most significant increase (p=0.015) in luciferase expression relative to its control. Clone D12 was therefore selected for further testing. Fold change results were attained using Luciferase Luminometry data. For all p-values: p*<0.05, p**<0.01, and p***<0.001. Bi.) Phase-contrast images displaying selected TCF/LEF TFAR transduced clone D12 treated with the vehicle control. Bii). Corresponding GFP images. Ci.) Phase-contrast images displaying selected TCF/LEF TFAR transduced clone D12 treated with 50mM LiCl$_2$ for 48 hours. Cii.) Corresponding GFP images. All images were taken at 20X magnification using Leica Live Cell Imaging System. Scale bar 50μm.
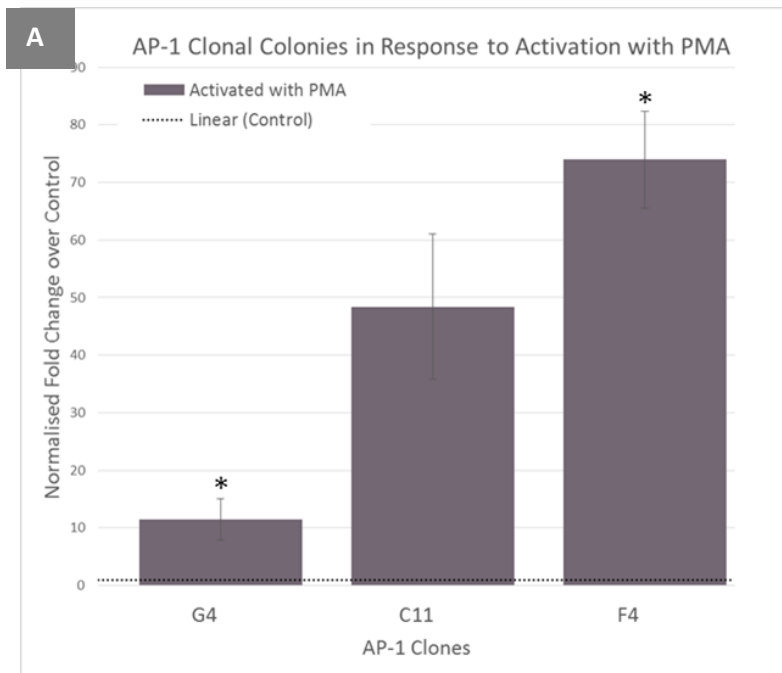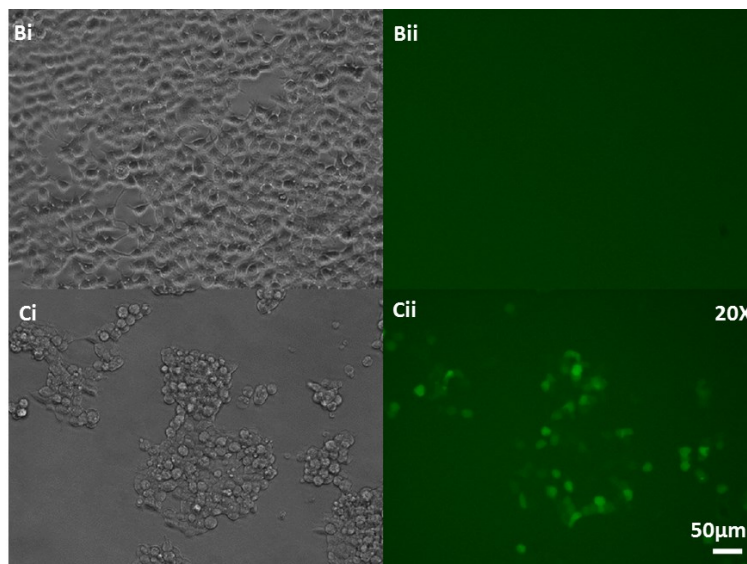
Figure 28. Clonal Population of HEK293Ts Transduced with STAT3 TFAR Activated by IL-6. A). Graph displaying activation of clonal populations integrated with the TFAR for STAT3 with the known agonist IL-6. On activation, clone A2 displayed the most significant increase (p<0.001) in luciferase expression relative to its control. However, Clone A2 didn't display any visible basal GFP expression, nor did it display an increase in GFP expression on activation. Increased GFP expression in response to an agonist is a required characteristic for all of the clones in the TFAR based cell screening model. Luciferase expression of Clone C7i was significantly increased (p=0.024) on activation with IL-6 and this clone displayed a visible increase in GFP. Therefore Clone C7i was selected. Fold change results were attained using Luciferase Luminometry data. For all p-values: p*<0.05, p**<0.01, and p***<0.001. Bi.) Phase-contrast images displaying selected STAT3 TFAR transduced clone C7i treated with the vehicle control. Bii). Corresponding GFP images. Ci.) Phase-contrast images displaying selected STAT3 TFAR transduced

clone C7i treated with 10ng/ml IL-6 for 16 hours. Cii.) Corresponding GFP images. All images were taken at 20X magnification using Leica Live Cell Imaging System. Scale bar 50µm.

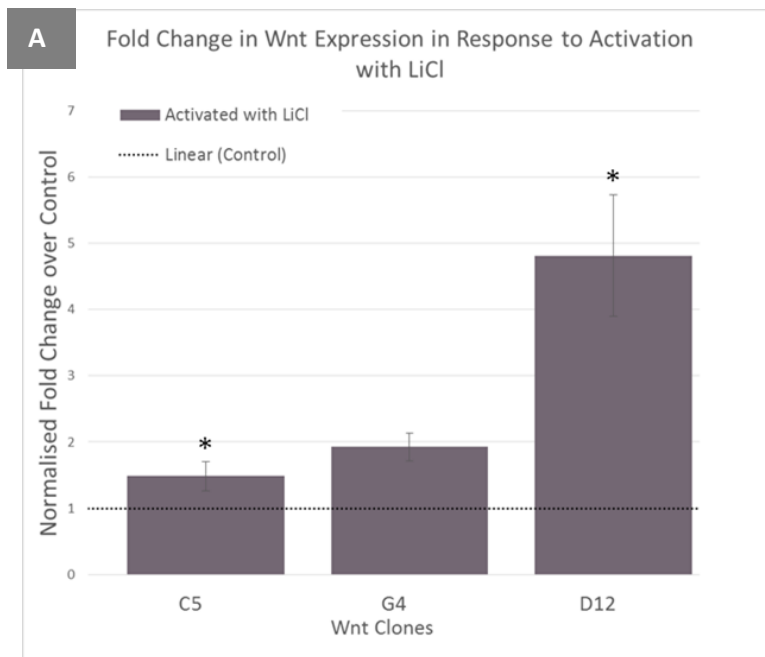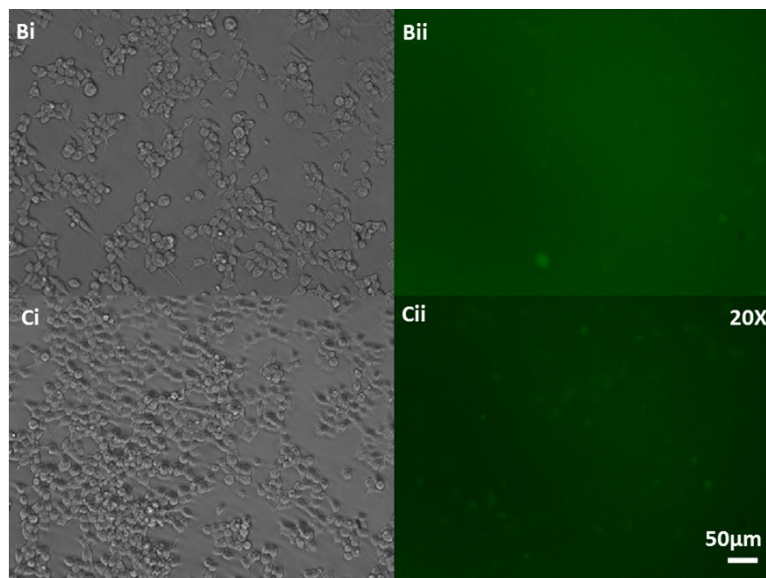**Figure 29. Clonal Population of HEK293Ts Transduced with NRF2 TFAR Activated by pyocyanin.** A). Graph displaying activation of clonal populations integrated with the TFAR for NRF2 with the known agonist pyocyanin. On activation, clone A9 displayed the greatest increase in luciferase expression relative to its control. The difference was not significant, however GFP images displayed clear activation of this clone on addition of pyocyanin, so clone A9 was selected. Fold change results were attained using Luciferase Luminometry data. For all p-values: p*<0.05, p**<0.01, and p***<0.001. Bi.) Phase-contrast images displaying selected NRF2 TFAR transduced clone A9 treated with the vehicle control. Bii). Corresponding GFP images. Ci.) Phase-contrast images displaying selected NRF2 TFAR transduced

clone A9 treated with 5µg/ml pyocyanin for 24 hours. Cii.) Corresponding GFP images. All images were taken at 20X magnification using Leica Live Cell Imaging System. Scale bar 50µm.
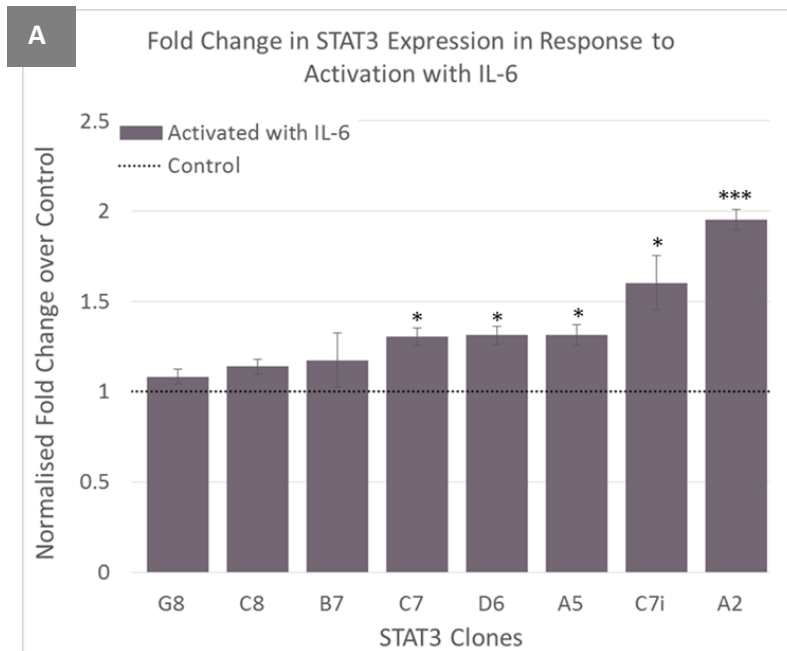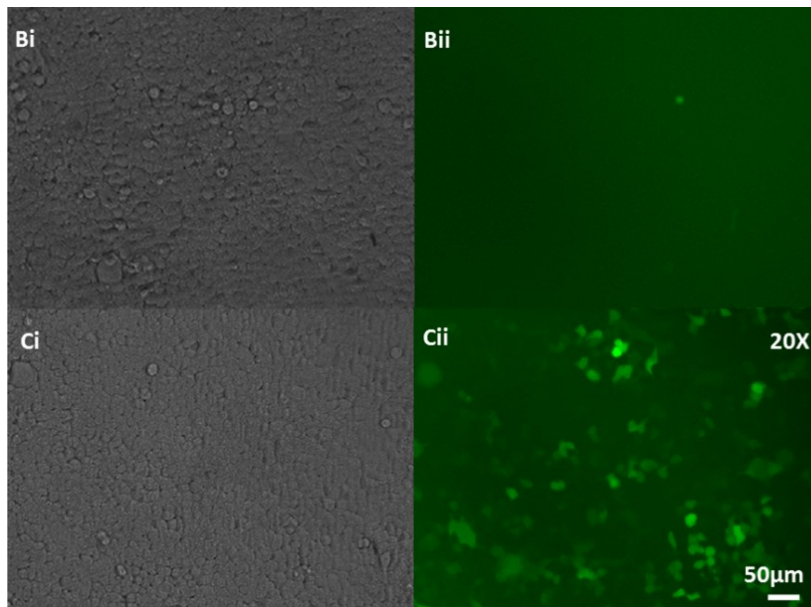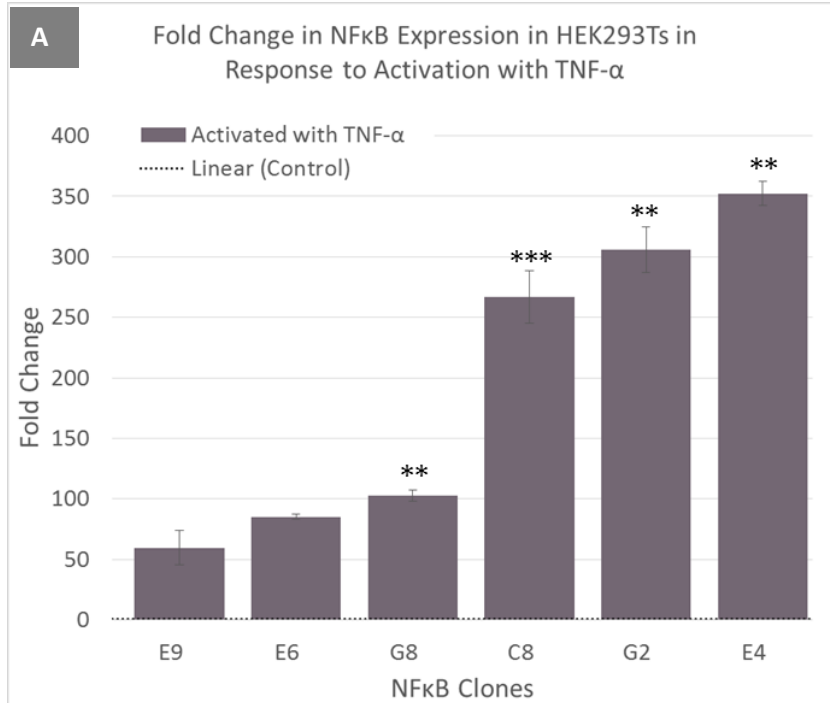
Figure 30. Clonal Population of HEK293Ts Transduced with NFκB TFAR Activated with TNF-α. A). Graph displaying activation of clonal populations integrated with the TFAR for NFκB with the known agonist TNF-α. Clonal populations integrated with the TFAR for NFκB were activated with the known agonist TNF-α. On activation, clone C8 displayed the most significant increase in luciferase expression relative to its control (p<0.001). However, GFP expression data did not correlate, so this clone was excluded. Clone G2 displayed significant increase in luciferase on addition of TNF-α (p=0.006) along with increased GFP expression. Therefore clone G2 was selected. Fold change results were attained using Luciferase Luminometry data. For all p-values: p*<0.05, p**<0.01, and p***<0.001. Bi.) Phase-contrast images displaying selected NFκB TFAR transduced clone G2 treated with the vehicle control. Bii). Corresponding GFP images. Ci.) Phase-contrast images displaying selected NFκB TFAR transduced clone G2 treated with 10ng/ml TNF-α for 16 hours. Cii.) Corresponding GFP images. All images were taken at 20X magnification using Leica Live Cell Imaging System. Scale bar 50µm.
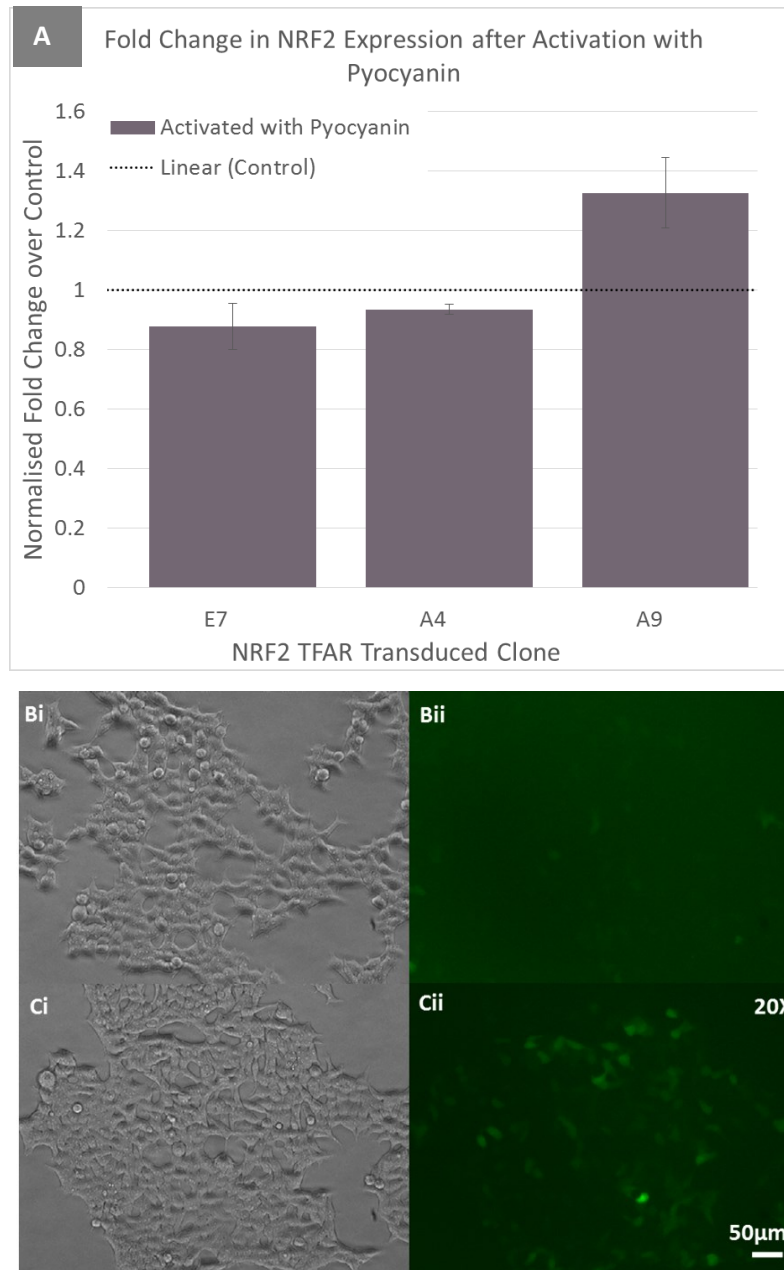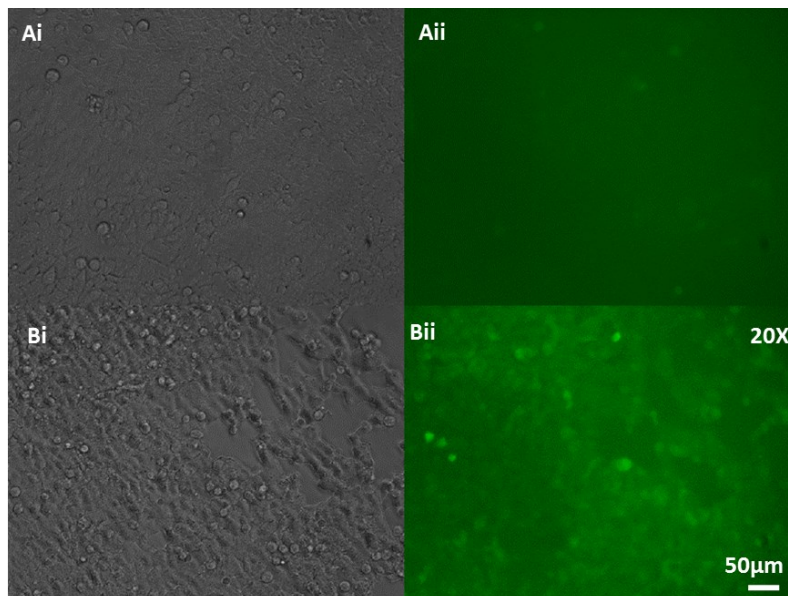

Figure 31. Clonal Population of HEK293Ts Transduced with TFEB TFAR Activated by Torin1. Ai.) Phase-contrast images displaying selected TFEB TFAR transduced clone G6 treated with the vehicle control. Aii). Corresponding GFP images. Bi.) Phase-contrast images displaying selected TFEB TFAR transduced clone G6 treated with Torin1 for 24 hours. Bii.) Corresponding GFP images. On activation, clone G6 displayed the greatest increase in GFP relative to its control. All images were taken at 20X magnification using Leica Live Cell Imaging System. Scale bar 50µm.

4.8 Model for drug screening

The clonal TFAR-HEK293T cell line panel was provisionally evaluated for responses to a pro-inflammatory cytokine (TNF-α), a cytokine-mediated phorbol ester (PMA) that acts as a PKC activator and a GSK-3β inhibitor (LiCl$_2$). HEK293Ts containing TFAR were plated in triplicate in a 24-well plate. One 24-well plate acted as a control and to the other plate, agonist was added. TF expression in response to pharmacological stimulation was quantified by luciferase luminometry and used to investigate TF modulation (Figure 28).
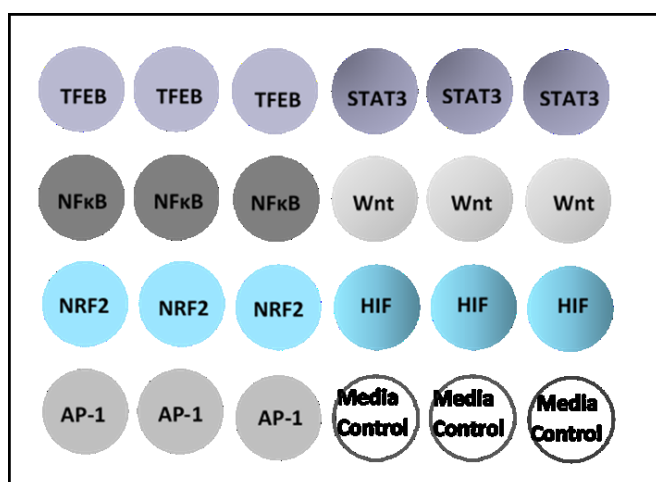
Figure 32. Representative formatting of the clonal TFAR integrated cell based drug screening model.

The clonal TFAR-HEK293T cell line panel was treated with 10ng/ml TNF-α for 16 hours for validation of the model. The clonal line transduced with the NFκB TFAR was used as a positive control. Results displayed in Figure 33. Indicate that TNF-α significantly upregulated gene expression of NFκB (p=0.006), STAT3, TCF/LEF (Wnt signalling) (p=0.039), NRF2 (p=0.002), TFEB (0.019), AP-1 (p<0.001) and HIF (0.037).

The clonal TFAR-HEK293T cell line panel was also used to investigate molecular response to pharmacological stimulation with known compounds. The panel was treated with 10ng/ml phorbol 12-myristate 13-acetate (PMA) for 16 hours. The clonal line transduced with the AP-1 TFAR was used as a positive control. Results displayed in Figure 34. indicate that PMA significantly upregulated gene expression of AP-1 (p=0.003), STAT3 (p=0.025), HIF (p=0.05), NFκB (p=0.004) and NRF2 (0.005).

The panel was then treated with 50mM Lithium Chloride (LiCl$_2$) for 3 days. The clonal line transduced with the TCF/LEF (Wnt signalling) TFAR was used as a positive control. Results displayed in Figure 35 indicate that LiCl$_2$ significantly upregulated gene expression of TFC/LEF (Wnt signalling) (p=0.034), TFEB (p=0.016), AP-1 (p=0.006) and STAT3 (p=0.024). LiCl2 significantly downregulated HIF gene expression (p=0.003). Changes in gene expression were quantified using luciferase luminometry and fluorescence microscopy. All results were normalised using VLuc and expressed as a fold change in activation from their individual control. Supporting GFP images are displayed in Appendix: (Figures 39-59).

Fully quantitative luciferase luminometry data showed that all three factors activated the predicted canonical cell signalling pathways (NFκB, AP-1 and TCF/LEF (Wnt signalling) respectively) but also activated non-canonical pathways. Results were broadly consistent with current literature, demonstrating that the clonal TFAR transduced cell based model could be a valuable first stage platform for evaluating newly synthesised drugs or screening drug libraries. The TFAR integrated cell based drug-screening model was further validated to test known agonists for off target effects.
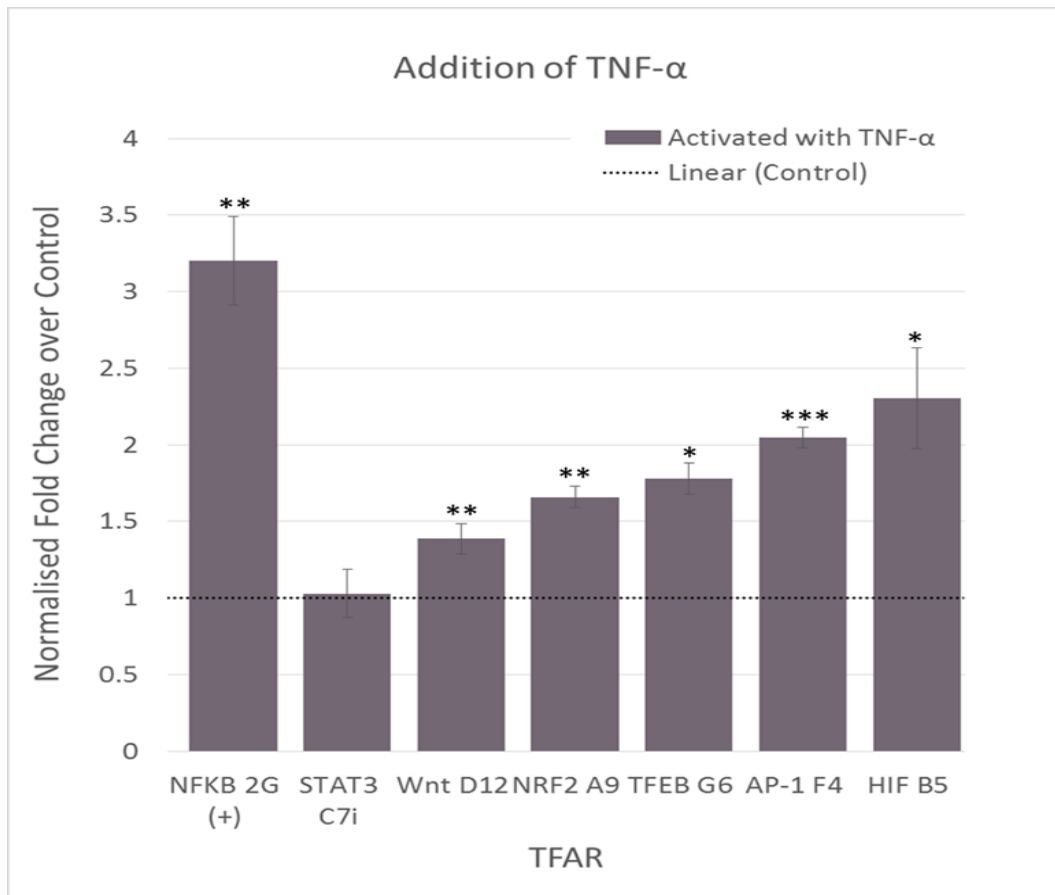
Figure 33. Validation of Cell Screening Model with TNF-α. Clonal HEK293Ts integrated with the TFAR for NFκB, STAT3, TCF/LEF (Wnt signalling), NRF2, TFEB, AP-1, HIF were treated with TNF-α. On activation with TNF-α, expression of NFκB was significantly increased (p=0.006), as was TCF/LEF (Wnt signalling) (p=0.039), NRF2 (p=0.002), TFEB (0.019), AP-1 (p<0.001) and HIF (0.037). STAT3 was also upregulated on addition of TNF-α. Fold change results were produced using Luciferase Luminometry data. For all p-values: p*<0.05, p**<0.01, and p***<0.001.

Figure 34. Addition of LiCl$_2$ for investigation of off-target effects. Clonal HEK293Ts integrated with the TFAR for NFκB, STAT3, TCF/LEF (Wnt signalling), NRF2, TFEB, AP-1, HIF were treated with LiCl$_2$. The positive control, TCF/LEF (Wnt signalling) was significantly upregulated by addition of LiCl$_2$ (p=0.034). Clonal NFκB was upregulated by LiCl$_2$ addition, but results were not significant. Clonal TFEB was upregulated by LiCl$_2$ (p=0.016) as were clonal AP-1 (p=0.006) and STAT3 (p=0.024). Clonal HIF displayed significant downregulation of gene expression on addition of LiCl$_2$ (p=0.003). For all p-values: p*<0.05, p**<0.01, and p***<0.001.

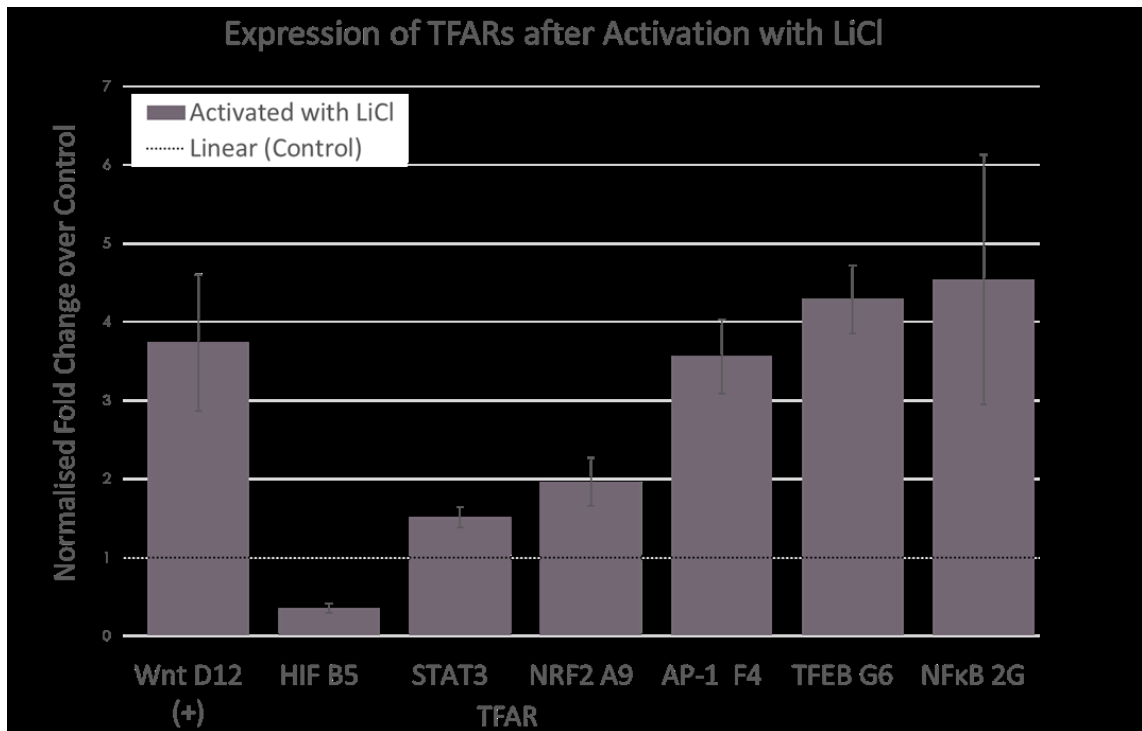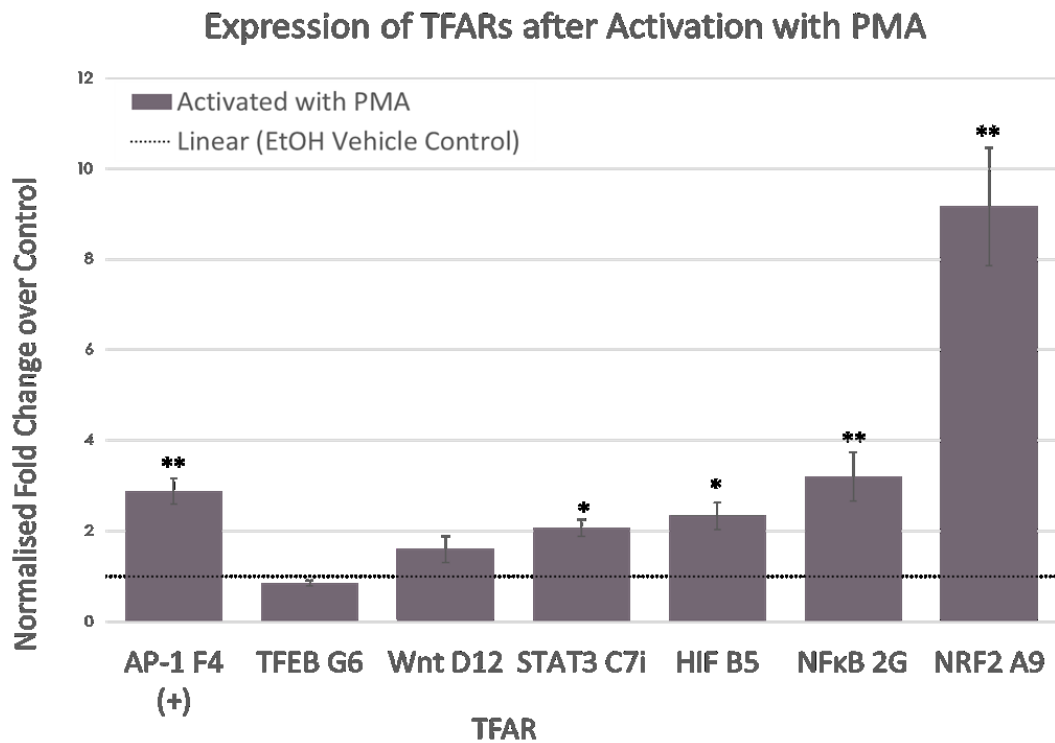**Figure 35. Addition of PMA for investigation of off-target effects.** Clonal HEK293Ts integrated with the TFAR for NFκB, STAT3, TCF/LEF (Wnt signalling), NRF2, TFEB, AP-1, HIF were treated with PMA. The positive control AP-1 was significantly upregulated by PMA (p=0.003), as were STAT3 (p=0.025), HIF (p=0.05), NFκB (p=0.004) and NRF2 (0.005). For all p-values: p*<0.05, p**<0.01, and p***<0.001.

5.0 Discussion

The aim of this project was to utilise lentiviral vectorology techniques to generate a clonal TFAR-HEK293T cell line panel model amenable to applications such as drug screening. TFAR constructs were generated and provided by the McKay Lab (Buckley *et al.,* 2015). These constructs contained a TFBM upstream of a minimal promoter (Figure 9.) TF binding to the specific TFBM initiated gene expression of associated NLuc and GFP genes in a dose responsive manner (Table 1. and Table 2.). HEK293T cells were co-transduced with the TFAR constructs and a lentiviral cassette consisting of a constitutively active promoter driving expression of secreted VLuc (Appendix: Figure 37.) Transduction was achieved using low concentrations of lentiviral vector for single lentiviral integration of each construct within target HEK293T cells. The panel was validated using known TF agonists for activation of each TFAR. NLuc measurements were taken from conditioned media and used to determine gene response to pharmacological stimulation. Results were normalised using VLuc values which were taken from the same conditioned media. Results were all displayed as a fold change from their individual control. The panel was then provisionally used to detect and measure off-target drug effects.

My results indicate successful development of a robust first line TFAR cell screening model which is fully quantified and able to produce significant results that are broadly consistent with current literature. The cell-screening model consists of clonal cell lines transduced with TFAR gene constructs for AP-1, NRF2, NFκB, HIF, STAT3, TCF/LEF (Wnt signalling) and TFEB.

TNF-α is a proinflammatory cytokine (Umare *et al.,* 2014). Many of the TFs investigated in the TFAR cell-screening model are known to be modulated during inflammation, (Ren and Hu., 2017), (Vion *et al.,* 2017), (Shanmugam *et al.,* 2016), (Lin *et al.,* 2016), (Sharma *et al.,* 2017), (Miscia *et al.,* 2002), TNF-α was therefore selected to validate the model. TNF-α is a well-defined NFκB agonist (Wu and Zhou, 2010) that binds to cell surface receptors to induce canonical NFκB signalling, NFκB was therefore used as the positive control for this experiment. Results showed TNF-α significantly increased activation of

the NFκB TFAR (p=0.006) as expected. TNF-α also significantly (p=0.039) upregulated Wnt signalling pathways (TCF/LEF TF activation). The Wnt/β-catenin pathway is involved in regulating inflammation in various diseases and there exists a crosstalk between NFκB and Wnt signalling pathways during inflammation. Sharma *et al.,* (2017) used the small molecule iCRT3 to inhibit Wnt signalling by binding to β-catenin. This blocked interactions between β-catenin and TCF and led to a reduction in TNF-α concentration. Ma and Hottiger, (2016) proposed that in tumour cells, macrophages release TNF-α which is able to activate β-catenin through GSK-3β and Akt signalling and promote tumour cell proliferation. NRF2 was shown to be significantly upregulated (p=0.002) in HEK293Ts after addition of TNF-α. Shanmugam *et al.,* (2016) described the complex interactions between NRF2 and TNF-α signalling, reporting that lower concentrations of TNF-α (2-5ng/ml) induced NRF2 nuclear translocation, increased DNA binding and transactivation of TF targets. However, increasing TNF-α concentration above 10ng/ml resulted in suppression of KEAP1/NRF2 signalling. This indicates concentration dependency in NRF2-TNF-α signalling.
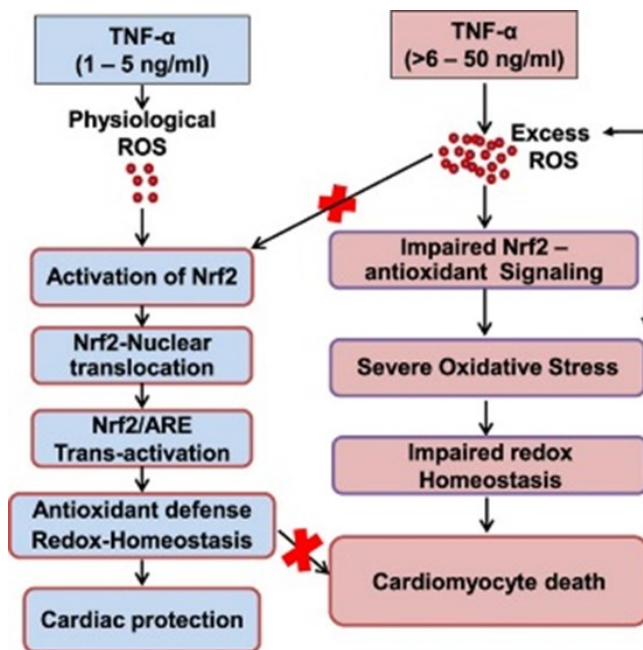

Figure 36. Schematic diagram showing potential NRF2 activation pathways in response to TNF-α (Shanmugam *et al.,* 2016).

Addition of TNF-α to HEK293Ts was shown to significantly upregulate cellular expression of the transcription factor TFEB (p=0.019). TNF-α induced TFEB activation is supported by Vion *et al.,* (2017) who reported that in the endothelium, a deficiency in autophagy promotes TNF-α induced inflammation. Brady *et al.,* (2017) described the autophagy-lysosome pathway as a key player in regulation of the inflammatory response and Uchida *et al.,* (2014) reported that in RC4 cells, expression of autophagy-related proteins was upregulated in the cornea after treatment with TNF-α. Treatment of HEK293Ts with TNF-α was shown to significantly upregulate expression of AP-1 (p<0.001). This result is supported by Westwick *et al.,* (1994) who determined that TNF-α prolonged activation of the c-jun kinase. Lin *et al.,* (2016) also described that c-jun N-terminal kinases (JNKs), extracellular signal-related kinases (ERKs) and p38s may be activated on stimulation with TNF-α via MAPK stimulation of AP-1. Gene expression of the HIF TF was significantly increased (p=0.037) on stimulation with TNF-α. TNF-α induced HIF-1 activation is supported by Ren and Hu., (2017) who found that chronic intermittent hypoxia (CIH) is positively associated with TNF-α, indicating that HIF-1α is upregulated by TNF-α. STAT3 gene expression was not significantly modulated by addition of TNF-α. Miscia *et al.,* (2002) reported that TNF-α activates Jak1/Stat3-Stat5B signaling through TNFR-1 in human B cells.

The clonal TFAR cell screening model was also used to investigate the off-target effects which may be produced on addition of a known pharmacological compound, for these experiments, the compounds used were Phorbol 12-myristate 13-acetate (PMA), a PKC activator and Lithium Chloride ($LiCl_2$), a GSK-3β specific kinase inhibitor. PMA and $LiCl_2$ are known agonists of AP-1 and Wnt signalling respectively, and were selected based on current literature due to their association with a vast range of cell signalling pathways. As AP-1 is known to be activated by PMA, it was used as a positive control (Colin *et al.,* 2011). Clonal HEK293T cells transduced with the AP-1 TFAR were activated with 10ng/ml PMA for 21 hours and displayed a statistically significant (P=0.003) increase in activation. Colin *et al.,* (2011) examined the intragenic region of HIV-1 for binding sites for TFs which can be induced by PMA (these included NF-κB, AP-1, AP-2 and AP-4). Clonal HEK293T cells transduced with the NRF2 TFAR were activated with 10ng/ml PMA for 21

hours and displayed a statistically significant (P=0.005) increase in activation. PMA induced NRF2 activation is supported by Zhang *et al.,* (2013), who reported increased NRF2 phosphorylation and ARE transcriptional activity on addition of PMA to HepG2 cells. Clonal HEK293T cells transduced with the NFκB TFAR were activated with 10ng/ml PMA for 21 hours and displayed a statistically significant (P=0.004) increase in activation. PMA induced NFκB activation is supported by Debelec-Butuner *et al.,* (2012) who reported a significant increase in levels of TNF-α on addition of PMA in U937 cells. Increased TNF-α leads to increased NFκB nuclear translocation (Wang *et al.,* 2013). Clonal HEK293 cells transduced with the HIF TFAR were activated with 10ng/ml PMA for 21 hours and displayed a statistically significant (P=0.050) increase in activation. PMA induced HIF activation is supported by Jung *et al.,* (2003) who noted that PMA induced increased expression of HIF-1α in normoxic cells. Clonal HEK293 cells transduced with the STAT3 TFAR were activated with 10ng/ml PMA for 21 hours and displayed a statistically significant (P=0.025) increase in activation. PMA induced STAT3 activation is supported by Kwon *et al.,* (2013) who reported PMA induced upregulation of STAT3 mRNA. Clonal HEK293 cells transduced with the TCF/LEF (Wnt signalling) TFAR were activated with 10ng/ml PMA for 21 hours and displayed an increase in activation. Seo *et al.,* (2016) described increased phosphorylation and thus inactivation of GSK3β on addition of PMA. Inhibition of GSK3β leads to increased Wnt signalling. Clonal HEK293 cells transduced with the TFEB TFAR were activated with 10ng/ml PMA for 21 hours and displayed downregulated protein expression on addition of PMA. Seo *et al.,* 2016 described PMA as an activator of PKC. Li *et al.,* (2015) describes that activation of PKC causes inactivation of GSK3β, which reduces phosphorylation, nuclear translocation and activation of TFEB, this indicates that PMA is expected to downregulate expression of TFEB, which correlates with the data achieved.

Wnt signalling pathways are known to be activated by $LiCl_2$, so the TFAR for TCF/LEF (Wnt signalling) was used as a positive control. Clonal HEK293 cells transduced with the TCF/LEF TFAR were activated with 50mM $LiCl_2$ for 3 days and displayed a statistically significant (p=0.034) increase in activation. This is supported by Galli *et al.,* (2013) who reported that $LiCl_2$ treatment induced TCF/LEF activation and expression of Wnt signalling markers in C2C12 cells on modSLA. Furthermore, Xia *et al.,* (2017) reported

increased Wnt/β-catenin signalling on addition of $LiCl_2$, which was activated through inhibition of GSK3β in the auditory cortex. Clonal HEK293 cells transduced with the NRF2 TFAR were activated with 50mM $LiCl_2$ for 3 days and displayed a statistically significant (p=0.033) increase in activation. Chen *et al.,* (2016) used $LiCl_2$ to inhibit GSK-3β *in vitro* and *in vivo* and described increased expression of nuclear and total NRF2, of NRF2-ARE binding activity and of NRF2/ARE pathway-driven gene expression. Chen *et al.,* (2016) also showed that overexpression of GSK-3β decreases NRF2 expression and the NRF2/ARE pathway in cerebral ischemia. Clonal HEK293 cells transduced with the AP-1 TFAR were activated with 50mM $LiCl_2$ for 3 days, and displayed a significant increase in activation (p=0.006). This is supported by Kwon *et al.,* (2008) who reported that $LiCl_2$ induced expression of Fra-2 and c-Fos in the amygdala. Clonal HEK293 cells transduced with the STAT3 TFAR were activated with 50mM $LiCl_2$ for 3 days and displayed a significant (p=0.024) increase in activation. Interactions between $LiCl_2$ and STAT3 differed in literature: Lim *et al.,* (2008) described that knock down of GSK3-β reduced activation of STAT3. $LiCl_2$ is a GSK3-β inhibitor and may reduce activation of STAT3. However, $LiCl_2$ upregulates Wnt/beta-catenin pathways which are interlinked with STAT3 signalling. Beurel and Jope., (2009) and Hao *et al.,* (2006) reported that Wnt3a upregulated STAT3 activation and nuclear translocation and that reducing STAT3 levels with siRNA eliminated Wnt3a related development and protection from oxidative stress. Clonal HEK293 cells transduced with the NFκB TFAR were activated with 50mM $LiCl_2$ for 3 days and displayed a significant (p=0.018) increase in activation. NFκB activation by $LiCl_2$ is supported by Chang *et al.,* (2013) who reported that inhibiting GSK-3β downregulated activation of NFκB and thus production of TNF-α in GAS-Infected RAW 264.7 Cells. $LiCl_2$ is an inhibitor of GSK-3β. Clonal HEK293 cells transduced with the HIF TFAR were activated with 50mM $LiCl_2$ for 3 days and displayed significant downregulation of HIF gene activation (p=0.003). GSK-3β has been shown to inhibit activation of HIF-1α transcription in hepatoma cells (Zhou *et al.,* 2012). Ko *et al.,* (2013) reported that inactivation of GSK-3β by hypoxia in gastric cancer cells contributes to accumulation of HIF-1α at translational but not transcriptional or post-translational levels. HIF and GSK-3β signalling may therefore be cell-type dependant (Ko *et al.,* 2013). Clonal HEK293 cells transduced with the TFEB TFAR were activated with 50mM $LiCl_2$ for 3 days. TFEB was significantly upregulated (p=0.016) by $LiCl_2$ as shown by the results

from Luciferase Luminometry. LiCl$_2$ activation of TFEB is supported by Parr *et al.,* (2012) who described that in N2a cells, inhibition of GSK-3β led to upregulation of TFEB nuclear translocation and autophagy.

The clonal TFAR-HEK293T cell line panel model is amenable to high throughput drug testing, is low cost to develop and use and produces reproducible results as it employs clonal cell lines. It also enables rapid identification of molecular pathways modulated and can improve understanding of interactions between molecular pathways. It therefore is advantageous as a drug screening model. The clonal TFAR model also displays advantages above other methods of measuring cell signalling and other reporter constructs as it uses secreted NLuc which can be collected at multiple time points and measured using conditioned media, thus enabling repeated measurements. NLuc is also smaller than other luciferases such as Luc and has a brighter luminescence intensity. On activation, the clonal TFAR-HEK293T cell line panel model also produces GFP to give two non-overlapping dual measures of gene expression. Limitations of the clonal TFAR-HEK293T cell line panel model are primarily related to the lentiviral vector used to deliver the TFAR gene construct to host cells, as lentiviruses are randomly integrating and immunogenic. Random integration of the TFAR construct has the potential to result in abhorrent protein expression and cancer. Furthermore, the exact number of viral integrations within each clonal cell line is unknown.

6.0 Future Work

To resolve concerns over TFAR integration sites within HEK293T cells, the genome of each clonal cell line will be sequenced and the site of TFAR insertion determined. This will clarify that insertions are within a section of the genome that doesn't lead to cancer-causing effects and will also enable determination of the number of viral integrations within each cell line. The clonal TFAR-HEK293T cell line panel model will also be used in collaboration with Dr. Ahad Rahim, UCL School of Pharmacy for screening of a candidate suitable for drug repurposing. Exendin-4 (Ex-4) is a short peptide GLP-1 analogue used in treatment of diabetes for upregulation of insulin secretion (Darsalia *et al.* 2014). Ex-4 has been shown to provide protective effects against acute brain injury after stroke and hypoxic/ischemic encephalopathy (HIE) (Chen *et al.* 2016). The precise mechanisms by

which this neuroprotection occurs are unclear thus may be studied using the clonal TFAR-HEK293T cell line panel model. Further work may also include transduction of a range of cell types with the TFAR construct, for example neural progenitor cells (NPCs) may be transduced with the TFAR constructs and used to measure fluctuation of TFs during neural differentiation.

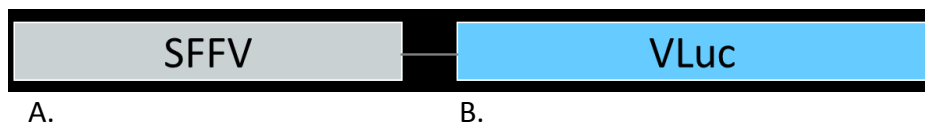## 7.0 Appendix

Figure 37. Representation of VLuc Gene construct consisting of A.) A Constitutively active control promoter, B.) The gene for secreted VLuc.

TFAR	Clone Selected
NFκB	G2
HIF	B5
TCF/LEF (Wnt)	D12
AP-1	F4
STAT3	C7i
NRF2	A9
TFEB	G6

Figure 38. Selected clonal populations transduced with the TFAR construct of choice.

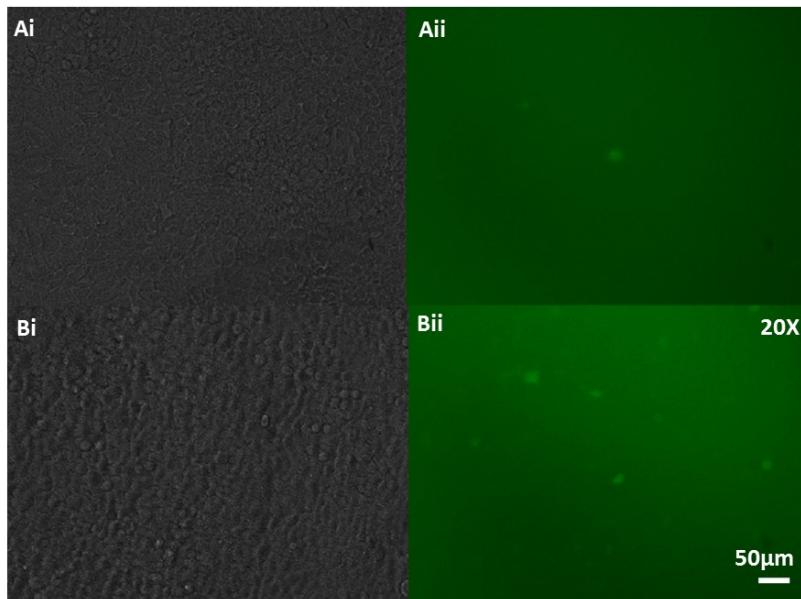# 7.1 Validation of cell screening model with TNF-α (GFP images)

Figure 39. Treatment of Clonal NFκB (G2) with TNF-α. Ai). Phase-contrast images of NFκB transduced clone G2 treated with the vehicle control. Aii). Correlating GFP images. Bi.)). Phase-contrast images of NFκB transduced clone G2 treated with TNF-α (10ng/ml, 16hrs). Bii). Correlating GFP images. GFP images displayed upregulated expression of NFκB on addition of TNF-α The NFκB TFAR was used as a positive control. All images were taken at 20X magnification using Leica Live Cell Imaging System. Scale bar 50µm.
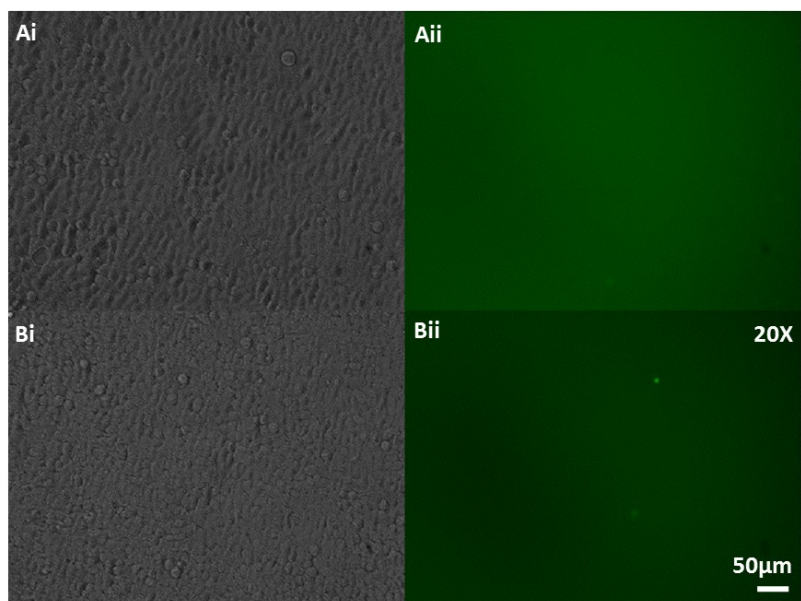

Figure 40. Treatment of Clonal AP-1 (F4) with TNF-α. Ai). Phase-contrast images of AP-1 transduced clone A9 treated with the vehicle control. Aii). Correlating GFP images. Bi.) Phase-contrast images of

AP-1 transduced clone G2 treated with TNF-α (10ng/ml, 16hrs). Bii). Correlating GFP images. GFP images did not display upregulated expression of AP-1 on addition of TNF-α. All images were taken at 20X magnification using Leica Live Cell Imaging System. Scale bar 50µm.

Figure 41. Treatment of Clonal HIF (B5) with TNF-α. Ai). Phase-contrast images of HIF transduced clone B5 treated with the vehicle control. Aii). Correlating GFP images. Bi.) Phase-contrast images of HIF transduced clone B5 treated with TNF-α (10ng/ml, 16hrs). Bii). Correlating GFP images. GFP images did not display clear upregulated expression of HIF on addition of TNF-α. All images were taken at 20X magnification using Leica Live Cell Imaging System. Scale bar 50µm.

Figure 42. Treatment of Clonal TFEB (G6) with TNF-α. Ai). Phase-contrast images of TFEB transduced clone G6 treated with the vehicle control. Aii). Correlating GFP images. Bi.) Phase-contrast images of TFEB transduced clone G6 treated with TNF-α (10ng/ml, 16hrs). Bii). Correlating GFP images. GFP images did not display clear upregulated expression of TFEB on addition of TNF-α. All images were taken at 20X magnification using Leica Live Cell Imaging System. Scale bar 50μm.
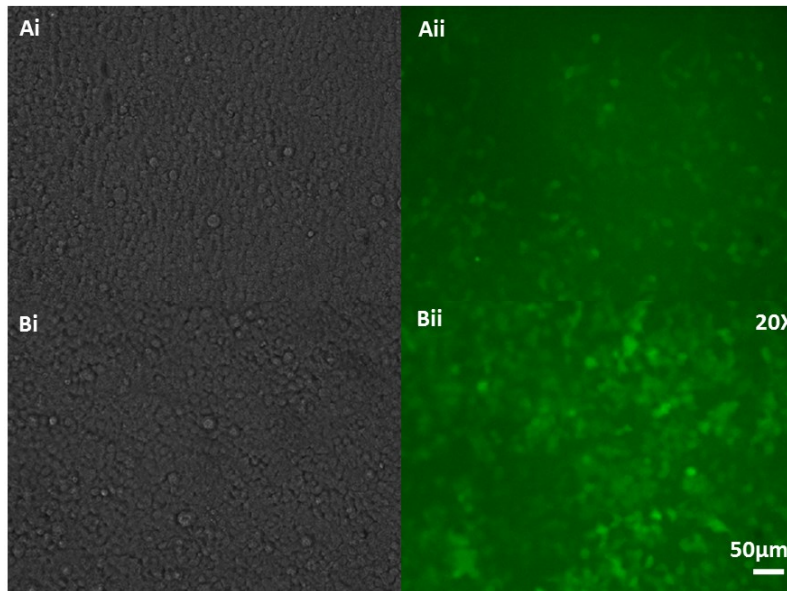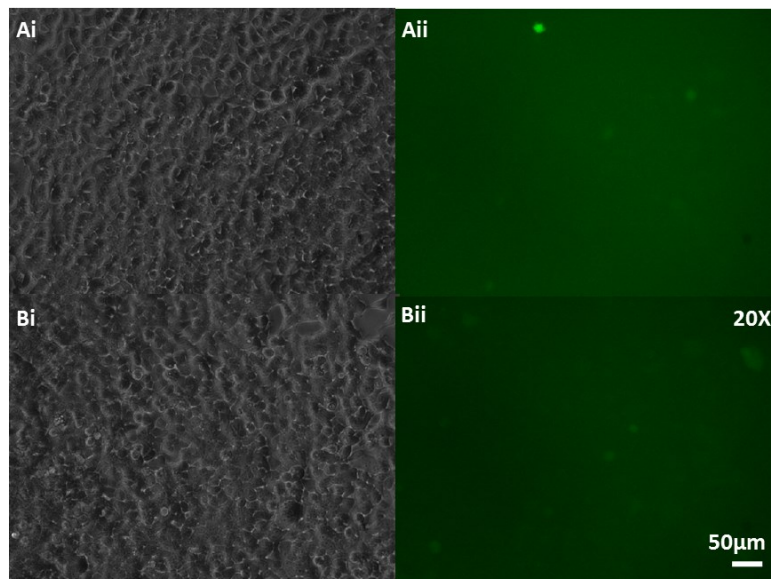

Figure 43. Treatment of Clonal STAT3 (C7i) with TNF-α. Ai). Phase-contrast images of STAT3 transduced clone C7i treated with the vehicle control. Aii). Correlating GFP images. Bi.) Phase-contrast images of STAT3 transduced clone C7i treated with TNF-α (10ng/ml, 16hrs). Bii). Correlating GFP images. GFP images did not display clear upregulated expression of TFEB on addition of TNF-α. All images were taken at 20X magnification using Leica Live Cell Imaging System. Scale bar 50μm.

Figure 44. Treatment of Clonal TCF/LEF (D12) with TNF-α. Ai). Phase-contrast images of TCF/LEF (Wnt signalling) transduced clone D12 treated with the vehicle control. Aii). Correlating GFP images. Bi.) Phase-contrast images of TCF/LEF (Wnt signalling) TFAR transduced clone D12 treated with TNF-α (10ng/ml, 16hrs). Bii). Correlating GFP images. GFP images did not display clear upregulated expression of TCF/LEF (wnt signalling) on addition of TNF-α. All images were taken at 20X magnification using Leica Live Cell Imaging System. Scale bar 50μm.

Figure 45. Treatment of Clonal NRF2 (A9) with TNF-α. Ai). Phase-contrast images of NRF2 TFAR transduced clone A9 treated with the vehicle control. Aii). Correlating GFP images. Bi.) Phase-contrast images of NRF2 clone A9 treated with TNF-α (10ng/ml, 16hrs). Bii). Correlating GFP images. GFP images did not display clear upregulated

expression of NRF2 on addition of TNF-α. All images were taken at 20X magnification using Leica Live Cell Imaging System. Scale bar 50µm.
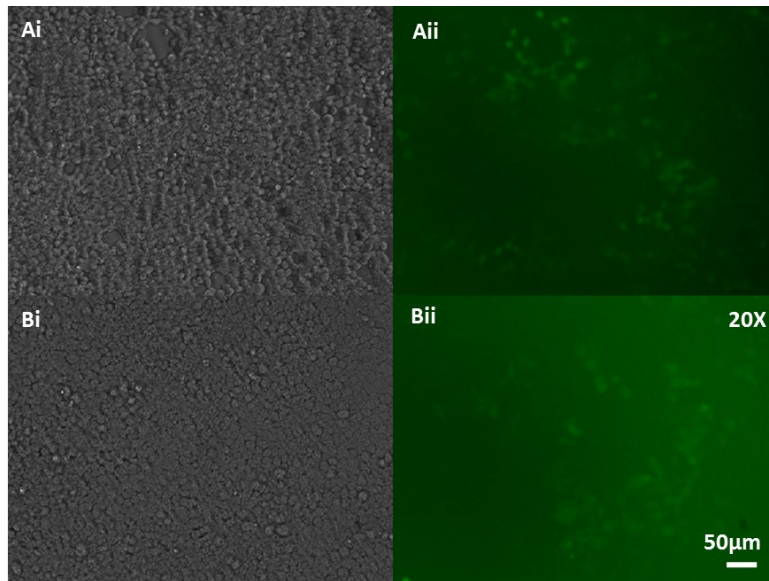
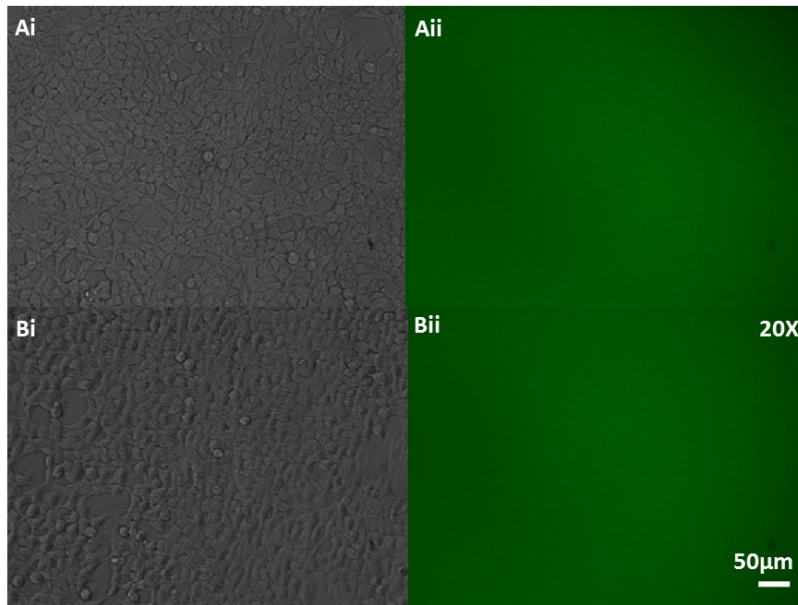## 7.2 Model for drug testing: LiCl2 (GFP images)
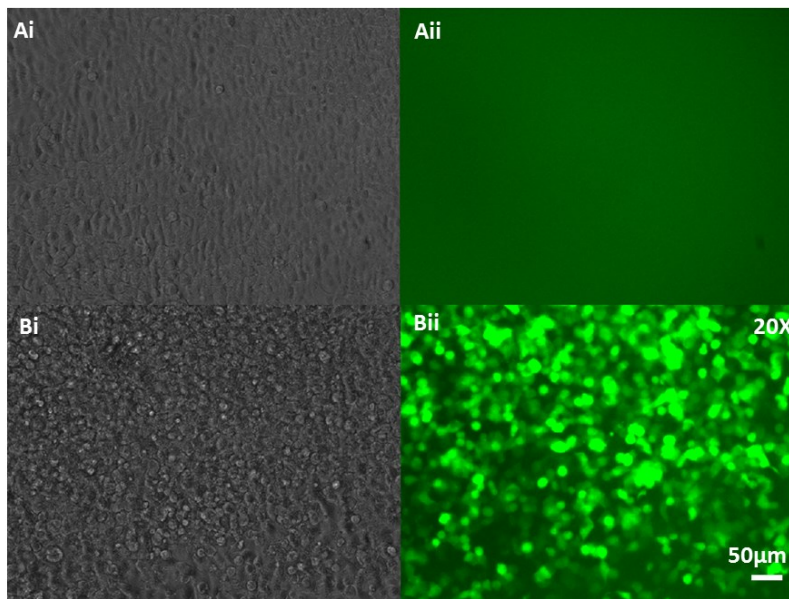
Figure 46. Treatment of Clonal TCF/LEF (D12) with LiCl2. Ai). Phase-contrast images of TCF/LEF (Wnt signalling) transduced clone D12 treated with the vehicle control. Aii). Correlating GFP images. Bi.) Phase-contrast images of TCF/LEF (Wnt signalling) TFAR transduced clone D12 treated with 50mM $LiCl_2$ (48 hours). Bii). Correlating GFP images. GFP images displayed clear upregulated expression of TCF/LEF (Wnt signalling) on addition of $LiCl_2$. All images were taken at 20X magnification using Leica Live Cell Imaging System. Scale bar 50µm.
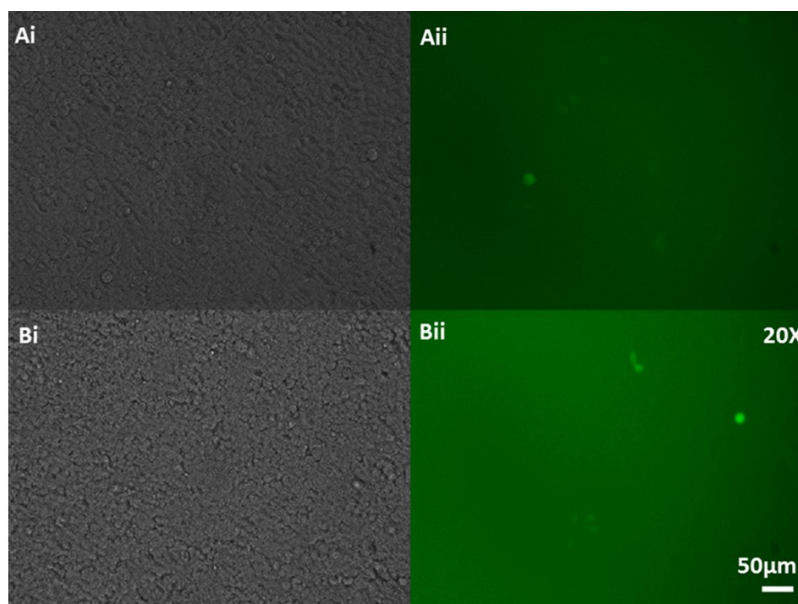
Figure 47. Treatment of Clonal HIF (B5) with LiCl2. Ai). Phase-contrast images of HIF transduced clone B5 treated with the vehicle control. Aii). Correlating GFP images. Bi.) Phase-contrast images of HIF TFAR transduced clone B5 treated with 50mM $LiCl_2$ (48 hours). Bii). Correlating GFP images. GFP images displayed clear upregulated expression of HIF on addition of $LiCl_2$. All images were taken at 20X magnification using Leica Live Cell Imaging System. Scale bar 50μm.

Figure 48. Treatment of Clonal STAT3 (C7i) with LiCl2. Ai). Phase-contrast images of STAT3 transduced clone C7i treated with the vehicle control. Aii). Correlating GFP images. Bi.) Phase-contrast images of

STAT3 TFAR transduced clone C7i treated with 50mM LiCl$_2$ (48 hours). Bii). Correlating GFP images. GFP images displayed clear upregulated expression of STAT3 on addition of LiCl$_2$. All images were taken at 20X magnification using Leica Live Cell Imaging System. Scale bar 50µm.

Figure 49. Treatment of Clonal NRF2 (A9) with LiCl2. Ai). Phase-contrast images of NRF2 transduced clone A9 treated with the vehicle control. Aii). Correlating GFP images. Bi.) Phase-contrast images of NRF2 TFAR transduced clone A9 treated with 50mM LiCl$_2$ (48 hours). Bii). Correlating GFP images. GFP images displayed clear upregulated expression of NRF2 on addition of LiCl$_2$. All images were taken at 20X magnification using Leica Live Cell Imaging System. Scale bar 50µm.
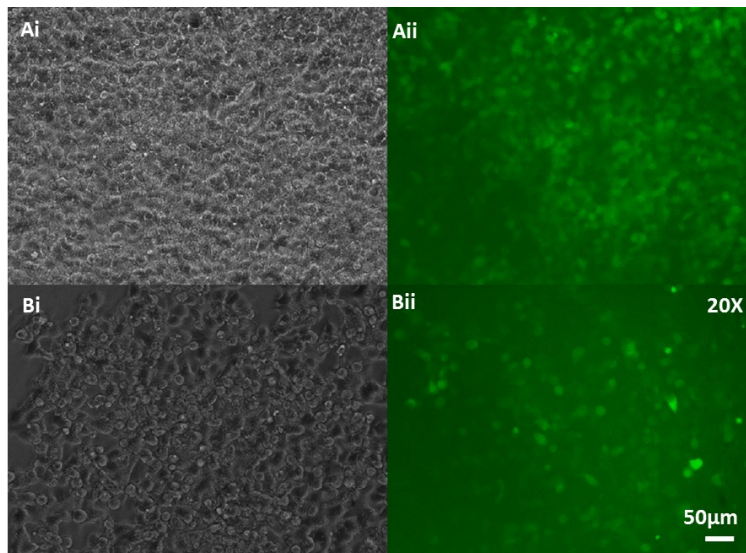
Figure 50. Treatment of Clonal AP-1 (F4) with LiCl2. Ai). Phase-contrast images of AP-1 transduced clone F4 treated with the vehicle control. Aii). Correlating GFP images. Bi.) Phase-contrast images of AP-1 TFAR transduced clone F4 treated with 50mM $LiCl_2$ (48 hours). Bii). Correlating GFP images. GFP images displayed clear upregulated expression of AP-1 on addition of $LiCl_2$. All images were taken at 20X magnification using Leica Live Cell Imaging System. Scale bar 50μm.
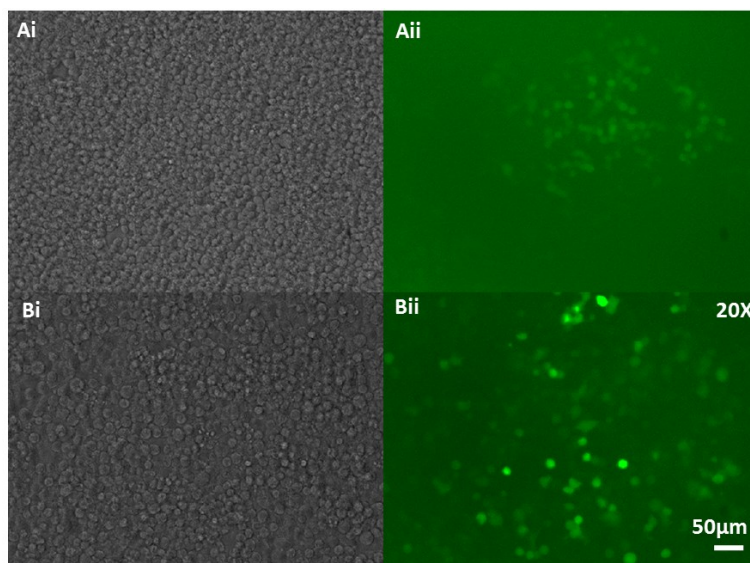

Figure 51. Treatment of Clonal TFEB (G6) with LiCl2. Ai). Phase-contrast images of TFEB transduced clone G6 treated with the vehicle control. Aii). Correlating GFP images. Bi.) Phase-contrast images of TFEB TFAR transduced clone G6 treated with 50mM $LiCl_2$ (48 hours). Bii). Correlating GFP images. GFP images displayed clear upregulated expression of TFEB on addition of $LiCl_2$. All images were taken at 20X magnification using Leica Live Cell Imaging System. Scale bar 50μm.

Figure 52. Treatment of Clonal NFκB (G2) with LiCl2. Ai). Phase-contrast images of NFκB transduced clone G2 treated with the vehicle control. Aii). Correlating GFP images. Bi.) Phase-contrast images of NFκB TFAR transduced clone G2 treated with 50mM $LiCl_2$ (48 hours). Bii). Correlating GFP images. GFP images displayed clear upregulated expression of NFκB on addition of $LiCl_2$. All images were taken at 20X magnification using Leica Live Cell Imaging System. Scale bar 50μm.
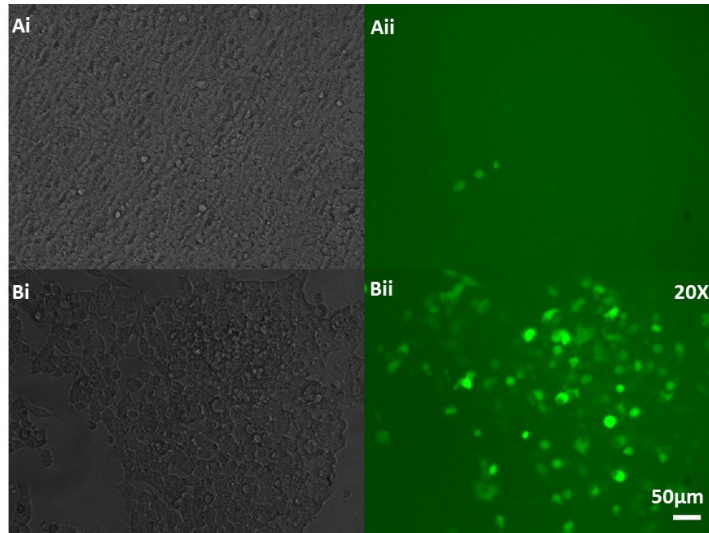
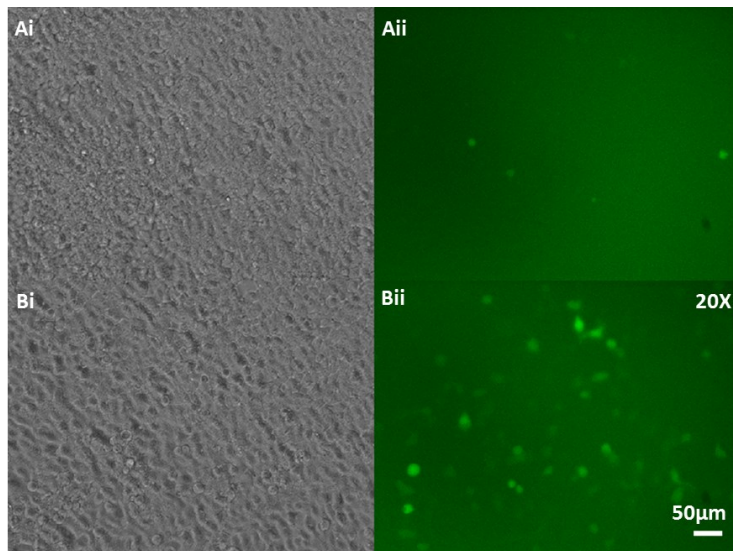## 7.3 Model for drug testing: PMA (GFP images)

Figure 53. Treatment of Clonal AP-1 (F4) with PMA. Ai). Phase-contrast images of AP-1 transduced clone F4 treated with the vehicle control. Aii). Correlating GFP images. Bi.) Phase-contrast images of AP-1 TFAR transduced clone F4 treated with 10ng/ml PMA (21 hrs). Bii). Correlating GFP images. GFP images displayed clear upregulated expression of AP-1 on addition of PMA. All images were taken at 20X magnification using Leica Live Cell Imaging System. Scale bar 50μm.
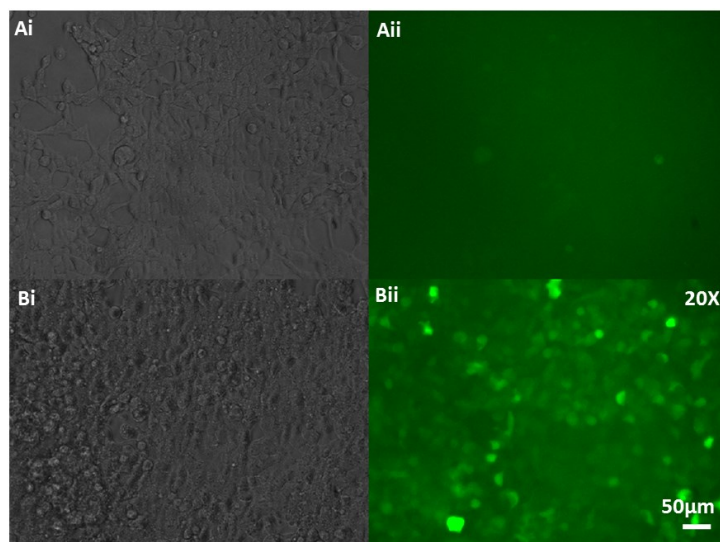
Figure 54. Treatment of Clonal TFEB (G6) with PMA. Ai). Phase-contrast images of TFEB transduced clone G6 treated with the vehicle control. Aii). Correlating GFP images. Bi.) Phase-contrast images of TFEB TFAR transduced clone G6 treated with 10ng/ml PMA (21 hrs). Bii). Correlating GFP images. GFP images displayed upregulated expression of TFEB on addition of PMA. All images were taken at 20X magnification using Leica Live Cell Imaging System. Scale bar 50µm.
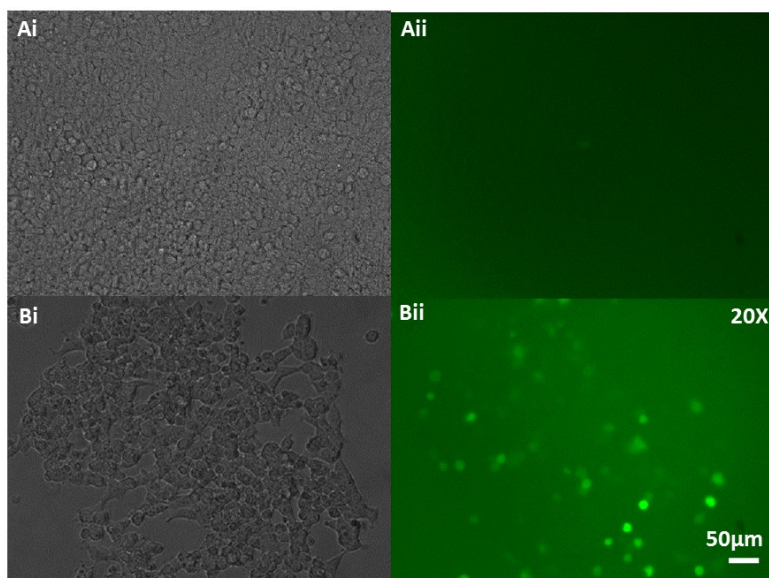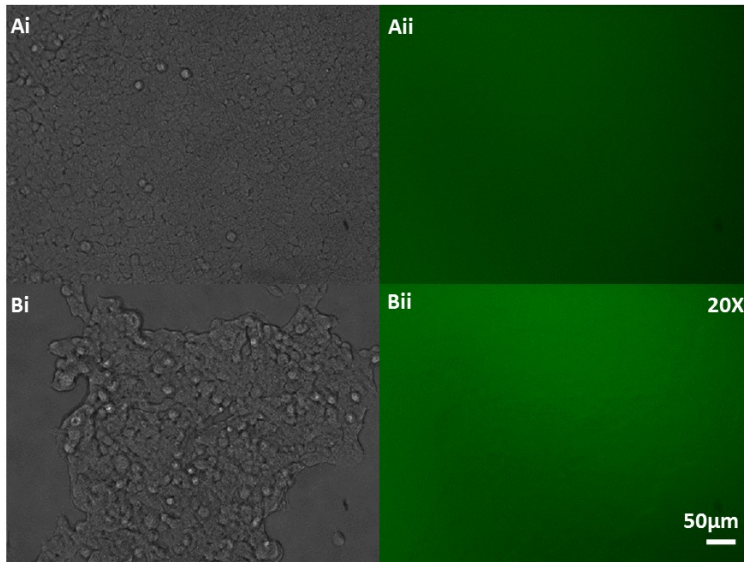

Figure 55. Treatment of Clonal TCF/LEF (Wnt signalling) (D12) with PMA. Ai). Phase-contrast images of TCF/LEF transduced clone D12 treated with the vehicle control. Aii). Correlating GFP images. Bi.) Phase-contrast images of TCF/LEF TFAR transduced clone D12 treated with 10ng/ml PMA (21 hrs). Bii). Correlating GFP images. GFP images did not display modulation of TCF/LEF (Wnt signalling) on addition of PMA. All images were taken at 20X magnification using Leica Live Cell Imaging System. Scale bar 50µm.
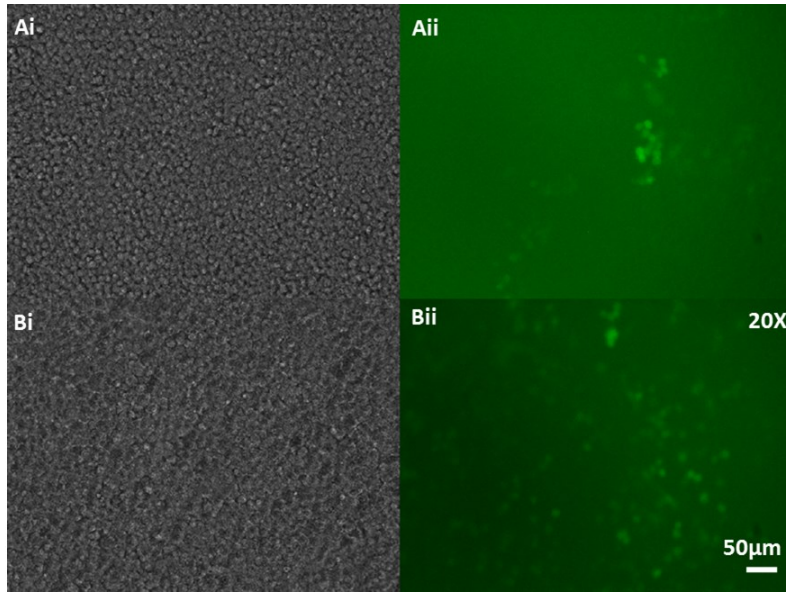
Figure 56. Treatment of Clonal STAT3 (C7i) with PMA. Ai). Phase-contrast images of STAT3 transduced clone C7i treated with the vehicle control. Aii). Correlating GFP images. Bi.) Phase-contrast images of STAT3 TFAR transduced clone C7i treated with 10ng/ml PMA (21 hrs). Bii). Correlating GFP images. GFP images displayed upregulation of STAT3 on addition of PMA. All images were taken at 20X magnification using Leica Live Cell Imaging System. Scale bar 50µm.
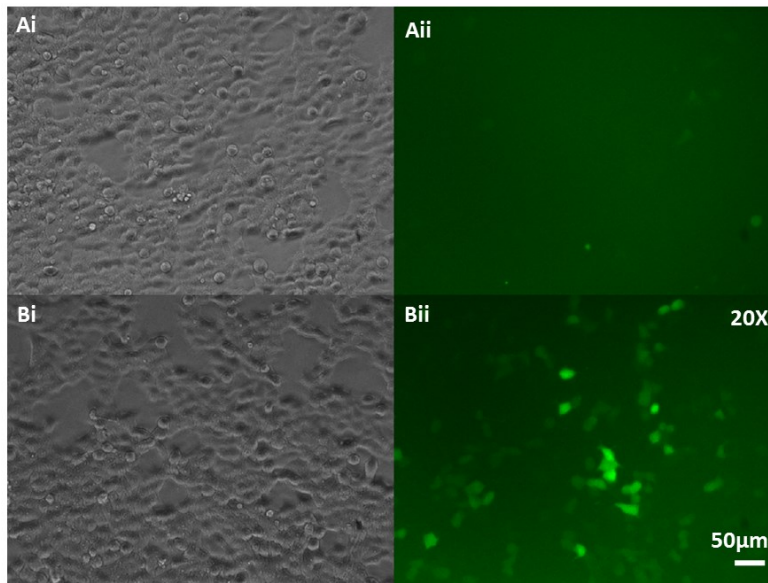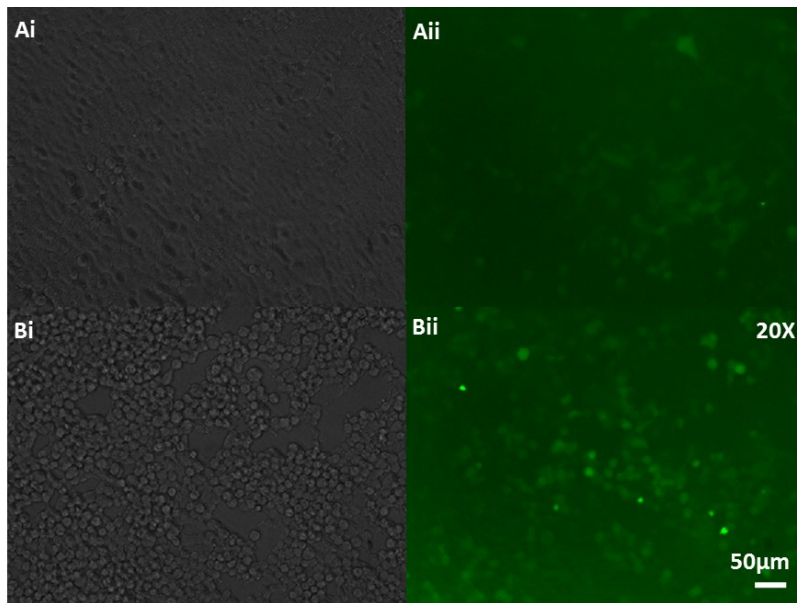

Figure 57. Treatment of Clonal HIF (B5) with PMA. Ai). Phase-contrast images of HIF transduced clone B5 treated with the vehicle control. Aii). Correlating GFP images. Bi.) Phase-contrast images of HIF TFAR transduced clone B5 treated with 10ng/ml PMA (21 hrs). Bii). Correlating GFP images. GFP images displayed upregulation of HIF on addition of PMA. All images were taken at 20X magnification using Leica Live Cell Imaging System. Scale bar 50µm.
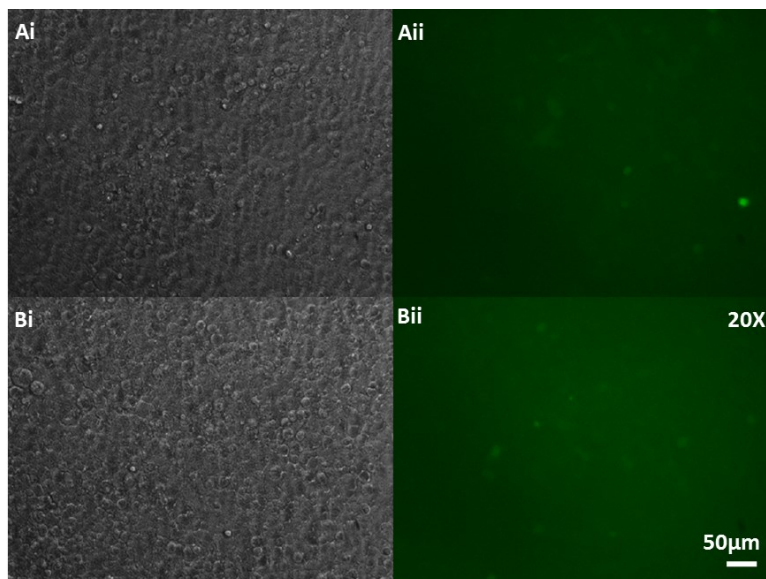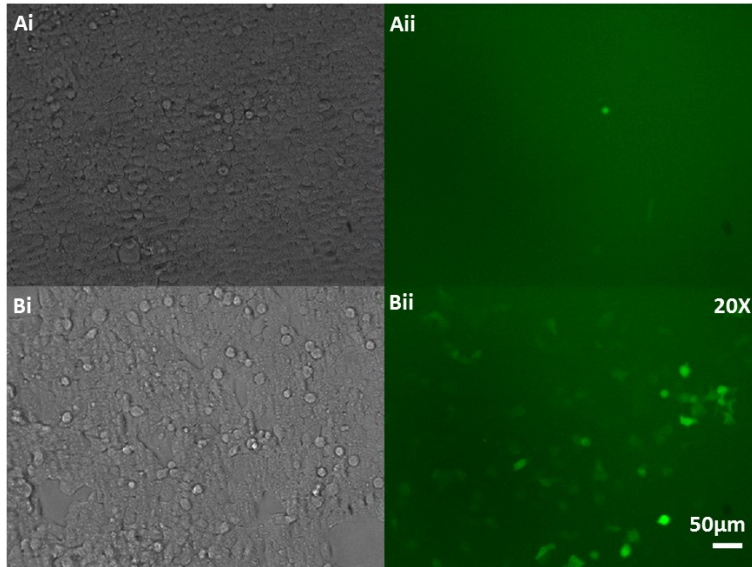
Figure 58. Treatment of Clonal NFκB (G2) with PMA. Ai). Phase-contrast images of NFκB transduced clone G2 treated with the vehicle control. Aii). Correlating GFP images. Bi.) Phase-contrast images of NFκB TFAR transduced clone G2 treated with 10ng/ml PMA (21 hrs). Bii). Correlating GFP images. GFP images displayed upregulation of NFκB on addition of PMA. All images were taken at 20X magnification using Leica Live Cell Imaging System. Scale bar 50μm.
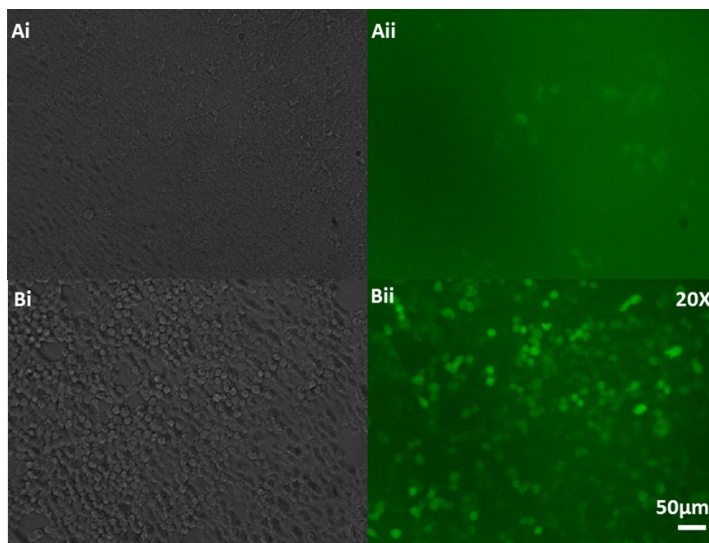
Figure 59. Treatment of Clonal NRF2 (A9) with PMA. Ai). Phase-contrast images of NRF2 transduced clone A9 treated with the vehicle control. Aii). Correlating GFP images. Bi.) Phase-contrast images of NRF2 TFAR transduced clone A9 treated with 10ng/ml PMA (21 hrs). Bii). Correlating GFP images. GFP images displayed upregulation of NRF2 on addition of PMA. All images were taken at 20X magnification using Leica Live Cell Imaging System. Scale bar 50μm.

8.0 References

Attia, Y. M., Tawfiq, R. A., Ali, A. A. and Elmazar, M. M. (2017) 'The FXR Agonist, Obeticholic Acid, Suppresses HCC Proliferation & Metastasis: Role of IL-6/STAT3 Signalling Pathway.' *Sci Rep*, 7(1), Oct, 2017/10/02, p. 12502.

Barriscale, K. A., O'Sullivan, S. A. and McCarthy, T. V. (2014) 'A single secreted luciferase-based gene reporter assay.' *Anal Biochem*, 453, May, 2014/02/28, pp. 44-49.

Beurel, E. and Jope, R. S. (2009) 'Glycogen synthase kinase-3 promotes the synergistic action of interferon-gamma on lipopolysaccharide-induced IL-6 production in RAW264.7 cells.' *Cell Signal*, 21(6), Jun, 2009/03/01, pp. 978-985.

Boute, N., Lowe, P., Berger, S., Malissard, M., Robert, A. and Tesar, M. (2016) 'NanoLuc Luciferase - A Multifunctional Tool for High Throughput Antibody Screening.' *Front Pharmacol*, 7 2016/02/18, p. 27.

Brady, O. A., Martina, J. A. and Puertollano, R. (2017) 'Emerging roles for TFEB in the immune response and inflammation.' *Autophagy*, Jul, 2017/07/24, pp. 1-9.

Bryan, H. K., Olayanju, A., Goldring, C. E. and Park, B. K. (2013) 'The Nrf2 cell defence pathway: Keap1-dependent and -independent mechanisms of regulation.' *Biochem Pharmacol*, 85(6), Mar, 2012/12/05, pp. 705-717.

Buckley, S. M., Delhove, J. M., Perocheau, D. P., Karda, R., Rahim, A. A., Howe, S. J., Ward, N. J., Birrell, M. A., Belvisi, M. G., Arbuthnot, P., Johnson, M. R., Waddington, S. N. and McKay, T. R. (2015) 'In vivo bioimaging with tissue-specific transcription factor activated luciferase reporters.' *Sci Rep*, 5, Jul, 2015/07/03, p. 11842.

Caamaño, J. and Hunter, C. A. (2002) 'NF-kappaB family of transcription factors: central regulators of innate and adaptive immune functions.' *Clin Microbiol Rev*, 15(3), Jul, pp. 414-429.

Chang, Y. T., Chen, C. L., Lin, C. F., Lu, S. L., Cheng, M. H., Kuo, C. F. and Lin, Y. S. (2013) 'Regulatory role of GSK-3 β on NF- κ B, nitric oxide, and TNF- α in group A streptococcal infection.' *Mediators Inflamm*, 2013 2013/03/05, p. 720689.

Chen, F., Wang, W., Ding, H., Yang, Q., Dong, Q. and Cui, M. (2016) 'The glucagon-like peptide-1 receptor agonist exendin-4 ameliorates warfarin-associated hemorrhagic transformation after cerebral ischemia.' *J Neuroinflammation*, 13(1), Aug, p. 204.

Chen, X., Liu, Y., Zhu, J., Lei, S., Dong, Y., L., L., Jiang, B., Tan L, Wu, J., Yu, S. and Zhao, Y. (2008) 'GSK-3β downregulates Nrf2 in cultured cortical neurons and in a rat model of cerebral ischemia-reperfusion.' *Scientific Reports*, 2016 Feb 3,

Colin, L., Vandenhoudt, N., de Walque, S., Van Driessche, B., Bergamaschi, A., Martinelli, V., Cherrier, T., Vanhulle, C., Guiguen, A., David, A., Burny, A., Herbein, G., Pancino, G., Rohr, O. and Van Lint, C. (2011) 'The AP-1 binding sites located in the pol gene intragenic regulatory region of HIV-1 are important for viral replication.' *PLoS One*, 6(4), Apr, 2011/04/19, p. e19084.

D'Ignazio, L., Batie, M. and Rocha, S. (2017) 'Hypoxia and Inflammation in Cancer, Focus on HIF and NF-κB.' *Biomedicines*, 5(2), May, 2017/05/09,

Darsalia, V., Hua, S., Larsson, M., Mallard, C., Nathanson, D., Nyström, T., Sjöholm, Å., Johansson, M. E. and Patrone, C. (2014) 'Exendin-4 reduces ischemic brain injury in normal and aged type 2 diabetic mice and promotes microglial M2 polarization.' *PLoS One*, 9(8) p. e103114.

Debelec-Butuner, B., Alapinar, C., Varisli, L., Erbaykent-Tepedelen, B., Hamid, S. M., Gonen-Korkmaz, C. and Korkmaz, K. S. (2014) 'Inflammation-mediated abrogation of androgen signaling: an in vitro model of prostate cell inflammation.' *Mol Carcinog*, 53(2), Feb, 2012/08/21, pp. 85-97.

Elsner, C. and Bohne, J. (2017) 'The retroviral vector family: something for everyone.' *Virus Genes*, Jul, 2017/07/31,

Esch, E. W., Bahinski, A. and Huh, D. (2015) 'Organs-on-chips at the frontiers of drug discovery.' *Nat Rev Drug Discov*, 14(4), Apr, 2015/03/20, pp. 248-260.

Farley, D. C., Iqball, S., Smith, J. C., Miskin, J. E., Kingsman, S. M. and Mitrophanous, K. A. (2007) 'Factors that influence VSV-G pseudotyping and transduction efficiency of lentiviral vectors-in vitro and in vivo implications.' *J Gene Med*, 9(5), May, pp. 345-356.

Galli, C., Piemontese, M., Lumetti, S., Manfredi, E., Macaluso, G. M. and Passeri, G. (2013) 'GSK3b-inhibitor lithium chloride enhances activation of Wnt canonical signaling and osteoblast differentiation on hydrophilic titanium surfaces.' *Clin Oral Implants Res*, 24(8), Aug, 2012/05/25, pp. 921-927.

Garziera, M., Scarabel, L. and Toffoli, G. (2017) 'Hypoxic Modulation of HLA-G Expression through the Metabolic Sensor HIF-1 in Human Cancer Cells.' *J Immunol Res*, 2017 2017/07/11, p. 4587520.

Ghim, C. M., Lee, S. K., Takayama, S. and Mitchell, R. J. (2010) 'The art of reporter proteins in science: past, present and future applications.' *BMB Rep*, 43(7), Jul, pp. 451-460.

Ghosh, S. and Dass, J. F. (2016) 'Study of pathway cross-talk interactions with NF-κB leading to its activation via ubiquitination or phosphorylation: A brief review.' *Gene*, 584(1), Jun, 2016/03/09, pp. 97-109.

Gorrini, C., Harris, I. S. and Mak, T. W. (2013) 'Modulation of oxidative stress as an anticancer strategy.' *Nat Rev Drug Discov*, 12(12), Dec, pp. 931-947.

Guo, H., Zhou, H., Lu, J., Qu, Y., Yu, D. and Tong, Y. (2016) 'Vascular endothelial growth factor: an attractive target in the treatment of hypoxic/ischemic brain injury.' *Neural Regen Res*, 11(1), Jan, pp. 174-179.

Gào, X. and Schöttker, B. (2017) 'Reduction-oxidation pathways involved in cancer development: a systematic review of literature reviews.' *Oncotarget*, 8(31), Aug, 2017/04/16, pp. 51888-51906.

Hao, J., Li, T. G., Qi, X., Zhao, D. F. and Zhao, G. Q. (2006) 'WNT/beta-catenin pathway up-regulates Stat3 and converges on LIF to prevent differentiation of mouse embryonic stem cells.' *Dev Biol*, 290(1), Feb, 2005/12/05, pp. 81-91.

Hoesel, B. and Schmid, J. A. (2013) 'The complexity of NF-κB signaling in inflammation and cancer.' *Molecular Cancer*, 12(86) 02.08.2013,

Hong, W. X., Hu, M. S., Esquivel, M., Liang, G. Y., Rennert, R. C., McArdle, A., Paik, K. J., Duscher, D., Gurtner, G. C., Lorenz, H. P. and Longaker, M. T. (2014) 'The Role of Hypoxia-Inducible Factor in Wound Healing.' *Adv Wound Care (New Rochelle)*, 3(5), May, pp. 390-399.

Huang, H., Kong, D., Liu, Y., Cui, Q., Wang, K., Zhang, D., Wang, J., Zhai, M., Yan, J., Zhang, C. and Wu, G. (2017) 'Sapylin promotes wound healing in mouse skin flaps.' *Am J Transl Res*, 9(6) 2017/06/15, pp. 3017-3026.

Jayant, R. D., Sosa, D., Kaushik, A., Atluri, V., Vashist, A., Tomitaka, A. and Nair, M. (2016a) 'Current status of non-viral gene therapy for CNS disorders.' *Expert Opin Drug Deliv*, 13(10), Oct, 2016/06/01, pp. 1433-1445.

Jayant, R. D., Sosa, D., Kaushik, A., Atluri, V., Vashist, A., Tomitaka, A. and Nair, M. (2016b) 'Current status of non-viral gene therapy for CNS disorders.' *Expert Opin Drug Deliv*, 13(10), Oct, 2016/06/01, pp. 1433-1445.

Jun, J. C., Rathore, A., Younas, H., Gilkes, D. and Polotsky, V. Y. (2017) 'Hypoxia-Inducible Factors and Cancer.' *Curr Sleep Med Rep*, 3(1), Mar, 2017/01/28, pp. 1-10.

Jung, Y., Isaacs, J. S., Lee, S., Trepel, J., Liu, Z. G. and Neckers, L. (2003) 'Hypoxia-inducible factor induction by tumour necrosis factor in normoxic cells requires receptor-interacting protein-dependent nuclear factor kappa B activation.' *Biochem J*, 370(Pt 3), Mar, pp. 1011-1017.

Kamel, M. and Ninov, N. (2017) 'Catching new targets in metabolic disease with a zebrafish.' *Curr Opin Pharmacol*, 37, Sep, 2017/09/06, pp. 41-50.

Kappelmann, M., Bosserhoff, A. and Kuphal, S. (2014) 'AP-1/c-Jun transcription factors: regulation and function in malignant melanoma.' *Eur J Cell Biol*, 93(1-2), 2014 Jan-Feb, 2013/10/26, pp. 76-81.

Karuppagounder, S. S. and Ratan, R. R. (2012) 'Hypoxia-inducible factor prolyl hydroxylase inhibition: robust new target or another big bust for stroke therapeutics?' *J Cereb Blood Flow Metab*, 32(7), Jul, 2012/03/14, pp. 1347-1361.

Khan, M. S., Ali, T., Abid, M. N., Jo, M. H., Khan, A., Kim, M. W., Yoon, G. H., Cheon, E. W., Rehman, S. U. and Kim, M. O. (2017) 'Lithium ameliorates lipopolysaccharide-induced neurotoxicity in the cortex and hippocampus of the adult rat brain.' *Neurochem Int*, 108, Sep, 2017/05/13, pp. 343-354.

Kim, J. Y. and Lee, J. Y. (2017) 'Targeting Tumor Adaption to Chronic Hypoxia: Implications for Drug Resistance, and How It Can Be Overcome.' *Int J Mol Sci*, 18(9), Aug, 2017/08/25,

Kim, M. H., Kim, E. H., Jung, H. S., Yang, D., Park, E. Y. and Jun, H. S. (2017) 'EX4 stabilizes and activates Nrf2 via PKCδ, contributing to the prevention of oxidative stress-induced pancreatic beta cell damage.' *Toxicol Appl Pharmacol*, 315, Jan, 2016/12/07, pp. 60-69.

Ko, Y. S., Cho, S. J., Park, J., Choi, Y., Lee, J. S., Youn, H. D., Kim, W. H., Kim, M. A., Park, J. W. and Lee, B. L. (2016) 'Hypoxic inactivation of glycogen synthase kinase-3β promotes gastric tumor growth and angiogenesis by facilitating hypoxia-inducible factor-1 signaling.' *APMIS*, 124(9), Sep, 2016/07/01, pp. 748-756.

Kumar, H. and Choi, D. K. (2015) 'Hypoxia Inducible Factor Pathway and Physiological Adaptation: A Cell Survival Pathway?' *Mediators Inflamm*, 2015 2015/09/27, p. 584758.

Kwon, B., Goltz, M. and Houpt, T. A. (2008) 'Expression of AP-1 family transcription factors in the amygdala during conditioned taste aversion learning: role for Fra-2.' *Brain Res*, 1207, May, 2008/02/09, pp. 128-141.

Kwon, M. J., Ma, J., Ding, Y., Wang, R. and Sun, Z. (2012) 'Protein kinase C-θ promotes Th17 differentiation via upregulation of Stat3.' *J Immunol*, 188(12), Jun, 2012/05/14, pp. 5887-5897.

Lee, C. T., Bendriem, R. M., Wu, W. W. and Shen, R. F. (2017a) '3D brain Organoids derived from pluripotent stem cells: promising experimental models for brain development and neurodegenerative disorders.' *J Biomed Sci*, 24(1), Aug, 2017/08/20, p. 59.

Lee, C. T., Bendriem, R. M., Wu, W. W. and Shen, R. F. (2017b) '3D brain Organoids derived from pluripotent stem cells: promising experimental models for brain development and neurodegenerative disorders.' *J Biomed Sci*, 24(1), Aug, 2017/08/20, p. 59.

Li, L., Saliba, P., Reischl, S., Marti, H. H. and Kunze, R. (2016) 'Neuronal deficiency of HIF prolyl 4-hydroxylase 2 in mice improves ischemic stroke recovery in an HIF dependent manner.' *Neurobiol Dis*, 91, Jul, pp. 221-235.

Lim, J., Chun, Y. and Park, J. (2008) 'Hypoxia-inducible factor1alpha obstructs a Wnt signaling pathway by inhibiting the hARD1-mediated activation of beta-catenin .' *Cancer Research.*, 68(13) 2008 Jul 1, pp. 5177-5184.

Lin, B., Xu, D. and Leaman, D. W. (2016) 'X-linked inhibitor of apoptosis-associated factor 1 regulates TNF receptor 1 complex stability.' *FEBS Lett*, 590(23), Dec, 2016/11/03, pp. 4381-4392.

Liu, A. M., New, D. C., Lo, R. K. and Wong, Y. H. (2009) 'Reporter gene assays.' *Methods Mol Biol*, 486 pp. 109-123.

Liu, K., Wang, X., Sha, K., Zhang, F., Xiong, F., Chen, J., Li, J., Churilov, L. P., Chen, S., Wang, Y. and Huang, N. (2017) 'Nuclear protein HMGN2 attenuates pyocyanin-induced oxidative stress via Nrf2 signaling and inhibits Pseudomonas aeruginosa internalization in A549 cells.' *Free Radic Biol Med*, 108, Jul, 2017/04/10, pp. 404-417.

Loor, G. and Schumacker, P. T. (2008) 'Role of hypoxia-inducible factor in cell survival during myocardial ischemia-reperfusion.' *Cell Death Differ*, 15(4), Apr, 2008/02/08, pp. 686-690.

Ma, B. and Hottiger, M. O. (2016) 'Crosstalk between Wnt/β-Catenin and NF-κB Signaling Pathway during Inflammation.' *Front Immunol*, 7 2016/09/22, p. 378.

Ma, Q. (2013a) 'Role of nrf2 in oxidative stress and toxicity.' *Annu Rev Pharmacol Toxicol*, 53 pp. 401-426.

Ma, Q. (2013b) 'Role of nrf2 in oxidative stress and toxicity.' *Annu Rev Pharmacol Toxicol*, 53 pp. 401-426.

MacRae, C. A. and Peterson, R. T. (2015) 'Zebrafish as tools for drug discovery.' *Nat Rev Drug Discov*, 14(10), Oct, 2015/09/11, pp. 721-731.

Medina, D. L., Di Paola, S., Peluso, I., Armani, A., De Stefani, D., Venditti, R., Montefusco, S., Scotto-Rosato, A., Prezioso, C., Forrester, A., Settembre, C., Wang, W., Gao, Q., Xu, H., Sandri, M., Rizzuto, R., De Matteis, M. A. and Ballabio, A. (2015) 'Lysosomal calcium signalling regulates autophagy through calcineurin and TFEB.' *Nat Cell Biol*, 17(3), Mar, pp. 288-299.

MH, P. and JT, H. (2016) 'Roles of NF -κB in Cancer and Inflammatory Diseases and Their Therapeutic Approaches .' *Cells*, 5(2) 29.05.2016,

Miscia, S., Marchisio, M., Grilli, A., Di Valerio, V., Centurione, L., Sabatino, G., Garaci, F., Zauli, G., Bonvini, E. and Di Baldassarre, A. (2002) 'Tumor necrosis factor alpha (TNF-alpha) activates Jak1/Stat3-Stat5B signaling through TNFR-1 in human B cells.' *Cell Growth Differ*, 13(1), Jan, pp. 13-18.

Nennig, S. E. and Schank, J. R. (2017) 'The Role of NFkB in Drug Addiction: Beyond Inflammation.' *Alcohol Alcohol*, 52(2), Mar, pp. 172-179.

Osorio, J. S. and Bionaz, M. (2017) 'Plasmid transfection in bovine cells: Optimization using a realtime monitoring of green fluorescent protein and effect on gene reporter assay.' *Gene*, 626, Aug, 2017/05/10, pp. 200-208.

Parr, C., Carzaniga, R., Gentleman, S. M., Van Leuven, F., Walter, J. and Sastre, M. (2012) 'Glycogen synthase kinase 3 inhibition promotes lysosomal biogenesis and autophagic degradation of the amyloid-β precursor protein.' *Mol Cell Biol*, 32(21), Nov, 2012/08/27, pp. 4410-4418.

Ramamoorth, M. and Narvekar, A. (2015) 'Non viral vectors in gene therapy- an overview.' *J Clin Diagn Res*, 9(1), Jan, 2015/01/01, pp. GE01-06.

Ranga, A., Gjorevski, N. and Lutolf, M. P. (2014) 'Drug discovery through stem cell-based organoid models.' *Adv Drug Deliv Rev*, 69-70, Apr, 2014/02/26, pp. 19-28.

Rapp, J., Jaromi, L., Kvell, K., Miskei, G. and Pongracz, J. E. (2017) 'WNT signaling - lung cancer is no exception.' *Respir Res*, 18(1), Sep, 2017/09/05, p. 167.

Ren, H. and Hu, K. (2017) 'Inflammatory and oxidative stress-associated factors in chronic intermittent hypoxia in Chinese patients, rats, lymphocytes and endotheliocytes.' *Mol Med Rep*, Sep, 2017/09/26,

Seo, H. H., Lee, C. Y., Lee, J., Lim, S., Choi, E., Park, J. C., Lee, S. and Hwang, K. C. (2016) 'The role of nuclear factor of activated T cells during phorbol myristate acetate-induced cardiac differentiation of mesenchymal stem cells.' *Stem Cell Res Ther*, 7(1), Jul, 2016/07/12, p. 90.

Shanmugam, G., Narasimhan, M., Sakthivel, R., Kumar R, R., Davidson, C., Palaniappan, S., Claycomb, W. W., Hoidal, J. R., Darley-Usmar, V. M. and Rajasekaran, N. S. (2016) 'A biphasic effect of TNF-α in regulation of the Keap1/Nrf2 pathway in cardiomyocytes.' *Redox Biol*, 9, Oct, 2016/06/27, pp. 77-89.

Sharma, A., Yang, W. L., Ochani, M. and Wang, P. (2017) 'Mitigation of sepsis-induced inflammatory responses and organ injury through targeting Wnt/β-catenin signaling.' *Sci Rep*, 7(1), Aug, 2017/08/23, p. 9235.

Smith, R. E., Tran, K., Smith, C. C., McDonald, M., Shejwalkar, P. and Hara, K. (2016) 'The Role of the Nrf2/ARE Antioxidant System in Preventing Cardiovascular Diseases.' *Diseases*, 4(4), Nov, 2016/11/11,

Stacer, A. C., Nyati, S., Moudgil, P., Iyengar, R., Luker, K. E., Rehemtulla, A. and Luker, G. D. (2013) 'NanoLuc reporter for dual luciferase imaging in living animals.' *Mol Imaging*, 12(7), Oct, pp. 1-13.

Supuran, C. T. (2017) 'Carbonic Anhydrase Inhibition and the Management of Hypoxic Tumors.' *Metabolites*, 7(3), Sep, 2017/09/16,

Suzuki, T. and Yamamoto, M. (2017) 'Stress-sensing mechanisms and the physiological roles of the Keap1-Nrf2 system during cellular stress.' *J Biol Chem*, Aug, 2017/08/24,

Sykiotis, G. P. and Bohmann, D. (2010a) 'Stress-activated cap'n'collar transcription factors in aging and human disease.' *Sci Signal*, 3(112), Mar, 2010/03/09, p. re3.

Sykiotis, G. P. and Bohmann, D. (2010b) 'Stress-activated cap'n'collar transcription factors in aging and human disease.' *Sci Signal*, 3(112), Mar, 2010/03/09, p. re3.

Szabo, M., Svensson Akusjärvi, S., Saxena, A., Liu, J., Chandrasekar, G. and Kitambi, S. S. (2017) 'Cell and small animal models for phenotypic drug discovery.' *Drug Des Devel Ther*, 11 2017/06/28, pp. 1957-1967.

Tewari, D., Nabavi, S. F., Nabavi, S. M., Sureda, A., Farooqi, A. A., Atanasov, A. G., Vacca, R. A., Sethi, G. and Bishayee, A. (2017) 'Targeting activator protein 1 signaling pathway by bioactive natural agents: Possible therapeutic strategy for cancer prevention and intervention.' *Pharmacol Res*, Sep, 2017/09/23,

Uchida, K., Unuma, K., Funakoshi, T., Aki, T. and Uemura, K. (2014) 'Activation of Master Autophagy Regulator TFEB During Systemic LPS Administration in the Cornea.' *J Toxicol Pathol*, 27(2), Jul, 2014/04/17, pp. 153-158.

Umare, V., Pradhan, V., Nadkar, M., Rajadhyaksha, A., Patwardhan, M., Ghosh, K. K. and Nadkarni, A. H. (2014) 'Effect of proinflammatory cytokines (IL-6, TNF-α, and IL-1β) on clinical manifestations in Indian SLE patients.' *Mediators Inflamm*, 2014 2014/12/07, p. 385297.

Velichkova, M. and Hasson, T. (2005) 'Keap1 regulates the oxidation-sensitive shuttling of Nrf2 into and out of the nucleus via a Crm1-dependent nuclear export mechanism.' *Mol Cell Biol*, 25(11), Jun, pp. 4501-4513.

Vion, A. C., Kheloufi, M., Hammoutene, A., Poisson, J., Lasselin, J., Devue, C., Pic, I., Dupont, N., Busse, J., Stark, K., Lafaurie-Janvore, J., Barakat, A. I., Loyer, X., Souyri, M., Viollet, B., Julia, P., Tedgui, A., Codogno, P., Boulanger, C. M. and Rautou, P. E. (2017) 'Autophagy is required for endothelial cell alignment and atheroprotection under physiological blood flow.' *Proc Natl Acad Sci U S A*, Sep, 2017/09/25,

Wang, L., Zhao, Y., Liu, Y., Akiyama, K., Chen, C., Qu, C., Jin, Y. and Shi, S. (2013) 'IFN-γ and TNF-α synergistically induce mesenchymal stem cell impairment and tumorigenesis via NFκB signaling.' *Stem Cells*, 31(7), Jul, pp. 1383-1395.

Wang, M. X., Cheng, X. Y., Jin, M., Cao, Y. L., Yang, Y. P., Wang, J. D., Li, Q., Wang, F., Hu, L. F. and Liu, C. F. (2015) 'TNF compromises lysosome acidification and reduces α-synuclein degradation via autophagy in dopaminergic cells.' *Exp Neurol*, 271, Sep, 2015/05/19, pp. 112-121.

Wang, Y., van Boxel-Dezaire, A. H., Cheon, H., Yang, J. and Stark, G. R. (2013) 'STAT3 activation in response to IL-6 is prolonged by the binding of IL-6 receptor to EGF receptor.' *Proc Natl Acad Sci U S A*, 110(42), Oct, 2013/09/30, pp. 16975-16980.

Wei, J., Zhang, Y., Jia, Q., Liu, M., Li, D., Song, L., Hu, Y., Xian, M., Yang, H., Ding, C. and Huang, L. (2016) 'Systematic investigation of transcription factors critical in the

protection against cerebral ischemia by Danhong injection.' *Sci Rep*, 6, Jul, 2016/07/19, p. 29823.

Wu, Y. and Zhou, B. P. (2010) 'TNF-alpha/NF-kappaB/Snail pathway in cancer cell migration and invasion.' *Br J Cancer*, 102(4), Feb, 2010/01/19, pp. 639-644.

Xia, M., Zhao, X., Huang, Q., Sun, H., Sun, C., Yuan, J., He, C., Sun, Y., Huang, X., Kong, W. and Kong, W. (2017) 'Activation of Wnt/β-catenin signaling by lithium chloride attenuates d-galactose - induced neurodegeneration in the auditory cortex of a rat model of aging .' *FEBS Open Bio*, 7(6) 2017 Apr 25, pp. 759-776.

Xiong, A. and Liu, Y. (2017) 'Targeting Hypoxia Inducible Factors-1α As a Novel Therapy in Fibrosis.' *Frontiers in Pharmacology*, 8(326) May 30.,

Xu, Y. Z., Kanagaratham, C., Jancik, S. and Radzioch, D. (2013) 'Promoter deletion analysis using a dual-luciferase reporter system.' *Methods Mol Biol*, 977 pp. 79-93.

Yu, T., Tang, B. and Sun, X. (2017) 'Development of Inhibitors Targeting Hypoxia-Inducible Factor 1 and 2 for Cancer Therapy.' *Yonsei Med J*, 58(3), May, pp. 489-496.

Zhang, M., An, C., Gao, Y., Leak, R. K., Chen, J. and Zhang, F. (2013) 'Emerging roles of Nrf2 and phase II antioxidant enzymes in neuroprotection.' *Prog Neurobiol*, 100, Jan, 2012/09/29, pp. 30-47.

Zhang, Z., Stickney, Z., Duong, N., Curley, K. and Lu, B. (2017a) 'AAV-based dual-reporter circuit for monitoring cell signaling in living human cells.' *J Biol Eng*, 11 2017/06/05, p. 18.

Zhang, Z., Stickney, Z., Duong, N., Curley, K. and Lu, B. (2017b) 'AAV-based dual-reporter circuit for monitoring cell signaling in living human cells.' *J Biol Eng*, 11 2017/06/05, p. 18.

Zhou, J., Yao, W., Li, C., Wu, W., Li, Q. and Liu, H. (2017) 'Administration of follicle-stimulating hormone induces autophagy via upregulation of HIF-1α in mouse granulosa cells.' *Cell Death Dis*, 8(8), Aug, 2017/08/17, p. e3001.

Zhou, T., Zhang, M., Zhao, L., Li, A. and Qin, X. (2016) 'Activation of Nrf2 contributes to the protective effect of Exendin-4 against angiotensin II-induced vascular smooth muscle cell senescence.' *Am J Physiol Cell Physiol*, 311(4), Oct, 2016/08/03, pp. C572-C582.

Zhou, W., Wang, L., Gou, S. M., Wang, T. L., Zhang, M., Liu, T. and Wang, C. Y. (2012) 'ShRNA silencing glycogen synthase kinase-3 beta inhibits tumor growth and angiogenesis in pancreatic cancer.' *Cancer Lett*, 316(2), Mar, 2011/11/02, pp. 178-186.

Ziello, J. E., Jovin, I. S. and Huang, Y. (2007) 'Hypoxia-Inducible Factor (HIF)-1 regulatory pathway and its potential for therapeutic intervention in malignancy and ischemia.' *Yale J Biol Med*, 80(2), Jun, pp. 51-60.